ABSTRACT

FLEXIBLE ELECTRONICS: MATERIALS AND SENSOR FABRICATION

by
Katherine J Duncan

This dissertation demonstrates how to fabricate piezoelectric/pyroelectric thin films by using different printing techniques. These techniques could replace vacuum techniques for manufacturing piezoelectric/pyroelectric sensors. Ink-jet, screen and stencil printing techniques were developed to print these devices.

This work outlines attempts to develop a solution processable conductive ink for ink-jet printing. It then details the printing of commercial conductive ink on flexible substrates employing the three printing methods. Raman spectroscopy and Fourier transform infrared spectroscopy, are both used to investigate the structure of the P(VDF-TrFE) films. Optical microscopy is used to investigate the thickness and uniformity of the deposited films. The formulation of P(VDF-TrFE) for printing is also described for the three printing methods.

Piezoelectric accelerometers have been developed and demonstrated. The sensors are axial compression piezoelectric accelerometers which measure impacts in the direction perpendicular to the sensors themselves. When the sensors are moved downward the top electrode tends to move upward, inducing charge via the piezoelectric effect. The sensors were mounted on an electrodynamic shaker and tested with an input vibration up to 1.5 g's at 100 Hz. The test data show that the accelerometers track the frequency of the input vibration; the output increases with increasing input acceleration.

A comparison of the three printing methods to fabricate sensors on flexible substrates with commercial conductive inks and formulated P(VDF-TrFE) ink specific to the print method with similar geometries produces the following conclusions:

Excellent adhesion of the commercial silver ink for screen and stencil printing has been achieved. The stencil printed silver films are smoother and more uniform than the screen printed films. Adhesion of the commercial PEDOT/PSS ink-jettable was successful. However, smoothness and uniformity were issues that need to be resolved. Also, when the ink-jetted PDOT/PSS films were exposed to high temperatures the films tended to crack and adhesion was lost.

Functional devices were fabricated with screen and stencil printing quickly. In a one day period, multiple sheets of functional devices were obtained with both printing methods. Ink-jet printing, on the other hand, required greater then twenty four hours to fabricate one sheet of sensors even when the sensor size was reduced.

The cost of masks/cartridges was $0.75, $1.68 and $59 per layer for stencil, screen and ink-jet printing respectively. The ink-jet print system cartridges were manufactured for one time use, whereas the masks were reusable for both screen and stencil printing.

The best stencil and screen printed accelerometers demonstrated a voltage sensitivity of 145 mV/g. It is believed that the performance of these sensors can be enhanced with an automated printing system that is equipped with optical vision and automated alignment systems. The successful development of printed devices demonstrates that these print methods will be beneficial to the future of flexible electronics.

FLEXIBLE ELECTRONICS: MATERIALS AND SENSOR FABRICATION

by
Katherine J. Duncan

A Dissertation
Submitted to the Faculty of
New Jersey Institute of Technology and
Rutgers, The State University of New Jersey-Newark
in Partial Fulfillment of the Requirements for the Degree of
Doctor of Philosophy in Applied Physics

Federated Physics Department

August 2008

APPROVAL PAGE

FLEXIBLE ELECTRONICS: MATERIALS AND SENSOR FABRICATION

Katherine J. Duncan

7/21/08

Dr. John F. Federici, Dissertation Advisor — Date
Professor of Physics, NJIT

6/5/08

Dr. Zhen Wu, Committee Member — Date
Professor of Physics, Rutgers, The State University of New Jersey-Newark

6/5/08

Dr. Trevor A. Tyson, Committee Member — Date
Professor of Physics, NJIT

6/5/08

Dr. Gordon A. Thomas, Committee Member — Date
Professor of Physics and Biomedical Engineering, NJIT

6/5/08

Dr. Reginald Farrow, Committee Member — Date
Research Professor of Physics, NJIT

6/5/08

Dr. Hee Chuan Lim, Committee Member — Date
Assistant Research Professor of Physics, NJIT

BIOGRAPHICAL SKETCH

Author: Katherine J. Duncan

Degree: Doctor of Philosophy

Date: August 2008

Undergraduate and Graduate Education:

- Doctor of Philosophy in Electrical Engineering,
  New Jersey Institute of Technology, Newark, NJ, 2008
- Master of Engineering in Electrical Engineering,
  Stevens Institute of Technology, Hoboken, NJ, 1999
- Bachelor of Engineering in Computer Engineering,
  Stevens Institute of Technology, Hoboken, NJ, 1998

Major: Applied Physics

This dissertation is dedicated to John S. , who always comes first in my book.

ACKNOWLEDGMENT

I want to thank my dissertation advisor, Dr John Federici for introducing me to the field of flexible electronics also thank you for your unfailing support encouragement and guidance at every step of my research which led to this dissertation. In the same vain, I would like to thank Dr. Zhen Wu, Dr. Trevor A. Tyson, Dr. Gordon A Thomas, Dr. Reginald C. Farrow and Dr. Hee Chuan Lim, who actively participated in my dissertation committee providing valuable recommendation at every point in this work.

I gratefully acknowledge Laura Ayers of the US Army AMRDEC Redstone Arsenal, AL and James Zunino of the US Army ARDEC Picatinny Arsenal, NJ for providing the funding to facilitate this work. As well special thanks go to Dr John Rollino, Physics Department Rutgers Newark, for providing funding for the initial years of my PhD. degree.

I appreciate the assistance of the following people who facilitated and assisted me in my research; Dr Camelia Prodan and Ms. Corina T. Bot for providing the use of their microscope and invaluable advice; Dr. Zafar Iqbal and Mr. William Wagner for assisting with the Raman measurements; Dr. Daniel E. Murnick and Mr. Erhan Ilkman for assisting in the IR measurements, for the use of their CO_2 laser and for the informative discussions; Dr. Amit Goyal for assisting with many chemistry issues that arose and helping find the path to resolve them; Dr. Lukasz A. Lapok, for assisting at the most critical point and helping in finding the necessary resources to complete this work; Lastly I thank the NJIT Chemistry Department and specifically Mr. Yogesh Gandhi without this assistance most of my research would not have been possible.

I appreciate the assistance of the following people who supplied me with engineering samples and technical assistance in my research; Mr. Don Farrelly, Technical Specialist, DuPont HPF for the Kapton samples and the technical data; Mr. Patrick Reich, FUJIFILM Dimatix, Inc., for all your technical assistance when our printer had unusual failures; Dr Frank Keohan, Technical Marketing Specialist Electronics & Optics Group H.C. Starck Inc., for providing technical information on modifying the materials that my group had on hand, extensive technical information on the Baytron products and for providing a very generous sample of Baytron P Jet N material; Dr. Mitch Thompson, Measurement Specialties, Inc. for providing excellent resources on piezoelectric polymers and for the very generous sample of P(VDF-TrFE) material.

Lastly, I wish to thank my friends and family without whom my success in this endeavor would not have been possible.

TABLE OF CONTENTS

TABLE OF CONTENTS
(Continued)

TABLE OF CONTENTS
(Continued)

Chapter **Page**

LIST OF TABLES

LIST OF TABLES
(Continued)

LIST OF FIGURES

LIST OF FIGURES
(Continued)

LIST OF FIGURES
(Continued)

CHAPTER 1

INTRODUCTION

1.1 Background

Some of the early concepts of flexible electronics date back to the turn of the 20th century when the first patents [1] were filled for the flexible printed wires, as seen in Figure 1.1. Over time, flexible printed wiring found applications in flip chip technology, flexible interconnects and flexible electronics. Nearly every imaginable type of electrical and electronic product today contains flexible interconnections. Examples are computer keyboards, ipods and cell phones. The science of material and materials processing also contributed to major advancements in flexible electronic systems such as displays, sensors, and radio-frequency identification (RFID). As silicon technology progressed, the technology has been transferred to flexible electronics.

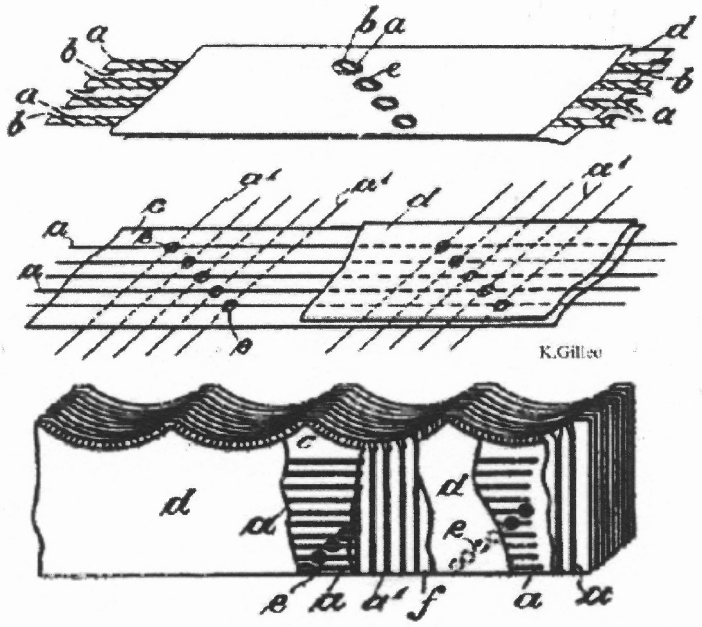

Figure 1.1 First flexible circuit patent [1].

Flexible electronics have found application as connectors in various systems where flexibility and space constraints limited the options of the engineer. Today flexible electronics have three main research concentrations: development of materials, device/system development and processing/fabrication. As materials research matured and special classes of polymers [2, 3] (with levels of conductivity between those of insulators and metals) began to be developed so have the imagination of engineers. Most conductive polymers have metal flakes or nanoparticles dispersed in polymers or resin. Studies on conductive polymers [4, 5] have included the effects of the particle size, the ratio of polymer to metal and the annealing temperature. Nano-materials have pushed the capabilities of processing and potential flexible devices. The ability to produce nanocomposite materials has given rise to conductive adhesives, embedded passives [6] such as capacitors, inductors and resistors. This has made material science a driving force of potential new devices applications.

In the past few years, a steady growth in research ranges from applications like sensing, RFID, flexible display, flexible solar cells [7, 8] and wearable electronics [9] while have been in the forefront of technology. The development of flexible electronics, in the area of systems and devices such as flexible display technology and electronic paper, has benefited from scientists carrying out studies of materials and processing. Furthermore, many research groups around the world have developed competing technologies. These advances in flexible display technologies have pushed the potential for flexible fuel cells, RFID technologies and wearable electronics. These advances can be seen in initial commercial offerings of rollable/foldable/flexible solar panels and flexible displays.

Presently, the field of flexible electronics is exploding due to the progress seen with materials. Flexible electronics is on the edge to make a great impact by integrating systems with the advantage of being mass producible, light weight and disposable. However, one crucial restraining factor that needs to be overcome is the fabrication process; currently people are working on printing methods [10, 11] as an alternative to standard cleanroom technology.

This section has attempted to highlight some of the more significant work. This by no means is an exhaustive compilation of work in the area of flexible electronics. Many monthly journals, internet websites and excellent books are published on the subject and can be consulted for current research trends [12, 13].

1.2 Motivation

Recently flexible electronics has become a rich area for researchers across different fields of science and yet some key aspects of this multidisciplinary subject remain immature. Specifically, the choices of low cost and low temperature processing on flexible substrates are still rather limited. Standard vacuum deposition and lithography technology [14-16] continue to be used to fabricate flexible electronics, in some cases techniques such as plasma etching and vapor deposition make the end product cost prohibitive.

Limitations in fabrication can be a disadvantage in many areas of flexible electronics application. In some situations, if standard silicon processing is chosen, one needs to tailor the processing for the vacuum system fixtures and photolithography fixtures. If ink-jet printing is the fabrication method is chosen, again in most cases, the

system needs to be modified. In certain cases, a system specifically designed to deposit different types of exotic inks can be purchased.

In the present study, the goal is to resolve some of the significant aspects related to flexible thin film deposition methods. The specific goal is to find low cost as well as low temperature methods for processing to accommodate various substrates and to eliminate the use of expensive clean room facilities. An in depth investigation of the following issues has been made:

- Comparison of multiple printing processes to deposit electrically conductive mechanically stable thin films and a similar study will be performed with an active polymer. This study will determine which if any is the most viable printing method of thin films suitable for flexible device fabrication.
- Design of a pyroelectric infrared sensor using a pyroelectric polymer. Pyroelectric infrared sensors detect variations in temperature which modify the electric polarization of the material in turn releasing charge. These devices would offer a possibility of reducing the complexity of fabrication and thus lowering the cost.
- Design of a compression type accelerometer using a piezoelectric polymer. Piezoelectric accelerometers detect changes in acceleration in turn imparting a mechanical stress on the polymer resulting in an electrical output voltage. These devices would offer a possibility of reducing the complexity of fabricating and thus lowering the cost and enabling the potential for integration into other flexible systems.

1.3 Overview of Thesis

The aim of this study has been to develop low cost, low temperature fabrication techniques to create piezoelectric and pyroelectric thin films for use in flexible sensors. The research involved designing, fabricating and testing flexible accelerometers and infrared sensors. A number of printing techniques have been used to fabricate devices with the potential to advance the development of flexible electronics.

In the current chapter, an introduction and the motivation of this work is outlined, with the current state of flexible electronics summarized. Chapter 2 presents a detailed review of flexible electronics, starting with typical materials and deposition techniques. The materials and techniques presently employed in this research and standards for flexible electronics are reviewed. Also different methods of sensing both infrared radiation and acceleration are outlined.

Chapter 3 details the three printing methods employed for fabricating thin films. This chapter describes the effects of modifying ink-jet printer parameters on the printed thin films along with the effects of printing multiple layers and drop spacing. Details of the effects of changing the mesh on the uniformity of the films for screen printing are also detailed. Modification to standard stencil printing is described to obtain uniform thin films.

Chapter 4 examines the material properties of the P(VDF-TrFE) films deposited in Chapter 3. This chapter also looks at the cross section of the films to determine the thickness and uniformity of the deposited films. Raman and Fourier transform spectrometry are employed to determine the crystalline phase of the material. The films were then cross sectioned and thickness and uniformity were measured with an optical microscope.

Chapter 5 goes through the design of a thermal infrared sensor and a compression accelerometer using P(VDF-TrFE). Fabrication of the devices entailed adjusting the physical parameters like layer thickness, and overlap of the contacts to modify the response of the devices. The sensitivity of the infrared sensors was measured and the frequency response of the accelerometers was tested using a comparison calibration

method. This study is an attempt to verify the piezoelectric and pyroelectric effect in the P(VDF-TrFE) polymer.

Chapter 6 contains the conclusion and the recommendations for further research in this field.

CHAPTER 2

REVIEW OF FLEXIBLE ELECTRONICS

2.1 Introduction

Flexible electronics is a growing field and has exhibited steady growth in fabrication techniques and development of new materials which in turn have opened up new application areas. Some applications utilize standard semiconductor fabrication techniques which result in robust devices. Developments have been slowed due to the thermal and chemical incompatibilities of the substrates with standard processing techniques. Another of the principal reasons for the slowing of development is that standard semiconductor fabrication techniques remain expensive and unavailable to many researchers. Moreover, the introduction of non-standard materials to these environments tends to be difficult.

Flexible electronics depends heavily on materials and fabrication techniques, which are suited for specific applications. Various commercial printable inks will be discussed in detail in the present chapter along with inks that can be formulated using nanoparticles or chemicals readily available from chemical supply companies like Sigma Aldrich. Three promising fabrication techniques, namely ink-jet printing, screen printing and stencil printing will be discussed in detail. Some less utilized techniques for deposition of thin films will also be discussed in detail in the present chapter along with some applications of these thin films. To understand these fabrication techniques properly, a review of presently available materials, printing technology along with some applications will be discussed.

2.2 Materials for Flexible Electronics

2.2.1 Flexible Substrates

Recently there has been an increased interest in the use of flexible substrates in microelectronic fabrication. The main benefits of flexible substrates are their lighter weight, lower cost and the potential for roll-to-roll processing. Flexible substrates are further classified into plastics and metal films.

2.2.1.1 Plastic Substrates. The two main plastic substrates used today are polyimide substrates, for example DuPont's Kapton, and polyester or PET substrates, for example DuPont's Mylar.

Polyester has dimensional stability, consistent color and good clarity. It is chemical resistant, non-yellowing, non-tearing, and heat resistant to 230 degrees C [17]. On the other hand, polyimides' thermal, mechanical, chemical and electrical properties are retained over a wide temperatures range (-200 C to 400 C). The upper temperature limit for Kapton HN is 400 C [18]. Polyimides' thermal coefficient of expansion and thermal conductivity are 20 ppm/K and 1.09 W/mK [19] respectively, whereas the thermal conductivity of silicon (300K) is 1.3 W/cmC [20]. These properties make polyimide an ideal candidate for devices that need high temperature and chemical insensitivity. The main drawback of polyimide is its relatively high moisture absorption. But researchers have minimized this by adding a passivation layer of Si3N4 [14].

Polyimide laminates with rolled annealed copper foil are commercially available and suited for fabricating single and double sided circuitry [21, 22]. These laminates have the same advantages of polyimide and can be processed in a similar manner to printed circuit boards.

2.2.1.2 Metallic Substrates. Plastic substrates have become a dominant force in flexible electronics, although in display applications metallic substrates have dominated when higher chemical resistance, higher temperature tolerance and affective heat dissipation are required.

Stainless steel is an excellent flexible substrate for fabricating circuits that need high temperature processing. Afentakis et al. [23] experimented with titanium, molybdenum, stainless steel type-304 and Kovar. Prior to fabrication, polishing was necessary as a surface preparation. Afentakis found that the best results were observed with stainless steel type-304 and Kovar. One potential issue found from this research is the possible diffusion of metal species from the steel during the thermal processing. Their research has deduced that the Kovar having high cobalt content diffuses and causes undesirable electrical properties in the layers deposited on the metallic substrate.

Recently, researchers have found that high-quality semiconductor thin films can be grown on metal substrates with large grains by using nitride buffer layers. The use of the semiconductor films grown the metallic substrates has advantages over conventional semiconductor device fabrication processes when they are used for large-area and low-cost applications [24].

Metallic substrates have a higher compatibility with standard CMOS processing due to their higher resistance to chemicals, higher thermal stability, better thermal dissipation and better long term substrate stability in reference to moisture absorption. They also have the potential of EMI shielding and common signal supply through conductive substrates compared to plastics [25].

2.2.2 Solution Processable Materials

Depending on the printing methods, specific ink solutions need to be formulated or purchased including conducting ink, semi-conducting ink and insulating ink. Inks for flexible electronics are a very broad class of materials. Printable solutions need to have their fluidic characteristics (viscosity, surface tension, shear behavior) tailored for the specific printing method.

A short list of commercially available inks is given in Table 2.1. Two main groups of solution processable metals are nanoparticles and orgo-metallic compounds. Many research groups are currently working on preparing stable solutions of nanoparticles. The details of the preparation of printable fluidic solutions will not be discussed in this section. Alternatively, the physical and chemical properties of printable inks and their applications will be summarized.

Table 2.1 Commercially Available Metals

Name	Producer	Printing Method	Ink Type
NanoGold/NanoSilver	Nanomas	Ink jet	Nano particle
Functionalized nanoparticles solution	Sigma Aldrich	Ink-jet	Nano particle
Baytron P Jet N	Baytron	Ink-jet	PEDT/PSS
Baytron S V3	Baytron	Screen and stencil	PEDT/PSS
C10903D14	Gwent Electronic Materials (UK)	Screen and stencil	Carbon paste
Orgacon® EL-P3000	AGFA	Screen and stencil	PEDT/PSS

2.2.2.1 Printable Metals. Two main groups of solution processable metals are nanoparticles and orgo-metallic compounds [26]. Many research groups are currently working on preparing stable solutions of nanoparticles with an eye toward device contacts. Two of the most common physical methods of synthesizing metal nanoparticles are laser ablation and solvated metal atom dispersion. Metal nanoparticles can also be synthesized chemically by reducing the salt forms of the metal with alcohols or other solvents. The details of the synthesis will not be discussed here. Instead, some applications of nanoparticles and other printable metals will be summarized.

In the past 25 years the synthesis of nanoparticles has become a major area of research. The dimensions of these particles, in the range of 1-20 nm, have resulted in different physical properties from those observed in their bulk materials. As particle sizes become smaller the surface properties start to influence the properties of the material. The electronic and chemical properties of these materials can be tuned by controlling their particle size.

Most precious metals have been utilized to form nanoparticles, chemical reduction techniques are the most common methods of synthesis. Zhao et al. [27] fabricated field-effect transistors using gold nanoparticle ink for source-drain electrodes and obtained higher output currents in their devices compared to devices fabricated using conducting polymers. They obtained channel lengths from 4 μm down to 60 nm by controlling the surface tension and drying time of the ink. A fluid dynamical model is given to explain the mechanism by which the channel forms in the self-aligned printing technique.

Green [28] has used techniques normally utilized in the production of semiconductor quantum dots and has applied these techniques in the synthesis of metal nanoparticles. By controlling parameters such as reaction temperature and chemistry, Green synthesized precise nanostructures that exhibited magnetic, optical and catalytic properties.

An inexpensive silver ink-jettable ink can be formulated as Liu et al. [29] demonstrated. Silver nitrate is mixed with water and dimethyl sulfoxide (DMSO) and then passed through a filtered syringe, to achieve the correct particle size. The viscosity of the ink can be adjusted by adjusting the ratio of water to DMSO. This ink was deposited on Kapton 500 FPC, the deposition temperature was set to 120 C to dry the ink quickly. The films were cured on a hot plate at 300 C for 20 minutes at ambient conditions. After curing, the films were still highly flexible. These films were also free from periodic wrinkles which have been observed with Ag nanoparticles depositions. Silver nitrate melts at 212 C creating smooth traces. The resistivity of the Ag film was 1.5 x 10-5 Ω*cm.

Intrinsically conductive polymers (ICPs), are a special class of polymers that have a range of conductivity up to 10^2 - 10^3 S/cm. Polypyrrole, polyaniline and polythiophene plus its derivatives have been actively studied since the early 1980s for their conductivity properties. The conductivity of these polymers is due to the delocalization of the π-bonded electrons in the conjugated double bonds. The degree of delocalization can be limited by the charge interaction and the conformation, sis or trans.

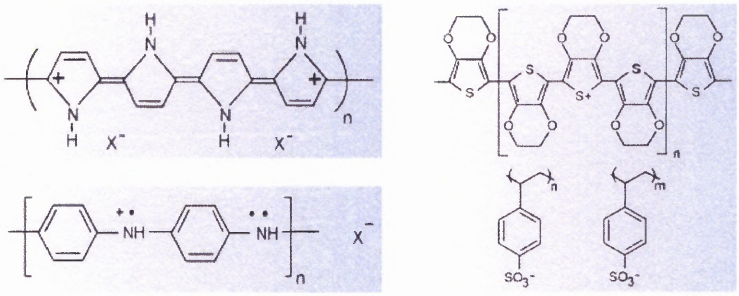

Figure 2.1 Polypyrrole, polyaniline and polythiophene [30].

Conducting polymers can be purchased from companies like H.C. Starck or they can be formulated. Morrin et al. [31] describe the formulation of polyaniline (PANI) nanoparticles films. PANI is a highly desirable conductive polymer due to the ease in which its properties can be adjusted. Morrin obtained high quality uniform films; conductivity was measured to be 0.2 to 04 mS*cm-1.

The most commonly used conducting polymers are formulated from 3,4-ethylenedioxythiophene and an EDT monomer, the conductive polymer poly-3,4-ethylenedioxythiophene-polystyrenesulfonate, (PEDOT/PSS). This polymer, PEDOT/PSS, exhibits good chemical stability in air and its fluidic properties can be adjusted for different printing methods. Intrinsically conductive polymers have found applications as in sensors [32, 33], solar cells [34, 35], electrochromic [36] and organic or polymer LEDs [37, 38]. Films exhibit conductivities in the range of 10^{-5} to 500 S/cm.

Solution processable metals used in current technology have been briefly summarized. The following section will concentrate on solution processable active materials for use in flexible electronics.

2.2.2.2 Printable Active Materials. Full-integration of printable devices on a single substrate requires the ability to print the active materials. These active materials can include ferroelectric ceramics, piezoelectric semiconductors, electro-active polymers, electrochromic polymers and electroluminescent polymers to name a few.

Lead zirconate titanate (PZT) is one of the most utilized ferroelectric ceramics due to its piezoelectric and pyroelectric properties. Devices fabricated with this material as its active layer include accelerometers, thermal sensors and ultrasonic motors. In 1999 Windle et al. [39] produced a dilute aqueous suspension of PZT and ink-jet printed complex two-dimensional shapes to be used for the rapid manufacture of devices. Tay et al. [40] prepared a ceramic ink and optimized the printing parameters. Phenomena occurring during the printing process were investigated such as the appearance of ridges, splattering, and non-vertical walls.

AlN and ZnO are common piezoelectric ceramics used in sensor applications. Both are wurtzite structured materials with a piezoelectric response along the [41] plane. Both are commonly sputtered [42] but ZnO has been deposited by a chemical bath deposition method [43]. ZnO films deposited at room temperature exhibit high resistivity. AlN on the other hand can be grown between 100 and 900 C without exhibiting conductivity issues.

Trindade et al. [44] have reviewed the synthesis of compound semiconductor nanoparticle materials and their potential use in areas such as catalysis and electronic device fabrication. Murray et al. [45] have demonstrated a simple method to synthesize CdE (E = S, Se, Te) semiconductor nanocrystallites. These crystallites are prepared in a single reaction, generating crystallites 12 A° to 115 A° in diameter with consistent crystal

properties. The controlled growth of nanocrystallites resulted in high sample quality in terms of the size of the crystallites samples with narrow size distributions. Which then resulted in sharp absorption features and strong "band-edge" emission this emission which was tunable with particle size and choice of material.

Electrochromic and electroluminescent devices utilize conjugate polymers to produce flexible displays, light emitting diodes, field effect transistors, solar cells and chemical sensors. Small et al. [46] discuss the synthesis, inkjet printing and characterization of a water dispersable polyaniline composite material with high carbon content. Printed films displayed electrochromic behavior allowing switching between yellow, green and blue. Sandee et al. [47] detail the synthesis of a solution-processible phosphorescent iridium complex. The solutions are readily spin-coated with the photoluminescence emission tunable from green to red.

Solution processable active materials used in current technology have been summarized. The following section will concentrate on possible deposition methods for the solutions processable materials discussed for use in functional flexible devices.

2.3 Deposition Methods

For this study a cleanroom facility was unavailable. Therefore, vacuum technology and standard semiconductor technology will not be reviewed here. Also, the intent of this study is to find alternative inexpensive rapid methods of fabricating thin films with an eye toward piezoelectric and pyroelectric sensors. So for brevity, only the methods that fall in this category will be reviewed.

2.3.1 Aqueous Solution Techniques

Many low temperature solution-based techniques for depositing ceramics have been developed as alternatives to vacuum deposition. Techniques like liquid flow deposition [48], photochemical deposition [49], chemical bath [50], and chemical surface deposition [51] all use aqueous solutions at temperatures below 100 C to deposit thin films.

Two solution based deposition techniques to be described encompass the following steps:

1. Equilibrium between the complexing agent and water.
2. Formation/dissociation of the ionic metal-ligand complex $[M(L)_i]^{n-ik}$, where L^{k-} denotes one or more ligands.
3. Hydrolysis of the chalcogenide source.
4. Formation of the solid.

The adjustment of the last three steps has the most control over the growth of the film. Step 3 is critical as it provides non-metal species to pull the metal cations out of solution to form the solid film. The kinetics of this step is highly sensitive to the solution's pH and temperature.

2.3.1.1 Chemical Bath Deposition. Chemical bath deposition (CBD) involves immersion of the substrate into a pre-heated liquid containing metal salts, a source of chalcogenides, and a complexing agent. Heat from the substrate causes a heterogeneous reaction between Group IIB and VIA ionic species in the solution. The process flow diagram is shown in Figure 2.2.

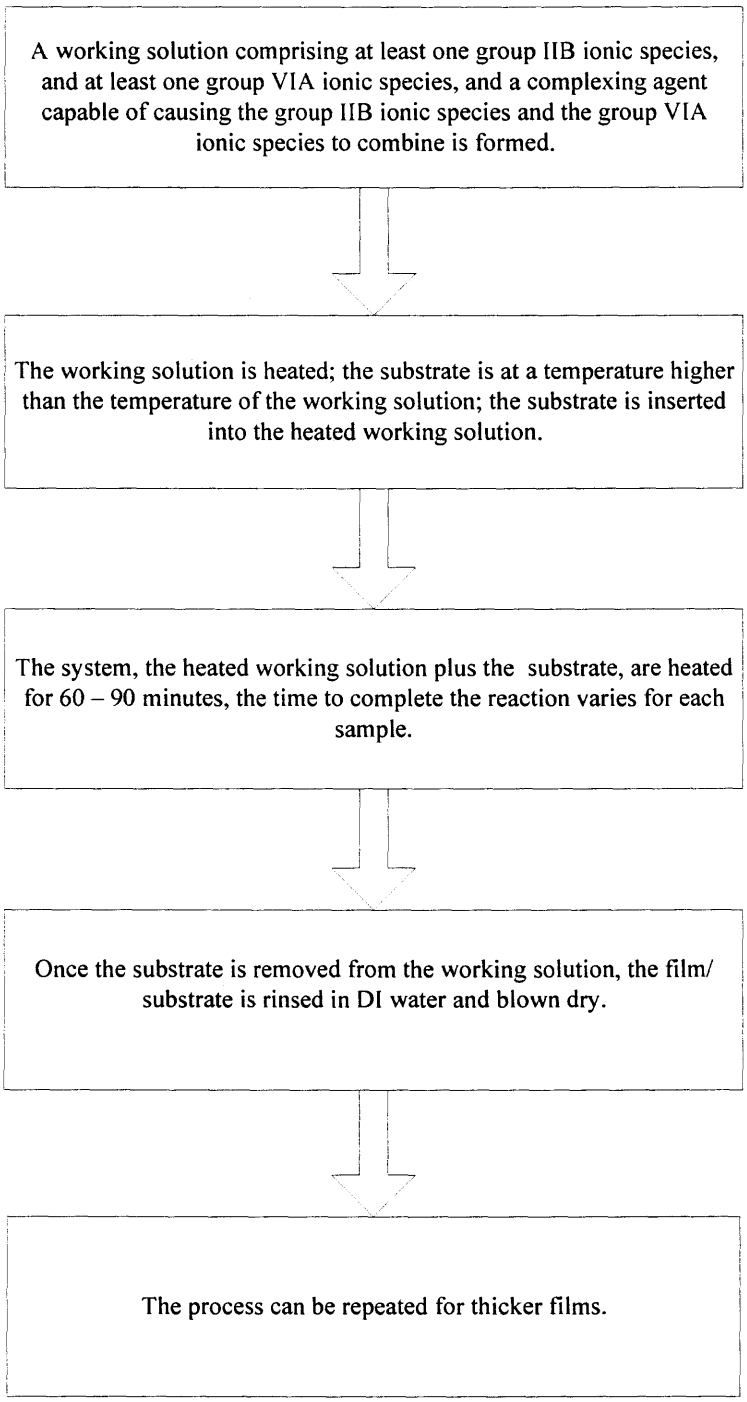

Figure 2.2 Chemical bath deposition process flow chart [52].

2.3.1.2 Chemical Surface Deposition. Chemical surface deposition (CSD) involves dispensing an aqueous solution containing Group IIB and Group VIA ionic species onto a preheated substrate. Heat from the substrate causes a heterogeneous reaction between the

Group IIB and VIA ionic species of the solution. The process flow diagram is shown in Figure 2.3.

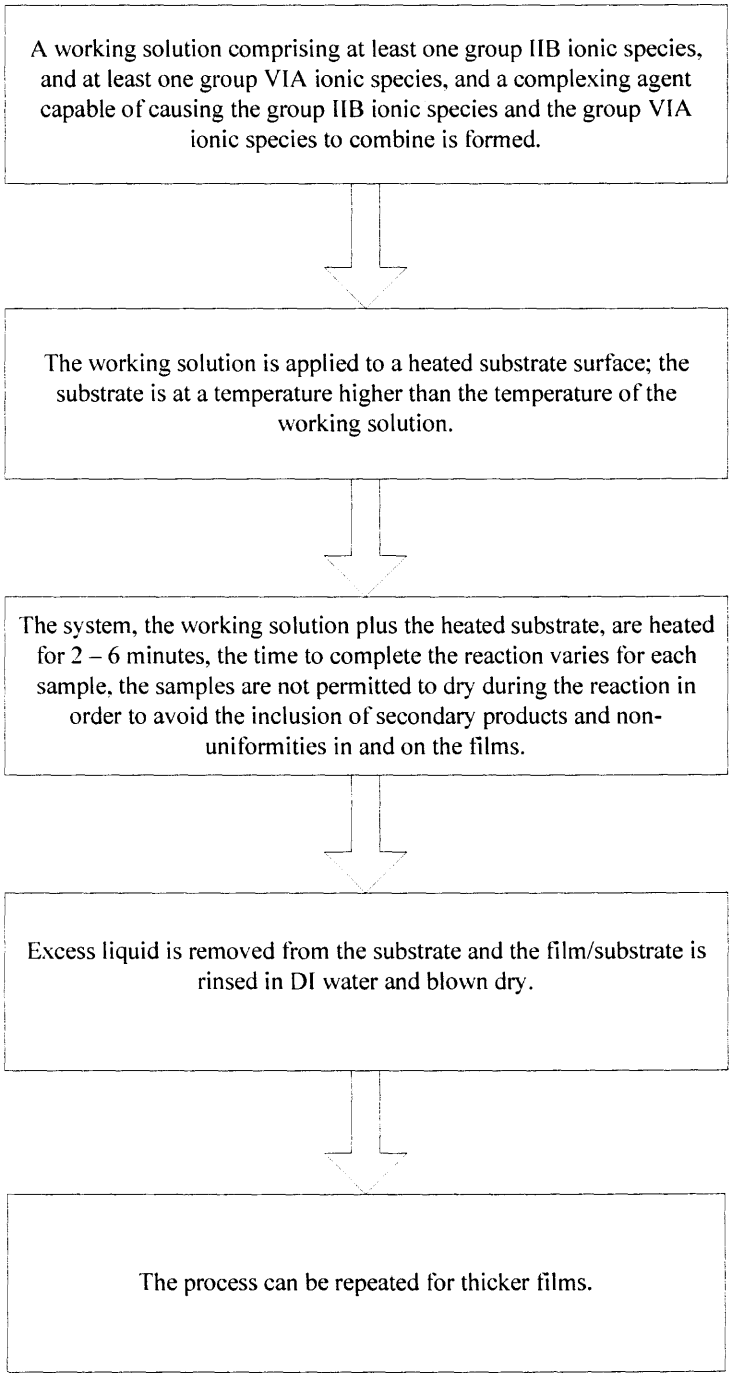

Figure 2.3 Chemical surface deposition process flow chart [52].

The chemistry involved with CSD parallels that of CBD. The difference in these methods is in how the solution and substrate interact. With CBD the substrate is immersed into a pre-heated solution, while in CSD the substrate is pre-heated and the solution which is maintained at room temperature is dispensed onto the pre-heated substrate. The advantage of CSD is that there is no particulate formation by homogeneous reactions in the bath which forms on the beaker in the CBD method. Also it has been reported that there is an increased utilization of Group IIB species and denser adherent films have been obtained.

2.3.2 Ink Jet Printing

Ink-jet printers were standard equipment in most offices and homes for printing all sorts of text, graphics onto paper and transparencies prior to the drop in cost of the laser printer. The ink-jet printer has turned into a versatile tool for many industrial manufacturing processes due to the development of solution processable materials.

The objective of ink-jet printers is to print images by creating tiny droplets of ink and precisely dropping them onto a substrate. The two main methods of forming the drops are continuous or drop on demand mode. Continuous mode is generally used in graphics and labeling industries. A schematic of a continuous mode print system detailing the drop formation is depicted in Figure 2.4. Pressurized fluid is pumped through a tiny nozzle; the typical diameter of the nozzle is 50 to 80 um. Drops are formed and charged by passing the pressurized fluid thorough an electrostatic field. The charged drops are then passed through a deflection plate to direct the drop to the substrate. This type of system is continuously producing droplets and the placement is

varied by the charge applied. Commercially available systems can produce droplets as small as 20 um with 150 um being the typical size. Typical commercial systems generate droplets in the range of 80 to 100 kHz; systems operating at 1 MHz are also available.

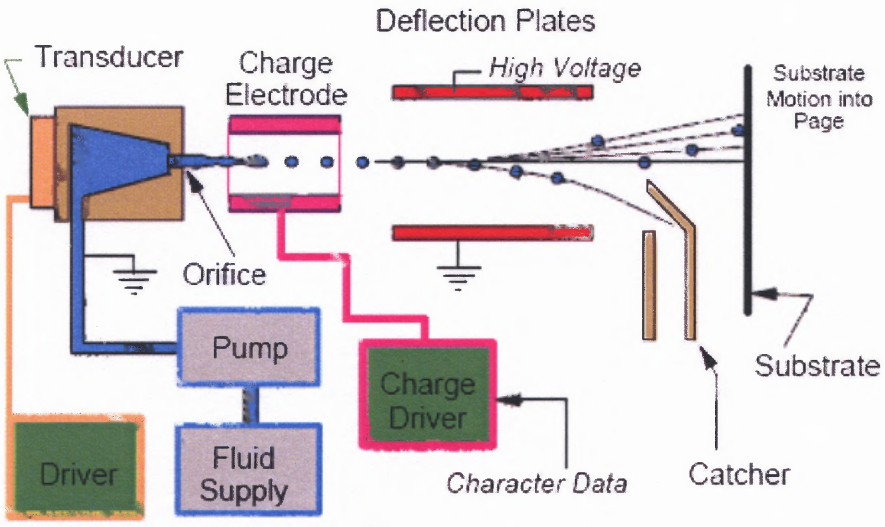

Figure 2.4 Schematic of a continuous mode ink-jet print system [53].

Drop-on-demand mode print systems, on the other hand, are utilized most often for fabrication of electronic devices, due to the capability of depositing smaller drops and the accuracy of the drops' placement.

A schematic of a drop-on-demand print system detailing the drop formation is depicted in Figure 2.5. A voltage pulse is applied to a piezoelectric material that is in contact with the fluid to be jetted. This contact induces a change in volume of the fluid causing pressure transients and forcing the fluid through the nozzle. This type of system only produces droplets when a potential is applied to the piezoelectric material. The piezoelectric transducer can be substituted with a resistor forming a thermal ink-jet print system. In this case, current passes through the resistor heating the fluid to form a bubble. This bubble forces the fluid through the nozzle.

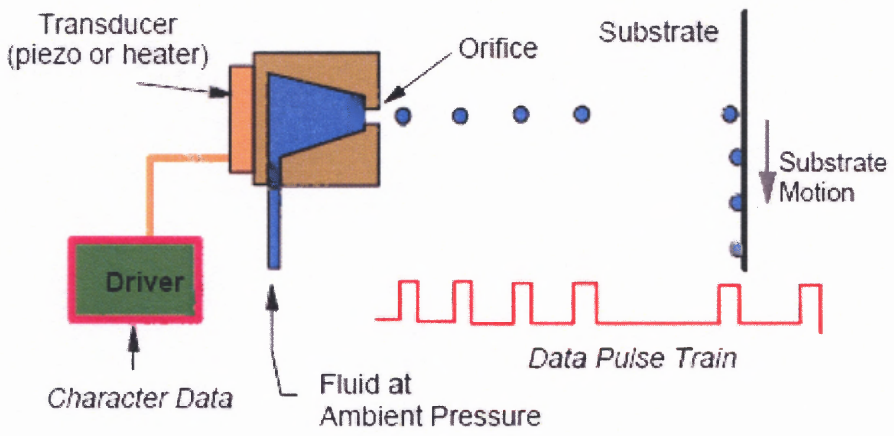

Figure 2.5 Schematic of a drop on demand mode ink-jet print system [53].

2.3.3 Screen Printing

Screen printing is a very mature technology, and has been used for industrial and graphic arts applications for most of the 20th century. This printing method is used to produce posters, labeling consumer goods and printed circuit boards. This method is attractive due to the availability of the equipment, minimal chemical waste, little required capital investment, and compatibility with most materials and substrates. Also, the simplicity of this process enables one to fabricate films rapidly.

Prior to printing, screens are fabricated with the desired image to be printed. The images are generated as stencils to be transferred to the screen. There are two common methods of transferring the stencil's image to the screen; the first is by using photo emulsion. Photo emulsion material is painted on the screen and then left to dry. The stencil is placed over the dried screen with emulsion and exposed to UV light to transfer the pattern to the screen. The photo emulsion in most cases is applied to only one side of the screen, the side that faces the substrate when printing. The thickness of the printed layer can be controlled by the thickness of this emulsion and with the correct choice of the screen mesh count. The second method is the direct block out or screen filler method.

In this method the stencil is traced onto the mesh and the resist material is painted onto the mesh.

Once the screen has been generated, the screen is placed above the substrate in a fixture so that the mesh is not directly in contact with the substrate. The ink is dispensed on top of the mesh, and then the ink is pressed through the screen with a squeegee. The ink only passes through to areas not covered by emulsion.

In recent years researchers have been working on characterizing thin films deposited by screen printing. Deitz et al. [54] have screen printed lead–zirconate–titanate (PZT) particulate and polyvinylidene-trifluoroethylene (PVDF-TrFE) copolymer on indium–tin-oxide (ITO)-coated glass substrates. They have investigated the material properties to demonstrate that screen printing is a cost-effective way of producing structured functional thin films for pyroelectric and piezoelectric applications. Hafaiedh et al. [55] deposited tin oxide by screen-printing on an alumina substrate with two gold electrodes for use in chemical vapor sensors. Tin dioxide thick films were studied with various techniques and highly reproducible films were produced with optimum characteristics for detecting gas.

To date, screen printing has been used as an alternative step in device fabrication, and not the total method to fabricate devices. Ito et al. [56] start by describing their process for producing screen-printing pastes used to form both the transparent and light-scattering layers of TiO2 electrodes for dye-sensitized solar cells with a conversion efficiency of global air mass 1.5 (AM 1.5, 1000 W/m2) for converting solar light to electric power of over 10%.

The main parameters in controlling the thickness of the films are the viscosity of the ink, screen mesh count, and the emulsion. The resolution of the printed image depends highly on the screen mesh and the emulsion layer. In this study, manual equipment was used. With fully automated screen printing production lines commercially available devices could, once optimized, be mass produced.

2.3.4 Stencil Printing

Stencil printing is a novel printing technique adapted from circuit board printing. This technology is similar to screen printing with the stencil replacing the screen. Stencil printing shares the benefits of simplicity and cost with screen printing but has the additional benefits of reduction of clean up time and ease in generating stencils.

Stencil printing is a well established technology, and has been used extensively for deposition of adhesives [57, 58] and solder pastes [59, 60]. Ufer et al. [61] used stencil printing to pattern the ion-selective membranes in sensor arrays where high viscosity pastes containing various membrane polymers, plasticizers, and ionophores were used due to their electrochemical performance. Due to the size and spacing of the sensors within the array, traditional casting methods were not able to be used to deposit the membranes. To date, in all fabricated devices, stencil printing has been used as an alternative step in device fabrication, mainly for deposition of solder paste and not the total method of fabrication.

Typical stencils are fabricated from metal foils with openings where the inks are free to be printed on the substrate. Fine lines and high height-to-width aspect ratios are achievable due to the availability of different thicknesses of metal foils. Fine line stencils can be fabricated by laser cutting or chemical means. Since the ink is not obstructed due

to a mesh like screen printing there are no issues with shading nor any issues with deformation of the mesh. Also, down time is reduced due to the ease of cleaning, longer life span and less wear of the stencil [62]. In this study, plastic stencils were used and the inks were rolled through the stencil.

2.4 Applications

In the last several decades, there has been tremendous growth in the number of functional flexible devices in the areas of displays, RFID, solar cells, sensors and wearable electronics. The experimentation with the materials and processes above has spurred some of this growth. The intent of this study is to print thin film piezoelectric flexible sensors

In 1880 the brothers Curie discovered the direct piezoelectric effect. The Curie brothers found that when pressure was applied to certain materials, they generate a potential. Piezoelectricity is a coupling between a material's mechanical and electrical behaviors. In the simplest of terms, when a piezoelectric material is squeezed, an electric charge builds up on its surface. On the other hand, when a piezoelectric material has a voltage applied across it, the material deforms mechanically.

There are two necessary conditions for a material to be considered piezoelectric [63]. The first is the lack of a crystal center of symmetry. If a crystal is symmetrical with respect to a point, a line, or a plane the body is centrosymmetrical; it can possess no polar properties and exhibits no piezoelectric effect. The second condition is that the material's bonds need to be either ionic or partially ionic.

All material crystal structures belong to one of thirty two point groups. Eleven of these thirty two point groups are centerosymmetric and non-polar [64]. The other twenty-one point groups do not exhibit a center of symmetry and are termed non-centrosymmetric. Twenty of the twenty one point groups display piezoelectric activity. Ten of the twenty point groups have a permanent dipole in which the positive charge is not aligned with the center of the negative charge resulting in one or more polar axes in these crystalline materials. The polarization of these ten crystals is temperature dependent, and termed ferroelectric. Crystals that exhibit polarization without the application of an applied field are known as pyroelectric [63]. The spontaneous polarization can be reoriented by an applied field and the materials can be termed ferroelectric. All ferroelectric crystals are pyroelectric and pyroelectric crystals are piezoelectric, but piezoelectric crystals are not necessarily pyroelectric. Ferroelectricity tends to dissipate above the Curie temperature of the material. The material is in a paraelectric state above the Curie temperature and obeys the Curie-Weiss Law.

Ferroelectric materials exhibit hysteresis, a typical hysteresis loop for polyvinylidene fluoride (PVDF) is seen in Figure 2.6. The remnant polarization, the polarization present after the applied field has been removed, governs the piezoelectric and pyroelectric activity. Tajitsu et al. [65] have shown that the remnant polarization as a function of the crystallinity increases as the content of the VDF increases.

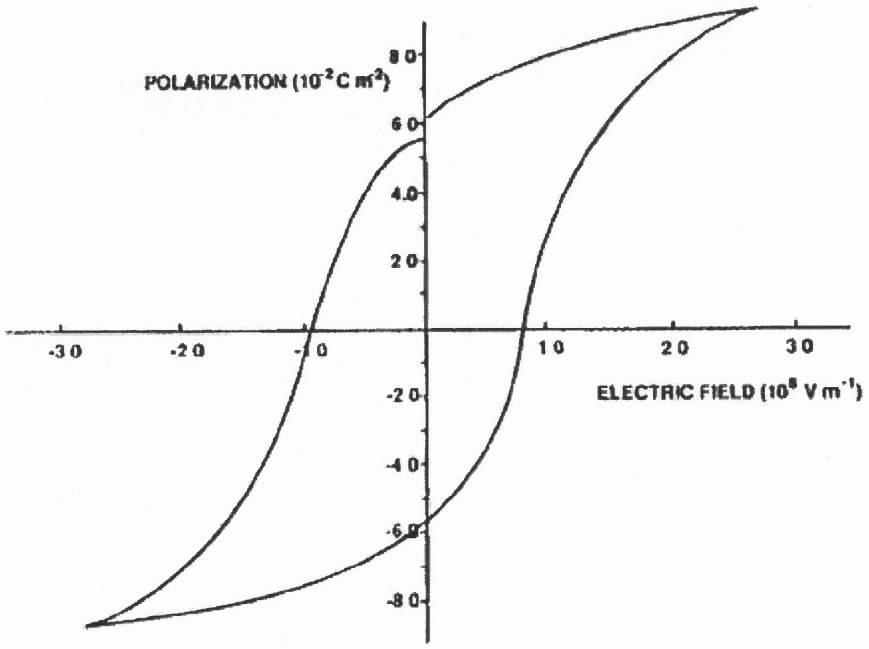

Figure 2.6 Hysteresis loop for PVF2 film 25um thick, swept with a symmetric triangular wave with a peak height of 280 MV m-1 [66].

It is observed in piezoelectric materials that mechanical stresses result in the accumulation of electric surface charge on the material. The direct piezoelectric effect, where a crystalline material with no center of symmetry, develops an electric charge proportional to a mechanical stress, was discovered by the brothers Curie in 1880 [63]. Piezoelectric materials are generally classified into two categories, ferroelectric and non-ferroelectric (sometimes called pure piezoelectric). The distinction is whether or not an applied electric field can reorient the spontaneous electric dipoles in the material without breaking bonds [64]. In ferroelectric materials such as PZT and BaTiO3, a process called poling is where the dipoles are aligned by electric fields, orient the dipoles and polarize the materials. The common method of poling consists of applying a high DC voltage (>2kV/mm) across a heated material. The material is heated above its Curie temperature.

If this temperature is exceeded the material loses its ferroelectric properties [67]. This is also the maximum temperature limit of the material.

In non-ferroelectric materials like AlN and ZnO the polarization direction is fixed by the crystal structure and an application of an electric field would result in breaking bonds. For good piezoelectric response in non-ferroelectric materials, like AlN and ZnO, c-oriented films with large grain size and narrow X-ray diffraction curves, are necessary [68-71]. Table 2.2 summarizes some of the common piezoelectric materials' properties.

Table 2.2 Reported piezoelectric properties for AlN, $BaTiO_3$, PVDF, PZT and ZnO [1, 71-82]

Material	ρ (kg/m^3)	ε_r	c_E (GPa)	d_{33} (pC/N)
AlN	3230	9 -11	395	3.4 - 5.1
$BaTiO_3$	5300 - 5700	1700	75	85
PVDF	1780 - 1850	8 - 13	2	-33 - 20
P(VDF-TrFE)	1820	7 - 8	2	-38
PZT	7500 - 7700	900 - 1300	98	90 - 223
ZnO	5680	8 - 12	208	7.5 - 12.4

Devices fabricated with ZnO include optical, accelerometers, solar cells and sensors [83-90] to name a few. For maximum piezoelectric response the films must be grown highly c-oriented [69]; this has been achieved with chemical bath deposition. AlN has a lower piezoelectric constant then ZnO but has lower dielectric loss and higher acoustic velocity. Both are compatible with standard cleanroom fabrication techniques and can be fabricated by low temperature means, such as chemical bath deposition. Compared with the other materials, lead zirconate titanate (PZT) exhibits a much higher response then the other materials listed in the table. PZT is commonly found in MEMS application such as actuators and sensors [91-94].

In 1969 Kawai discovered the piezoelectric polymer polyvinylidene fluoride (PVDF) or (PVF2). Two years later Bergman concurrently with Nakamura and Wanda discovered the pyroelectric effect in PVDF. Since the discovery of these effects many other ferroelectric polymers have been discovered including the copolymers of PVDF with trifluoroethylene (P(VDF-TrFE)) [95, 96] and with tetrafluroethylene (P(VDF-TFE)) [97] (CH2=CF2) and several nylons. The copolymers have the largest piezo and pyro effects out of the polymers but still the magnitude of these effects is much lower than the effects with those of ferroelectric ceramics.

PVDF is a semi-crystalline polymer with its crystal structure shown in Figure 2.7 and chemical structure shown in Figure 2.8. Due to their high energy density, excellent low power requirements, low mass, high flexibility and relatively low cost, PVDF and its copolymers have found applications as actuators and sensors. Polyvinylidene fluoride trifluoroethylene P(VDF-TrFe) is becoming the most widely used of the copolymers and has the highest response [98]. Due to the size of the additional fluorine atom in the copolymer P(VDF-TrFE), this copolymer crystallizes in the polar β phase [2.62]. Stretching of the copolymer is not necessary as is with PVDF. These materials are commercially available in pellet and powder form. These piezoelectric polymers can be deposited by screen printing, ink-jet printing and solution or spin casting.

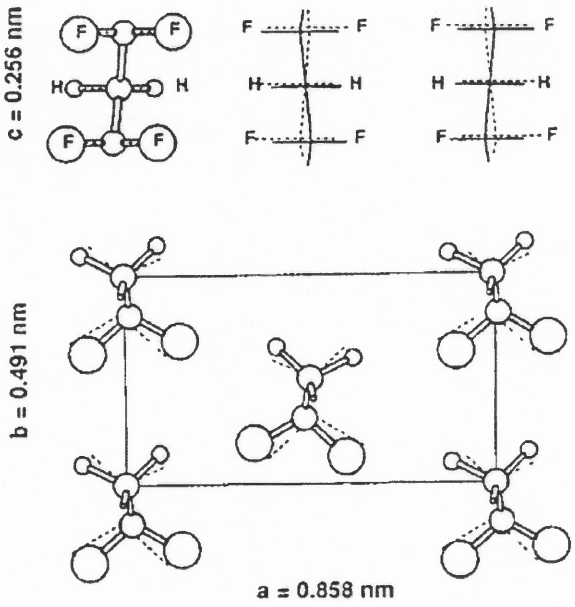

Figure 2.7 Crystal structure of the polar β phase of PVF2 [66].

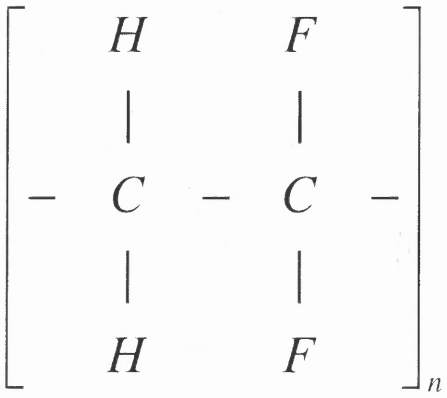

Figure 2.8 PVDF chemical structure.

A mean-field theory was used to predict the phase transitions for the phase diagram for PVDF given in Figure 2.9 [99]. The solid lines in the diagram delineate the regions of phase stability. The broken lines indicate the regions of metastability. An increase in the applied melting point of the α phase is lowered while the β phase melt temperature is increased. By increasing the stress of the α phase, every second chain has a rotation of 180 about its axis which forms the δ phase.

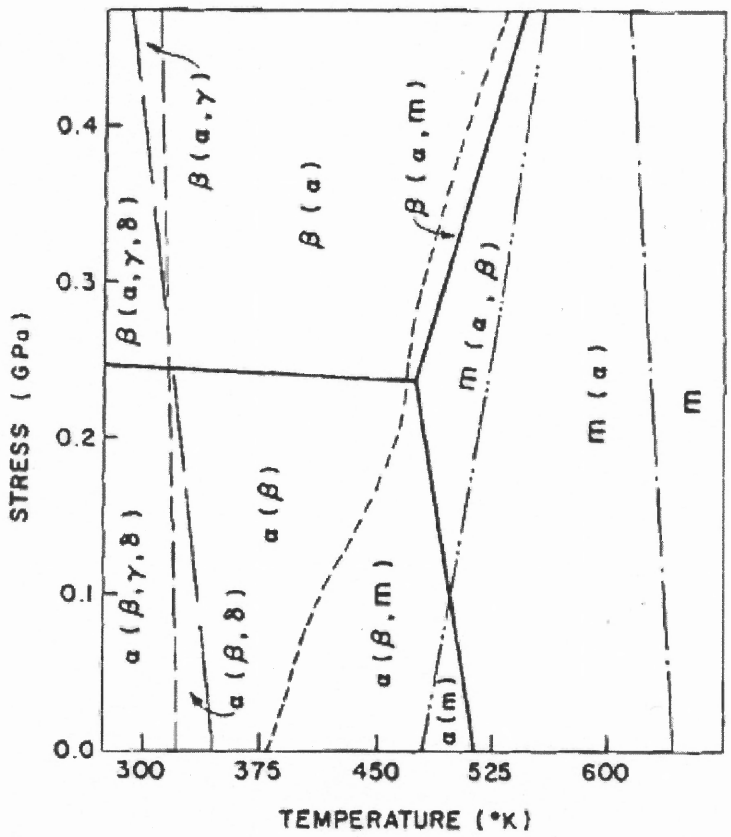

Figure 2.9 Uniaxial stress-temperature phase diagram for PVDF predicted by theory [99].

Piezoelectric sensors are designed on the piezoelectric effect which is the ability of the material to generate voltage in response to applied mechanical stress. Piezoelectric materials generate an electrical charge proportional to stress. This can be measured directly as a high- impedance signal (charge mode), or converted into a low-impedance voltage output by internal electronics. Integrated electronics are used only to condition the output signal allowing for the use of relatively simple electronic circuitry. Piezoelectric sensors cannot be used to measure frequencies below 0.1Hz such as steady-state tilt or static pressure.

The piezoelectric effect relates the electric field to the strain (the converse effect) and the charge density to the stress (the direct effect). The weighting factor for the direct

effect is the piezoelectric coefficient. Because the materials are anisotropic the coefficients are determined for the three poling directions of the material. Based on symmetry arguments the piezoelectric coefficient matrix for poled P(VDF-TrFE) can be written as,

$$d_{ij} = \begin{pmatrix} 0 & 0 & 0 & 0 & d_{15} & 0 \\ 0 & 0 & 0 & d_{15} & 0 & 0 \\ d_{31} & d_{31} & d_{33} & 0 & 0 & 0 \end{pmatrix} \tag{2.1}$$

Five of the coefficients are non-zero. Three of these coefficients are unique implying that there are three modes of operation [82]. The 3- direction is along the poling direction and the 1-direction is along the stretching direction, typically as seen in Figure 2.1. Typical values for the piezoelectric coefficient are: $d_{31} = pC/N$, $d_{32} = pC/N$ and $d_{33} = pC/N$. The negative values indicate that the material contracts in that direction. In order to generate a positive strain, the electric field would need to be applied to oppose the polarization field.

PVDF and their copolymers are the most widely investigated ferroelectric polymers due to their relatively high electromechanical properties. These polymers have been deposited by a variety of techniques, including micropaterning, ink-jet printing, electrospray deposition [100], and vacuum evaporation [101]. Ink, screen and stencil printing have been chosen as the deposition methods for this study due to the ease in which good quality films can be deposited. Other advantages include the low equipment cost and the ability to cover large areas.

One type of device that has capitalized on the piezoelectric effect is accelerometers. Designs are based on three different concepts- compression, shearing and bending. A piezoelectric material is formed on either a cantilever or a diaphragm, as a force is applied to the sensor a change in resistance will be observed.

Devices have been fabricated to exploit the pyroelectric characteristics of the films and include: infrared and ultraviolet fire sensor [102], microwave field-detecting elements [103], hydrogen sensor [104] and visible/infrared integrated double detector [105] to name a few.

Figure 2.10 diagrams the internal alignment of the domains in ferroelectric materials. Domains are regions of homogenous polarization in the crystalline material. As seen in Figure 2.10(a), initially the material is randomly aligned, (b) a potential is applied for an extended period and (c) materials with regions in which the domains are aligned is obtained.

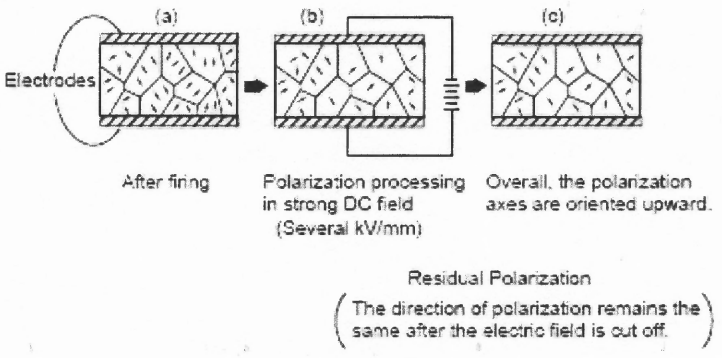

Figure 2.10 Polarization processing of piezoelectric material [106].

Mechanical drawing is necessary for PVDF to be transformed into its piezoelectric β phase. When PVDF is deposited, the CF2 dipoles are randomly oriented. Typically an electric field and elevated temperature are used to rotate the dipoles in the

direction of the applied field. It has been reported that the minimum poling field for PVDF films is 0.5 MV/cm [107]. It has also been reported that the poling is not time dependent, but the piezoelectric activity is highly dependent on the poling field [108]. The poling of piezoelectric polymers consists of applying an electric field, in some cases, at an elevated temperature for a period of time. Applying an electric field to a ferroelectric material induces alignment of dipoles. The applied field must be greater then the coercive field in order to align the dipoles. PVDF needs to be drawn prior to poling to convert its crystalline phase from non-polar α phase to ferroelectric β phase. The copolymer P(VDF-TrFE) crystallizes directly in the beta form due to the addition of fluorine atoms [67].

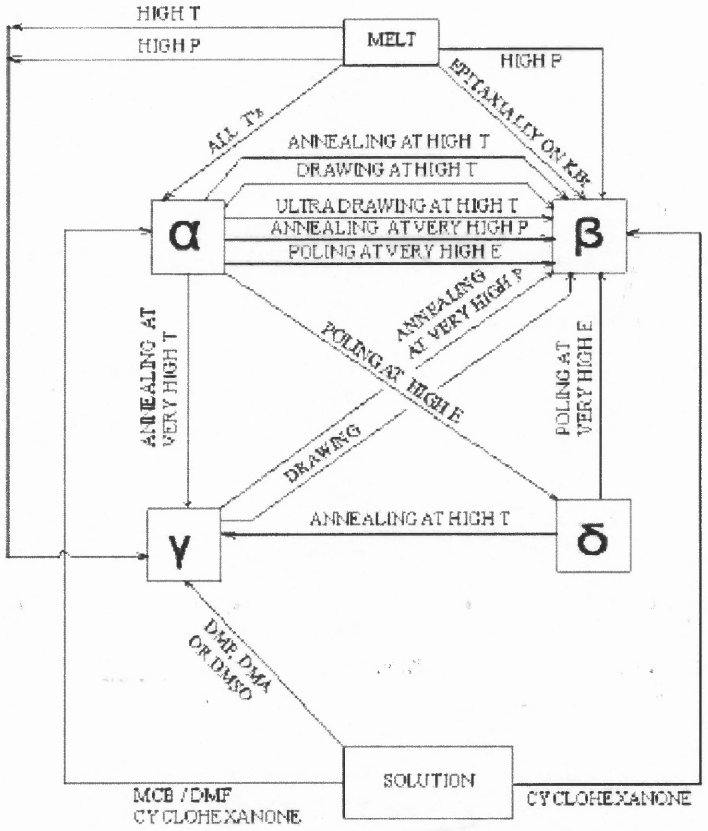

Figure 2.11 Interrelationship between the four established phases of PVF2, and the common solvents [109].

PVDF films are commonly poled utilizing the corona poling method. Tyler et al. [110] were the first to demonstrated corona poling on cellulose acetate films, and this technique has since been adapted for room temperature poling of PVDF thin films. Corona poling has also been used on polymer/ceramic composites [111]. There are two major advantages of corona poling, the first is the possibility of poling materials in which only one side of the film has a contact deposited. The second advantage is the possibility to pole large areas by moving the film through the poling set-up. Variations on corona poling consist of poling through a mask in which electrodes are patterned on the polymer to be poled. A related poling method is electron beam poling, in which an electron beam irradiates the piezoelectric polymer. This method allows for the control of the properties of the poled polymer by varying the electron beam [112].

Step-wise poling of the copolymer P(VDF-TrFE) has been demonstrated as a successful method of room temperature poling with a low breakdown rate. These films exhibit high pyroelectric coefficients [113].

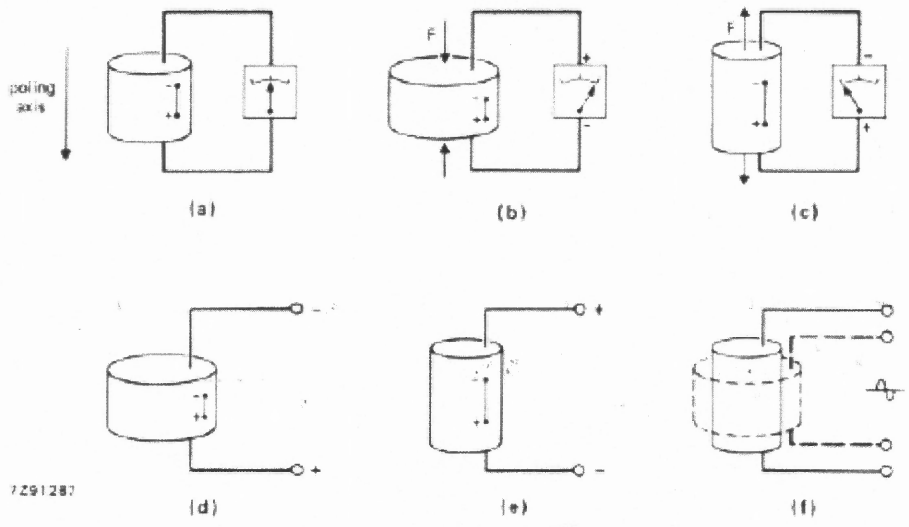

Figure 2.12 Actuation modes for piezoelectric materials [66].

These flexible devices are no longer the creation of academic researchers. There is a commercial demand for these devices due to the personal portable devices such as ipods and cell phones. The demand for wearable electronics is increasing every year, as seen in Table 2.3. The ipod consumer is looking for controls and headphones built in their clothes and the same is true of the cell phone user.

Table 2.3 Commercially Flexible Electronics Products

Application	Company Name	Address
Flexible active-matrix display modules	Plastic Logic	http://www.plasticlogic.com
P-OLED display technology	Add-Vision, Inc.	http://www.add-vision.com/
Electronic Paper Displays	E*INK	http://www.eink.com
Flexible Rollable Solar Cells	flexsolarcells	http://www.flexsolarcells.com
Power Plastic® - Ink jet printed photovoltaic products - used for charging portable devices with indoor or outdoor light	Konarka	http://www.konarkatech.com
Elektex® - smart fabric interfaces, to integrate five-button iPod controls	Koyono/Eleksen	http://www.koyono.com/
Paper electronics	Printed Systems	http://www.printed-systems.de/index.php?id=37&L=1
Printed semiconductor-based sensors	NANOIDENT	http://www.nanoident.com/
Audex Jacket Series - Bluetooth-enabled Speakers and a microphone are integrated in the hood	Motorola and Burton Snowboards	http://store.burton.com

Table 2.4 University Research in Printed Electronics

Application	Group	Address
Investigation of the electronic properties of organic materials and advance their applications in electronics and bioelectronics	The Malliaras Laboratory for Organic Electronics	http://people.ccmr.cornell.edu/~george/
Research in both semiconductor and organic optoelectronics High resolution active-matrix polymer light-emitting displays on flexible stainless steel	Center for Optical Technologies	http://www.lehigh.edu/optics/
The group spans a wide range of research interests with a focus on the processing-structure-mechanical properties relation in ceramics, glasses and biomaterials.	Advanced Processing Techniques and Mechanical Properties	http://www.materials.manchester.ac.uk/research/groups/ceramicsandglasses/advancedprocessingtechniques/
Research to improve understanding, characterization and modeling of fluid flow, fluid-nozzle and fluid-substrate interactions so that the inkjet process can be optimized.	Inkjet Research Centre	http://www.ifm.eng.cam.ac.uk/pp/inkjet/default.html

CHAPTER 3

PRINTING METHODS FOR FLEXIBLE THIN FILMS

3.1 Introduction

Low temperature deposition of metallic, electroactive, and dielectric thin films is critical for the fabrication of flexible electronics. In the prior chapter a review of present and past materials, fabrication methods and devices were discussed. The primary motivation of this study is to discuss three low temperature printing methods to deposit metallic and electroactive polymer thin films onto flexible substrates: ink-jet printing, screen printing and a modified stencil printing technique. Some basic electrical characterization of these films is performed and discussed.

With the advent of ink-jet technology, inexpensive fabrication of electronic devices has become possible. Associated with the development of ink-jet technology and techniques, the ink formulations have become crucial. Ink-jet printing is advantageous as useful substrates are virtually unlimited. This method eliminates the masking steps and vapor deposition steps in standard cleanroom fabrication. In the present study, H.C. Starck's Baytron materials, solution processable metal-organic complexes and an active polymer ink have been formulated for use with a commercially available ink-jet printer (Dimatix material printer DMP-2800 Series).

The inkjet printer has been placed in an Airfiltronix HEPA filtration enclosure fitted with two RF-1000 positive blowers. This enclosure is placed on a vibration damping table to reduce particle inclusion and errors in printing due to vibrations.

Screen printing on the other hand is a very mature technology. The equipment is readily available, the chemical waste is minimal, and minimal capital investment is required. The simplicity of this process enables one to fabricate films rapidly. In this

study manual equipment was used, although fully automated screen printing production lines are commercially available for large scale production once devices are optimized.

Stencil printing is similar to screen printing. The screen is replaced with a metal stencil. In this study a transparent polymer stencil is used instead of steel stencils. The fabrication of the polymer stencil is accomplished by printing the patterns on transparency films with a laser printer, and cutting the patterns from the film with an Exacto knife. In typical stencil printing the ink is squeegeed through the stencil. In this study the inks are applied with a roller. Stencil printing shares the benefits of simplicity and cost with screen printing and also reduces clean up time.

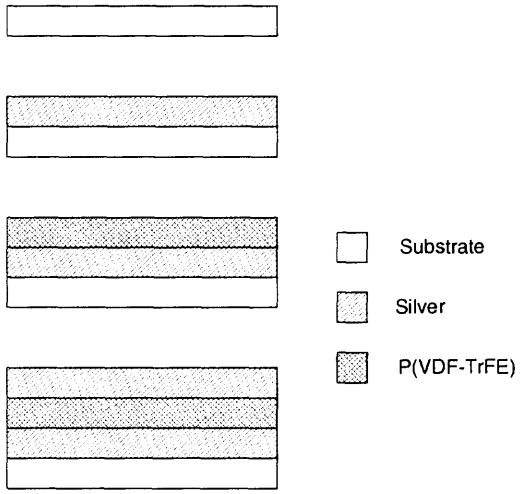

Figure 3.1 Fabrication of multiple screen printed layers.

In all three printing studies the substrates used were DuPont's Polyimide Kapton E and 3M transparency film. These films were cleaned in acetone, isopropanol, and distilled water. Multiple layers were deposited using the three different printing methods. The layer structure is depicted in Figure 3.1. H.C. Stark Baytron material and a metal-organic silver ink were deposited via ink-jet printing as the first layer depicted in Figure 3.1. The first layer deposited via screen and stencil printing was DuPont's microcircuit materials

CB028 silver conductor polymer thick film composition; this material had been designed for low temperature drying and good adhesion to polymer substrates such as Kapton [114]. The second layer was P(VDF-TrFE) which was printed directly on top of the silver, and the third layer deposited on the P(VDF-TrFE) was another layer of silver.

3.1 Ink-jet Printed Thin Films

A commercially available drop on demand ink-jet print system produced by FUJIFILM Dimatix, Inc [115] was used for this study. After considerable use it has been found that this system is capable of printing small proof of concept devices, and is by no means a production tool. Application specific software controls the system, and circuit designs can be drawn with this software or a bit map file can be imported.

The application specific software, Dimatix Drop Manager (DDM), allows the user to set the printing parameters and check the status of the printer. The standard parameters adjusted for a print job are the pattern to be printed, thickness of the substrate, cartridge settings, cartridge temperature, and substrate temperature, also referred to as the platen temperature.

The requirements of the ink to be jettable through the printhead are that the ink has a viscosity in the range of 10 - 30 cPs, a particle size smaller then 0.2 um, a surface tension range of 28 - 33 dynes/cm. The ink should have a low evaporation rate such that it will not clog the jets of the printer.

The acoustical resonances of the inks differ due to compressibility properties [116] of the various solvents that comprise the inks. Prior to printing the print parameters need to be set and the jetting waveform needs to be optimized. These waveforms activate the piezoelectric pumps in the printhead. While optimizing the jetting waveform, the jetting of the ink can be observed with the system camera that allows the user to view the

jetting nozzles. While viewing the printhead with the camera system, the voltage applied to each nozzle on the printhead can be individually addressed. By adjusting the waveform parameters, such as the pulse width and voltage, the parameters of the drop can be enhanced in velocity and size.

The print system is equipped with another camera for alignment of the circuit when multiple layers are deposited or the substrate has been removed from the print system. This camera can also be used to view the printed circuit features and to obtain pictures of the circuit after printing. Table 3.1 gives some of the more important parameters that can be varied and the range of values that these parameters can take for this printer system.

Table 3.1 Range of Dimatix Materials Printer System Parameters

Parameter	Range of Values
Drop Spacing (μm)	5 - 254
Platen Temperature (°C)	Ambient – 60
Cartridge Temperature (°C)	Ambient – 70
Number of Nozzles	1 – 16
Drop Volume (pL)	1 or 10
Substrate Size (mm)	Up to 210 x 315

3.2.1 Metal Organic (MO) Silver

Ink-jettable silver ink was formulated with a silver metal-organic complex(1,5-cyclooctadiene) (hexafluoroacetylacetonato) silver(I) , purchased from Sigma Aldrich. The solvents used for the ink were butanol and isopropyl alcohol, due to their low evaporation rates and low boiling temperatures. The formulation of the metal organic ink for inkjet printing of silver conductors follows from the work done by Sankir [117] in 2005. Sankir had dispensed metal organic silver into butanol, due to the low viscosity and increased adhesion of the silver to the substrate. Sankir's study had also found that

toluene due to its high evaporation rate clogged the print head. The properties of the solvents used for the inks in this study are given in Table 3.2 and the appropriate fluid properties of the Dimatix printer are given in Table 3.3.

Table 3.2 Solvent properties and Required Fluid Properties for the Dimatix Materials Printer DMP-2800 Series

	Acetone	Butanol	Dimethylformamide (DMF)	2-PROPANOL (isopropanol)	Methyl Ethyl Ketone (MEK)
Viscosity (cP @ 20 C)	0.32	3 (@ 25 C)	0.92	2.85 (@ 15 C)	0.43
Boiling Temperature (C)	56.5	118	153	82	80
Evaporation Rate (BuAc=1)	7.7	0.46	0.17	2.83	2.7

Table 3.3 Required Fluid Properties for the Dimatix Materials Printer DMP-2800 Series

	Dimatix Fluid Requirements
Viscosity (cP @ 20 C)	10 - 12
Surface Tension (dynes/cm)	28 - 33
Particle size (μm)	0.2 (max)

Table 3.4 Annealing Studies

	Adhesion	Conductivity
Box Oven	Poor	Poor
Vacuum Oven	Poor	Poor
Heat Lamp	Issues	Ok
Hotplate	Issues	Ok

Two silver metal organic compound inks were formed by first dissolving the silver compound in butanol, the second by dissolving the silver compound in isopropyl alcohol. Initial studies were conducted with the silver butanol ink to optimize the jetting of the ink by adjusting the jetting waveform on the Dimatix material printer.

The viscosities of both of the solvents used for the inks were similar. The larger the viscosity of the ink the more damping of the acoustic wave which in turn increases the jetting potential that is required to form a drop. The difference in the density of the solvents had little effect on the jetting waveform. The minimum jetting potential for these inks was found to be 9 V, while the maximum jetting potential for this printer is 40 V. When set to the maximum jetting potential the pattern was not well defined and exhibited drag marks. The jetting potential waveform pulse width was adjusted and a pulse width of 10μm resulted in a well defined pattern. A 1 μm pulse width was too short and nothing printed, while a 100 μm pulse width gave a pattern that was very messy with very little definition.

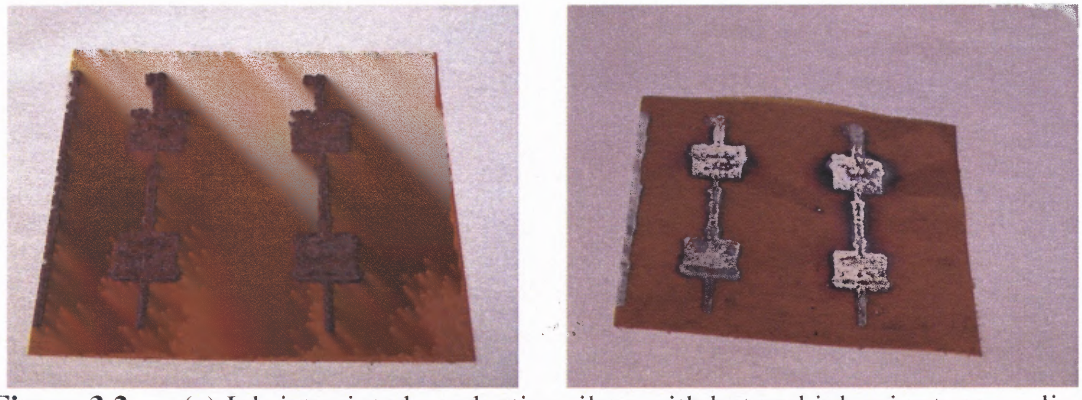

Figure 3.2 (a) Ink-jet printed conductive silver with butanol ink prior to annealing (b) ink-jet printed conductive silver ink after annealing.

The Kapton substrate was heated in a range from 30C to 60C during the printing of the silver ink. The printed contacts were not electrically conductive as deposited. Annealing was necessary for the films to become conductive as seen in Figure 3.2.

A vacuum oven, box oven, hotplate and heat lamp have been used for annealing. Annealing using a vacuum oven and a box oven had been ruled out as viable methods. Annealing in this way resulted in contacts that wipe off the surface with a q-tip and have shown little conductivity. The hotplate has yielded the most consistent results, producing conductive contacts, but also has problems with adhesion and conductivity. Table 3.4 summarizes the annealing results.

The number of layers printed, print temperature, anneal temperature and anneal time were adjusted to observe the effects on both conduction and adhesion. Print temperatures starting at 30 C increased in 5 degree steps to the maximum temperature of 60 C were examined. Layer thicknesses below fifty layers had spotty coverage and most had high resistance.

For each case in Table 3.5 the resolution was modified by changing the drop spacing. The drop spacing for this printer can be adjusted from 5 to 254 um in one micron increments; this is the center to center distance in x and y of the drops deposited. In this study it was found that drop spacing less then 25 um tends to overlap and results in puddles of ink. These puddles of ink do not have enough time to evaporate resulting in non-uniform films. Drop spacing greater then 75 um resulted in films that had discontinuities and were not conductive after the anneal process.

Conductive MO silver thin films that had good adhesion to Kapton were obtained, but were not repeatable. The next section details the ink-jet printing of the commercial ink Baytron P Jet on Kapton.

Table 3.5 Number of Layers of Ink-Jet Printed MO Silver on Kapton and Transparency Film

Number of Layers	Print Temperature (°C)	Anneal Temperature (°C)	Anneal Time (min)
5	30 - 60	100 - 250	5 – 60
10	30 - 60	100 - 250	5 – 60
25	30 - 60	100 - 250	5 – 60
50	40 - 50	100 - 250	30 – 60
75	40 - 50	100 - 250	30 – 60
100	40 - 50	100 - 250	30 – 60
150	40 - 50	200 - 250	30 – 60
200	40 - 50	100 - 250	30 – 60
225	40 - 50	100 - 250	30 – 60
250	40 - 50	100 - 250	30 – 60

3.2.2 Baytron Conductive Films

In order to obtain conductive ink-jettable thin films that adhere and depositions that are repeatable H.C. Starck materials were jetted.

Two jettable H.C. Starck Baytron products were available to this researcher for conductive contacts: Baytron P Jet and Baytron P VP AL 4083. The properties of these two Baytron materials can be seen in Table 3.6.

Table 3.6 Some Properties of Baytron Materials Used in This Study

	P Jet	P VP AL 4083
Solid content (%)	1.2 - 1.4	1.3 - 1.7
Viscosity (mPa*s)	5 - 11	5 - 12
Resistivity (Ωcm)	500 - 5000	500 - 5000

The P Jet material and the P VP AL 4083 Baytron material were jetted with no modification to the chemistry. Both materials jetted with no major issues, and all deposited similar to what was seen in Figure 3.3(a). All contacts were well defined with no over spray initially. Once the contacts were dry they did well with the scotch tape test and had little failure. The scotch tape test is a simple measure of adhesion; this test gives a quick indication of adhesion but gives no data as to the force required to pull the thin film from the substrate surface. Scotch brand tape is applied to the thin film and pulled off. If the thin film remains on the substrate the Scotch tape test has been passed.

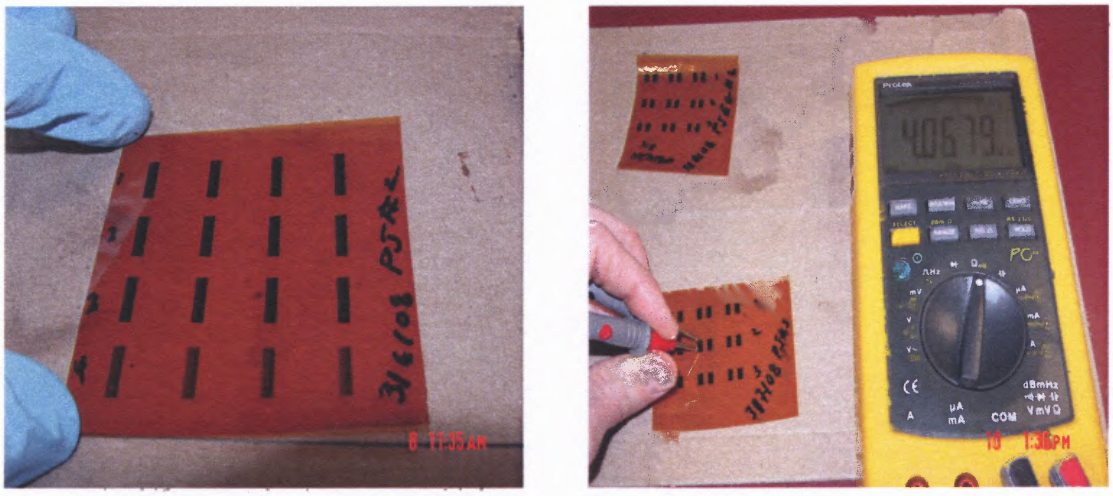

Figure 3.3 (a) Typical Baytron material bottom contacts (b) Measurement of resistance.

As seen in Figure 3.3 (b) the resistance was measured in the mega Ohms range for both Baytron products. The Baytron inks used in this study were originally developed for use as hole-injection layers in polymer or organic light emitting diodes. These inks were not developed for printing of conductive contacts. Layer thicknesses were jetted from 25 to 100 layers in 25 layer increments to see the optimum layer thickness. Resistance did

not change from 75 to 100 layers. The chemistry of these materials was adjusted to increase the conductivity [118].

The chemistry of the P Jet and the P VP AL 4083 was adjusted to see if an observable increase in the conductivity could be achieved. The adjusted Baytron materials jetted with no major issues. All contacts were well defined with no over spray initially. Once the contacts were dry they did well with the Scotch tape test and had little failure. The resistance of the P VP AL 4083 material stayed relatively the same in the range of 5 to 20 MΩ with the unmodified material having lower resistance. The modified P Jet had a resistance in the range of 0.250 to 4 MΩ and the unmodified P Jet had a resistance in the range of 1 to 10 MΩ. A summary or the results are given in Table 3.7.

After the deposition of the unmodified Baytron material samples, and given the film time to dry, the sample was immersed in ethylene glycol for two minutes to enhance the `conductivity of the thin films. As the sample sat in the solvent it was observed that the Baytron contacts were dissolving and after 2 minutes the contact was totally dissolved. This method of enhancing the conductivity was not recommended by H.C. Starck. It had been reported to increase the conductivity by three times the annealed value [3.4].

Table 3.7 Thickness Studies of Baytron Materials Used in This Study

	Unmodified		Modified	
Number of Layers	P Jet	P VP AL 4083	P Jet	P VP AL 4083
25	20 MΩ	20 MΩ	9 MΩ	18 MΩ
50	10 M Ω	18 M Ω	2 - 3 MΩ	18 MΩ
75	10 M Ω	10 M Ω	0.400 - 4 MΩ	9 MΩ
100	5 - 9 MΩ	3 - 8MΩ	0.250 -1.5 MΩ	4 - 12 MΩ

The H.C. Starck Baytron materials were successfully ink-jet printed. Adhesion and conductivity were good enough to use as conductive contacts for sensor applications. The next section will describe the ink-jet printing of P(VDF-TrFE) onto the MO silver contacts.

3.2.3 P(VDF-TrFE)

In order to create functional devices, multiple layers and or active material must be printed on the bottom contacts printed in the study. Therefore, two ink-jettable P(VDF-TrFE) polymer inks were formulated, the first was dissolved in Dimethylformamide (DMF) and the second was dissolved in methyl ethyl ketone (MEK) as seen in Figure 3.4.

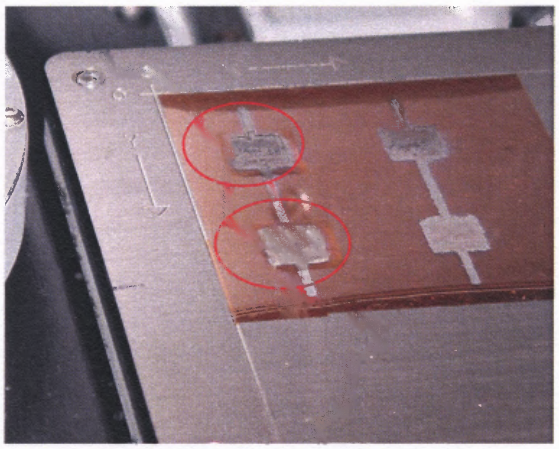

Figure 3.4 The two circuits on the left have polymer ink, jetted on top of MO silver.

Initially the optimum number of layers of the P(VDF-TrFE) ink had been studied along with the drop spacing, deposition temperature and ink concentration. As seen in Figure 3.5 an array of 1 cm2 rectangles had been deposited starting with 1 layer up to 150 layers in 5 layer increments. Using the formulation of polymer ink the number of layers necessary to make a uniform film is currently 125 to 150 layers. Also seen in Figure 3.5 are regions in which the printer cartridge may have clogged and not deposited entire lines

in the film which left regions where there would be conduction between layers or non-uniformities on the thickness of the films. When using brand new print heads uniform usable films were obtained, otherwise the polymer films had little definition.

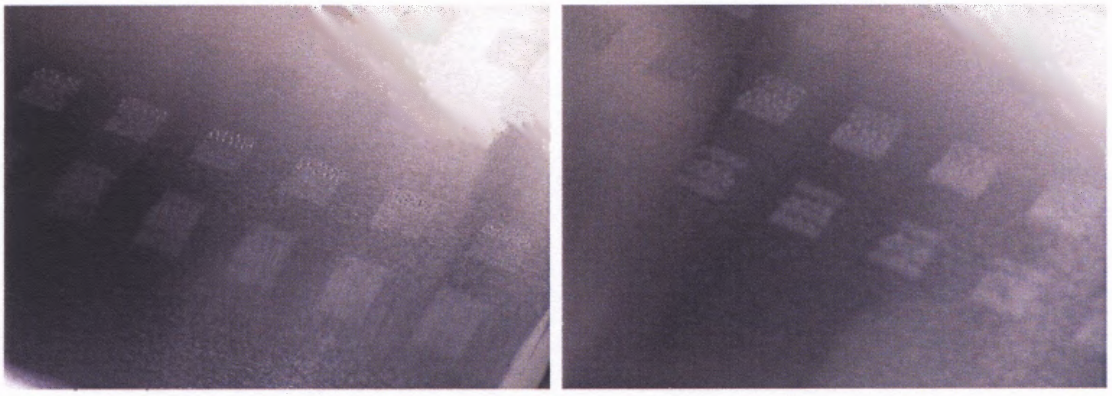

Figure 3.5 Piezoelectric polymer thickness study.

For each case in Table 3.8 the resolution was modified by changing the drop spacing. In this study it was found that drop spacing less then 50 um tended to be too close and did not give the solvent ample time to evaporate resulting in non-uniform films. Drop spacing greater then 75 um resulted in films that had discontinuities and were not very uniform after deposition. Platen temperatures greater then 45 C tended to evaporate the solvents rather quickly and resulted in clogged printer nozzles.

Table 3.8 Range of P(VDF-TrFE) Ink Printer System Parameters

Parameter	Range of Values
Drop Spacing (μm)	10 - 100
Platen Temperature (°C)	Ambient – 60
Cartridge Temperature (°C)	Ambient – 30
Number of Nozzles	16
Drop Volume (pL)	10

P(VDF-TrFE) inks were formulated, successfully jetted and studies were conducted to determine the number of layers necessary to form films that would isolate the bottom conductive layer. The next sections detail the ink-jet printing of this ink onto the conductive MO silver and the conductive Baytron films.

3.2.3.1 P(VDF-TrFE) onto MO Silver. Initially P(VDF-TrFE) ink was deposited on an unannealed MO silver contact. The solvent in the P(VDF-TrFE) ink tended to mix with the MO silver on the surface of the substrate and the sliver distributed throughout the polymer as seen in Figure 3.6.

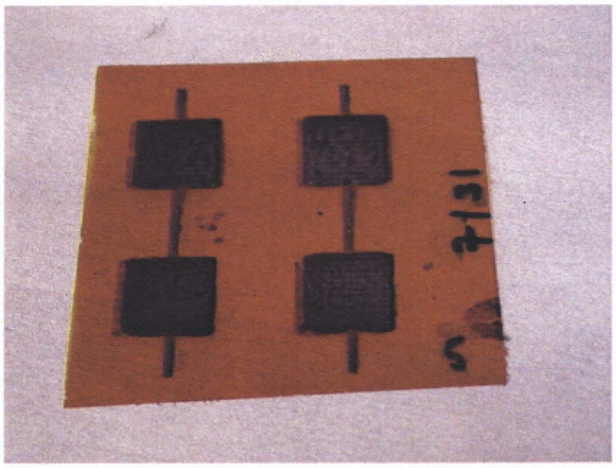

Figure 3.6 Unannealed bottom contacts with piezoelectric polymer printed on top.

Next, bottom contacts that had been annealed for 5 minutes at 100 C had 150 layers of P(VDF-TrFE) ink deposited on them. The bottom contacts had adhesion issues prior to the deposition of the piezoelectric polymer. These contacts were conductive but had spotty coverage and had silver flaking off the surface. When the polymer was deposited on these contacts, the polymer redistributed the silver flakes into the polymer.

This created an issue with both the uniformity of the piezoelectric polymer and deteriorated the conductivity of the bottom contacts.

Another set of thin films where the bottom contacts had been annealed for five minutes at 200 C had 150 layers of piezoelectric polymer deposited on them. In this case the increase in the anneal temperature resulted in better conductivity but had little effect on adhesion.

Further studies with anneal temperatures greater then 150 C not exceeding 250 C and anneal times of 30 to 60 minutes started to exhibit good conductivity and better adhesion. Figure 3.9 is an example of a typical sample prepared in this manner. Repeatability of results was difficult to achieve, so samples were hand picked for further processing. Samples annealed in such a way had 150 layers of the piezoelectric polymer deposited on them and were visually inspected for any defects. Three samples were fabricated that were free from defects and MO silver was deposited onto the polymer. The MO silver was dissolved in isopropanol in order not to interact with the P(VDF-TrFE).

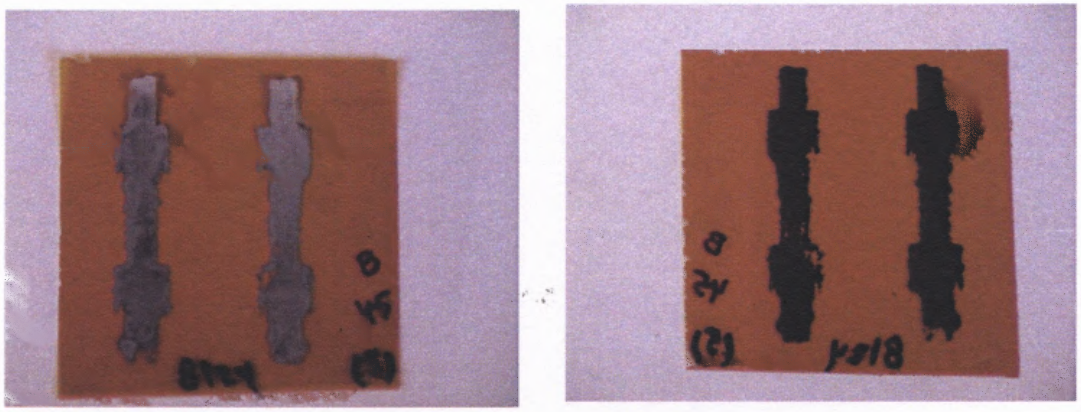

Figure 3.7 (a) Typical front view of ink-jet printed annealed Ag bottom contacts (b) Back side of ink-jet printed annealed Ag bottom contacts.

The first sample that had the MO silver deposited on the polymer was annealed at 200 C for 30 minutes. As seen in Figure 3.8, the anneal temperature was much to high and burned the polymer. For the next sample, the top contact was annealed with a heat lamp. This method of annealing the top contacts worked well, as it did not burn the polymer as seen in Figure 3.9. Problems with these samples arose from excessive handling leading to flaking of the silver from the bottom contact. As can be seen in Figure 3.8 there are discontinuities in the bottom contacts that lead to an inability of making good contacts.

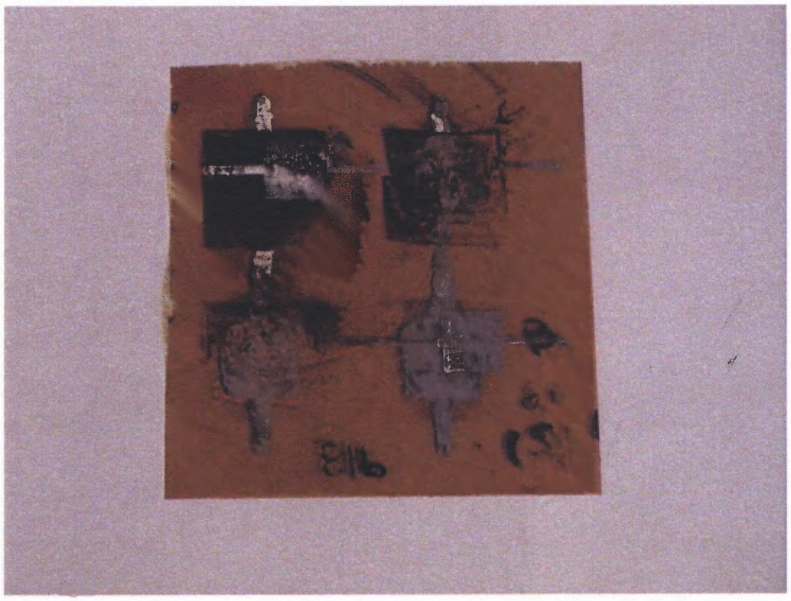

Figure 3.8 Sensor with burned polymer and top contact.

Many trials to perfect the MO silver ink have been performed. A summary is given in Table 3.9. Variations of deposition characteristics, utilizing different solvents and different concentrations of the metal organic silver compound have been experimented with along with different techniques for annealing the contacts. Single layers have been deposited then annealed and another layer deposited on top of the initial layer, neither layer has displayed conductivity. Contacts that adhere and are conductive

tend to look like those in Figure 3.7, where the contact remains in approximately 70% of the designed circuit area. Success was marginal. All bottom contacts were not well defined. Most of the thin films exhibited high conductivity and reasonable adhesion but repeatability was never achieved. Issues with repeatability lead the researcher to experiment with commercial inks.

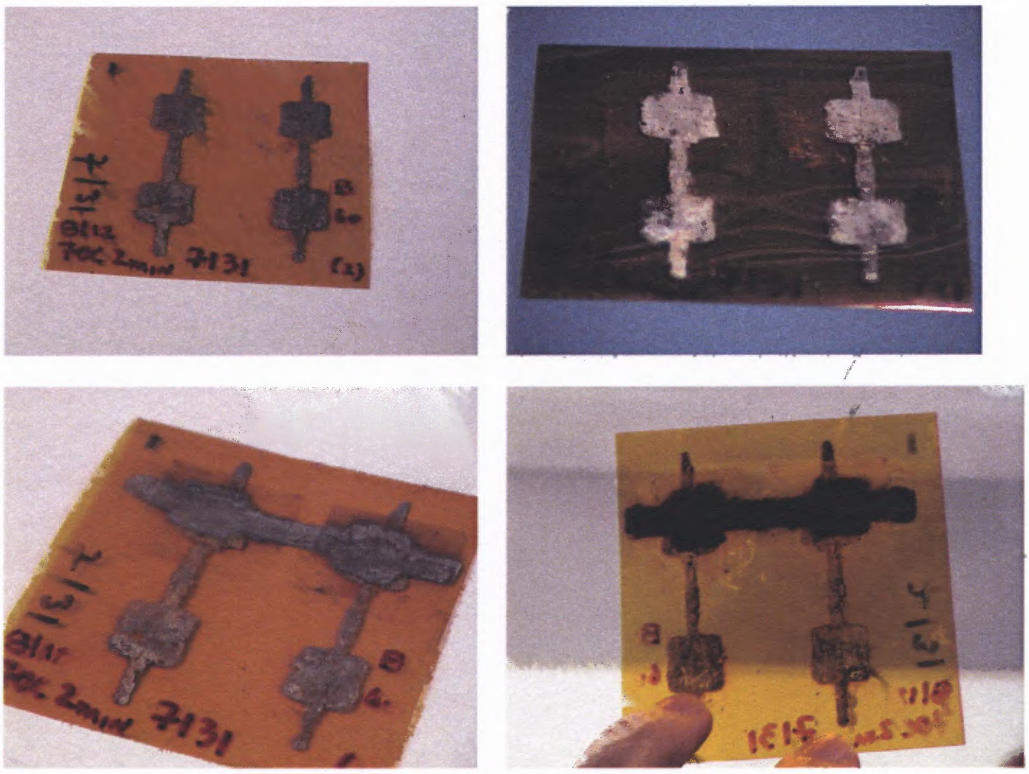

Figure 3.9 (a) Annealed Ag bottom contacts (b) piezoelectric polymer deposited on top of annealed contacts (c) conductive top contacts (d) discontinuity in the bottom contact.

Table 3.9 Summary of P(VDF-TrFE) Ink Deposited onto MO Silver

	Bottom Contacts			Top Contacts		
P(VDF-TrFE) Deposited On	Duration of Annealing	Temperature of Annealing	Top Contacts	Duration of Annealing	Temperature of Annealing	Observations
Unannealed MO Silver Bottom Contact	-	-	No	-	-	Absorbed MO silver from the substrate surface and mixed the silver with the polymer.
Annealed MO Silver Bottom Contact	Short	Low	No	-	-	Absorbed MO silver flakes from the substrate surface and mixed the silver with the polymer.
Annealed MO Silver Bottom Contact	Short	High	No	-	-	Better conductivity but poor adhesion.
Annealed MO Silver Bottom Contact	Long	High	No	-	-	Good conductivity, good adhesion, but not repeatable.
Annealed MO Silver Bottom Contact	Long	High	Yes	Long	High	P(VDF-TrFE) layer burned.
Annealed MO Silver Bottom Contact	Long	High	Yes	Short	Low	Not repeatable.

3.2.3.2 P(VDF-TrFE) onto Baytron Thin Films. Initially P(VDF-TrFE) ink was deposited on unmodified Baytron P Jet bottom contacts. Two hundred and seventy five layers of polymer were jetted onto the unmodified P Jet material to verify that the polymer would not dissolve or lift the Baytron contact from the substrate. The initial results were good. The polymer had excellent adhesion, the film was uniform and there was no interaction between the polymer and the P Jet material, as seen in Figure 3.10.

Figure 3.10 Polymer layer deposited on unmodified Baytron P Jet.

Variations of the printing parameters given in Table 3.10 were jetted. Lower platen temperature required a delay in the printing to give the solvent time to evaporate. Similar results were obtained for drop spacing closer then 50 um which gave poor results due to lack of evaporation of the solvents.

Table 3.10 Variations of P(VDF-TrFE) Ink Printed on Baytron Bottom Contacts

Parameters	Variations
Number of Layers	150 - 750
Drop spacing (um)	20 - 75
Platen Temperature (C)	Ambient - 35

A marked degradation of print quality was observed after eight or more hours of repeated use of the ink-jet cartridge. The pattern printed no longer had any definition and tended to smear as seen in Figure 3.11. Due to the degradation of the print quality and limited print head life span, more layers were needed to have isolation from the bottom contact. With a brand new cartridge 200 layers would exhibit excellent isolation. After many hours of use of the cartridge it became necessary to deposit well over 400 layers. These additional layers added hours to the print job.

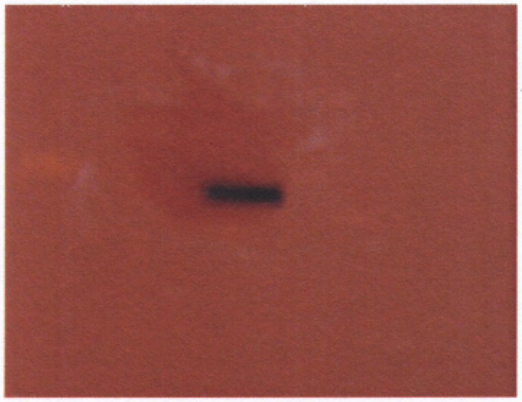

Figure 3.11 Polymer layer deposited on modified Baytron P Jet with little definition.

Once the issues with the printer cartridges were somewhat resolved, modified Baytron P Jet was deposited on top of the polymer layer. Measurements verified there was isolation between the top layer of Baytron P Jet and the bottom layer. Reductions in size of the contacts were made to speed the lengthy printing process. Arrays of 8 x 5 were printed for each of the three geometries given in Table 3.11. For the three geometries given in Table 3.11, one hundred layers of Baytron P Jet were jetted for each of the bottom and top geometries, two hundred plus layers of P(VDF-TrFE) ink were jetted for the middle layer. The variation in time to print these geometries was significant. The first array had a print time greater then 40 hours, the second array had a print time of

greater then twenty four hours, and the third array had a print time greater then fourteen hours. The geometry of each of these arrays as seen in Table 3.11 needed to have the size decreased to speed the printing process. Also, these printed arrays exhibited isolation between layers.

Table 3.11 Geometry of the Ink-Jet Printed Layers of Baytron Bottom and Top Layers, P(VDF-TrFE) Middle Layers

Array	Bottom Layer	Middle Layer	Top Layer
First (μm)	2.5 x 10	5 x 8	2.5 x 6
Second (μm)	2 x 5	3 x 3	2 x 2
Third (μm)	1.5 x 3	3 x 2	1.5 x 1

Many well defined working samples were fabricated. Issues with printer cartridges lead to the search for more time efficient printing methods.

3.2 Screen Printed Thin Films

So far, ink-jet printing of MO silver, Baytron materials and P(VDF-TrFE) inks has been discussed. Repeatability, reliability and speed negate utilizing that printing method. Screen printing was chosen as a low-tech alternative that has a proven track record of speed of deposition and is repeatable.

Screen printing is a very mature printing process. This method of printing has been used for printing graphics on tee-shirts, poster and advertising literature for years. Screen printing has also been used for hybrid circuits and Monolithic Microwave Integrated Circuits (MMICs) fabrication [119]. Due to the maturity of the process there are many research groups proceeding with fabricating devices that use this printing method [120, 121].

Stencils were generated, prior to printing, using the direct block out or screen filler method, as seen in Figure 3.12. Resist material was used to generate the circuit such that ink can be forced through the screen in the areas where the resist material has not been applied.

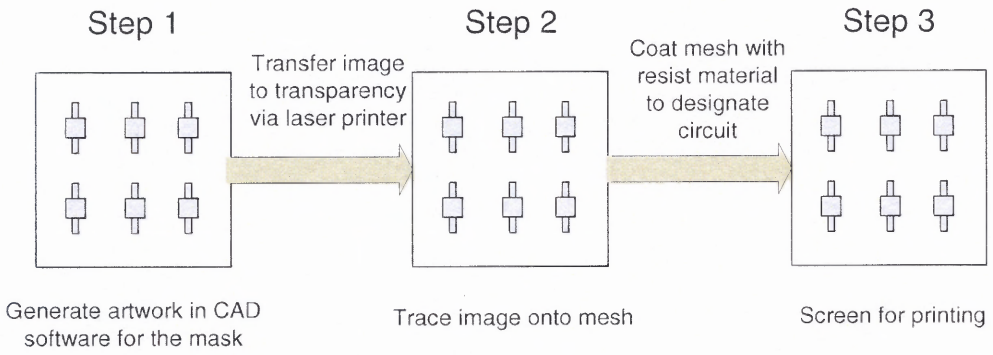

Figure 3.12 Procedure for generating screen for screen printing.

The substrates used were DuPont's Polyimide Kapton E and 3M transparency film. These films were cleaned in acetone, isopropanol, and distilled water. Multiple layers were deposited using screen printing, as is depicted in Figure 3.13. Each layer was deposited through three different screen meshes 12xx multifilament polyester, 8xx multifilament polyester and shear material with unspecified hole spacing. The first layer deposited was DuPont's microcircuit materials CB028 silver conductor polymer thick film composition; this material had been designed for low temperature drying and good adhesion to polymer substrates such as Kapton [122]. The second layer was P(VDF-TrFE) which was screen printed directly on top of the silver, and the third layer deposited on the P(VDF-TrFE) was another layer of DuPont's silver.

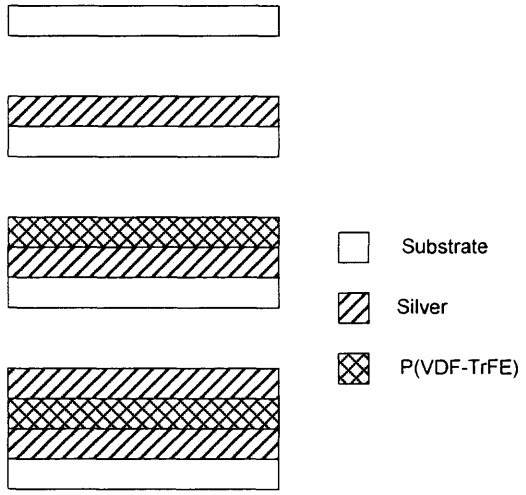

Figure 3.13 Fabrication of multiple screen printed layers.

Approximately 200 bottom silver contacts have been fabricated with the three different screen meshes. The geometry of the pattern is shown in Figure 3.14. The bottom silver layer was dried using a box oven, a heat lamp, a hot plate and by air drying at room temperature for 24 hours. Drying using these four methods resulted in low resistance, uniform contacts and excellent adhesion in all cases. The primary difference noted between drying on a hot plate or heat lamp vs. the box oven and room temperature was the respective anneal times of 10 minutes, 10 minutes, one hour and twenty four hours.

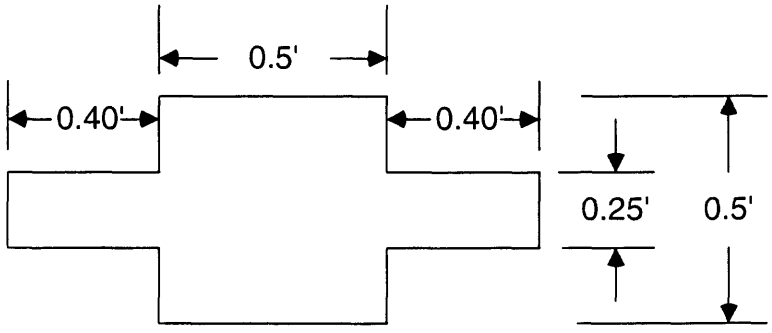

Figure 3.14 Geometry of the first layer.

The resistances of these silver contacts were measured to determine if there was an optimum method of drying to obtain low resistance silver layers. Also, the three different meshes were used to see if this had an effect on the resistance. As seen in Table 3.12 the resistance of the silver contact layer is well below 1 ohm for each drying method, and also for each mesh and substrate used. The best definition of the silver layers was obtained using the 12xx mesh. For the 8xx and the undefined mesh the silver ink tended to flow under the screen and distort the pattern. All contacts had been subjected to the scotch tape test. All have passed and were flexed to see if the silver would crack and peel. Resistance was measured after flexing the contacts; the resistance did not change.

The silver bottom contact on Kapton and Transparency film can be seen in Figure 3.15, and the mesh pattern can be seen in the silver contact. Adjustments were made to correct this by adding thumb tacks under the frame to act as spacers to keep the mesh from sitting in the ink. This did not totally correct the problem but it did help in making the films somewhat more uniform.

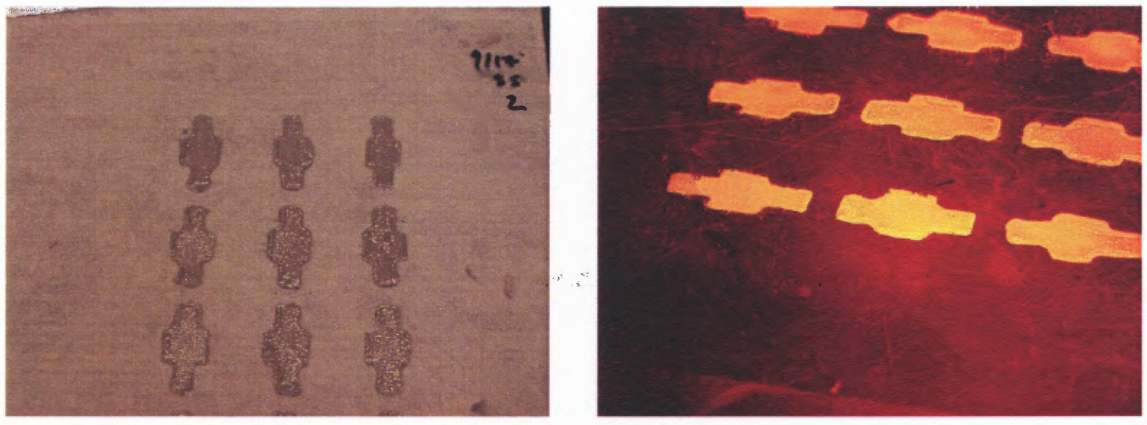

Figure 3.15 Pictures of the screen printed silver bottom contact on (a) Kapton (b) transparency film.

Table 3.12 Resistance Values of Different Drying Methods and Mesh Sizes for Screen Printing

Material	Mesh	Drying Method	Rmin (Ω)	Rmax(Ω)
Kapton	12	Box oven	0.09	0.31
		Heat Lamp	0.77	0.87
		Hot Plate	0.17	0.26
		Air Dry	0.02	0.12
	8	Box oven		
		Heat Lamp	.04	.190
		Hot Plate		
		Air Dry	0.03	0.08
Transparency	12	Box oven	0.27	0.32
		Heat Lamp	0.34	0.48
		Hot Plate	0.12	0.19
		Air Dry	0.06	0.14
	8	Box oven		
		Heat Lamp		
		Hot Plate	0.04	0.11
		Air Dry	0.03	

Two different solvents, acetone and MEK, were used to dissolve the P(VDF-TrFE) in different ratios to form screen printable inks. Approximately 60 of the bottom silver layers had this polymer ink deposited on them with the three different screen meshes. The geometry of the polymer layer was a one inch square. The mesh that worked best for depositing the polymer layer was the mesh with unspecified hole spacing, as it allows sufficient material flow for good coverage. Two to three printed layers permit enough material build up so that there are no pin holes allowing isolation of the bottom silver layer. Figure 3.16 shows typical polymer layers. The polymer tended to have many bubbles due to the mesh sticking in the polymer; this was resolved by reducing the viscosity of the ink, thereby allowing the trapped gasses to escape from the thinner bodied material. Also noted, the screen filler material had a tendency after many

uses to deteriorate and the screen material had in some cases become embedded in the printed material. This problem was corrected by simply discarding the screens after a set number of uses. Once printing was completed, the resistances of the silver bottom contacts were checked and demonstrated good conductivity before and after they had polymer deposited on them. The bottom contacts were no longer being dissolved by the polymer.

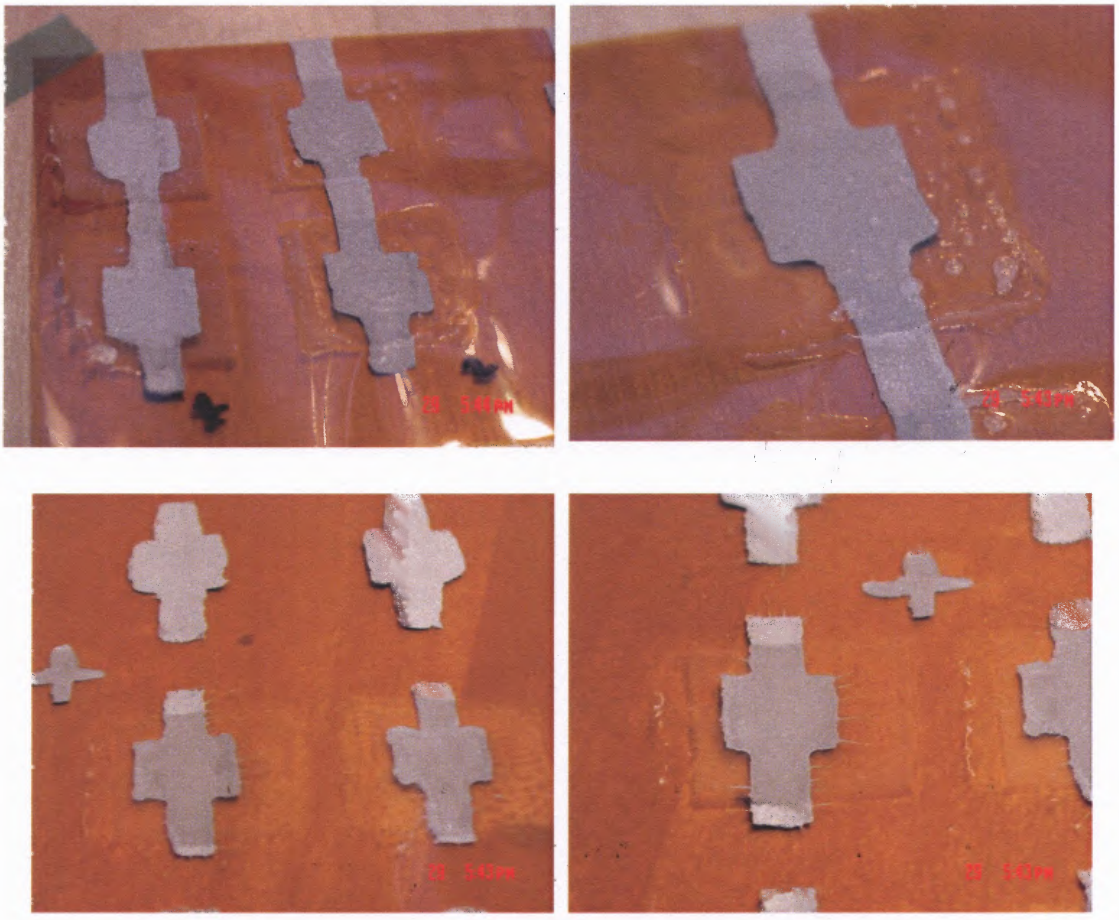

Figure 3.16 (a) Annealed Ag bottom contacts with piezoelectric polymer screen printed on top (b) close up view of piezoelectric polymer deposited on top of annealed contact (c) second generation annealed contact with polymer deposited (d) close up view of second generation contact with polymer deposited.

Approximately 30 of the fabricated films had top silver contacts screen printed on top of the polymer samples, and had been left to dry at room temperature. The top contact layer has been deposited through the 12xx multifilament polyester mesh. All the top contacts have been tested for resistance and have exhibited resistances below 1 ohm.

The silver top contact on Kapton film can be seen in Figure 3.17. As can be seen in the photo, the polymer had shrinkage but the top contact was still successfully printed and the top contacts were functional. Six of the approximate thirty top contacts were isolated from the bottom contacts; the potential cause for the electrical short in the twenty four samples is due to the layer thickness of the polymer being too thin. Further characterization of these films will be discussed in Chapter 4 and Chapter 5.

Table 3.13 Range of Resistance Values of Top Silver Layer Deposited by Screen Printing

Material	$R_t(\Omega)$	$R_{tb}(\Omega)$
Kapton	0.02 - 0.05	0.02 - 54 M
Transparency	0.02 - 0.04	0.02 - 23 M

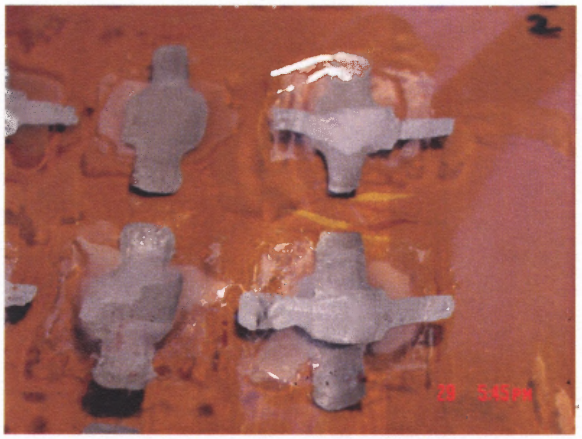

Figure 3.17 Pictures of the screen printed silver top contact on Kapton.

3.3 Stencil Printed Thin Films

Screen printing has been found to be a rapid method of depositing thin films. Issues had been encountered with this method where the screen stuck to the wet films that were deposited, creating non-uniform films. To improve the uniformity of the silver layers a modified stencil printing method was performed.

Prior to printing, plastic stencils were generated, as seen if Figure 3.18, in which the artwork was transferred to transparency film via a laser printer. The areas were cut out to generate the pattern such that ink could be rolled through the open areas where the transparency material had been cut away. Three such plastic stencils were generated, one for each of the layers, the bottom silver layer, top silver layer and the middle polymer layer.

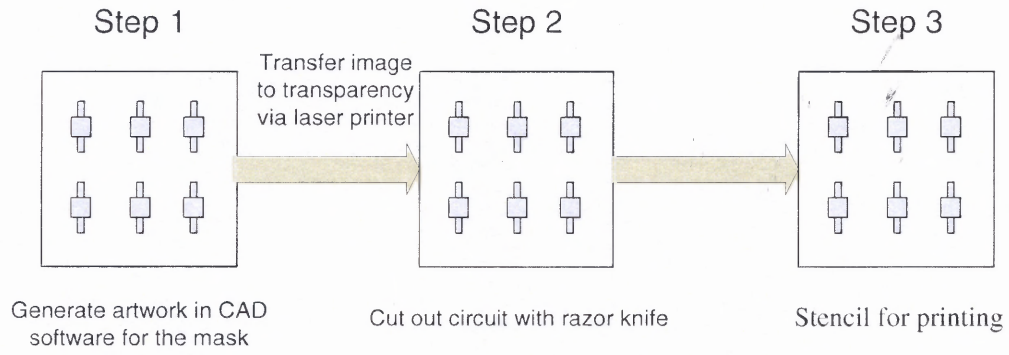

Figure 3.18 Process for generating stencil for stencil printing.

The substrates used were DuPont's Polyimide Kapton E, 3M transparency film and copy paper. The Kapton and transparency films were cleaned in acetone, isopropanol, and distilled water. Multiple layers were deposited using stencil printing; the same layers were deposited for screen printing as is depicted in Figure 3.1. The first layer deposited was DuPont's silver conductor polymer; the second layer was P(VDF-

TrFE) which was printed directly on top of the silver, and the third layer deposited on the P(VDF-TrFE) was another layer of DuPont's silver conductor polymer.

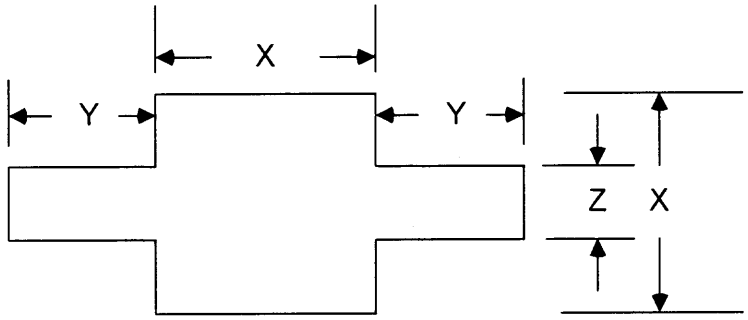

X	Y	Z
0.5	0.4	0.25
0.375	0.5	0.12
0.31	0.53	0.06

Figure 3.19 Geometries of the first layer via stencil printing.

Approximately 200 bottom silver films have been fabricated using stencil printing, with the geometry shown in Figure 4.19. The bottom silver layer was dried using a hot plate set at 125 C for 20 minutes. The resistances of these silver contacts were measured and the average data for all the silver contacts is seen in Table 3.14. Some distortion of the pattern was observed due to the flexibility of the stencil. The silver ink tended to get under the stencil and distort the pattern, contributing to the fluctuations in resistance values. A 10% sample of the contacts were subjected to the scotch tape test. All passed and were flexed to see if the silver would crack and peel. The measured resistance did not change after flexing the contacts.

Table 3.14 Resistance Values of Different Stencil Printed Geometries

Substrate	Geometry	$R_{min}(\Omega)$	$R_{max}(\Omega)$
Transparency	Large	0.08	0.53
	Medium	0.3	0.71
	Small	0.49	1.83
Kapton	Large	0.06	1.21
	Medium	0.1	1.3
	Small	0.28	5.07
Paper	Large	0.62	1.37
	Medium	0.91	1.85
	Small	1.1	2.27

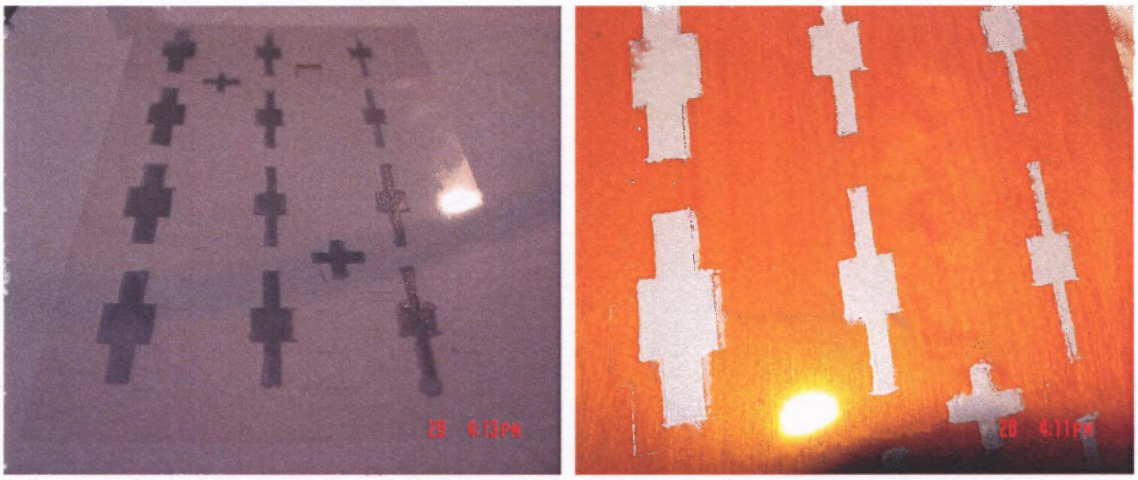

Figure 3.20 Pictures of the stencil printed silver bottom contact on (a) transparency film (b) Kapton.

Acetone was used to dissolve the P(VDF-TrFE) in different ratios to form screen printable inks. Approximately 15 of the bottom silver films had this polymer ink deposited through the stencil with a roller and some with an acid brush. The geometry of the polymer layer was a one inch square. The roller worked well but would stick and tear the polymer off the surface if rolled too long; the acid brush worked well also as it allows sufficient material to be applied for good coverage and more material could be applied with the brush than the roller. Two to three rolled layers allowed for enough material build-up so that there was isolation of the bottom silver layer. Figure 3.21 shows typical polymer layers, the polymer tended to adhere very well. The resistances of the silver bottom contacts were checked. They maintained good conductivity after they had polymer deposited on them and none had any issue with being dissolved by the polymer.

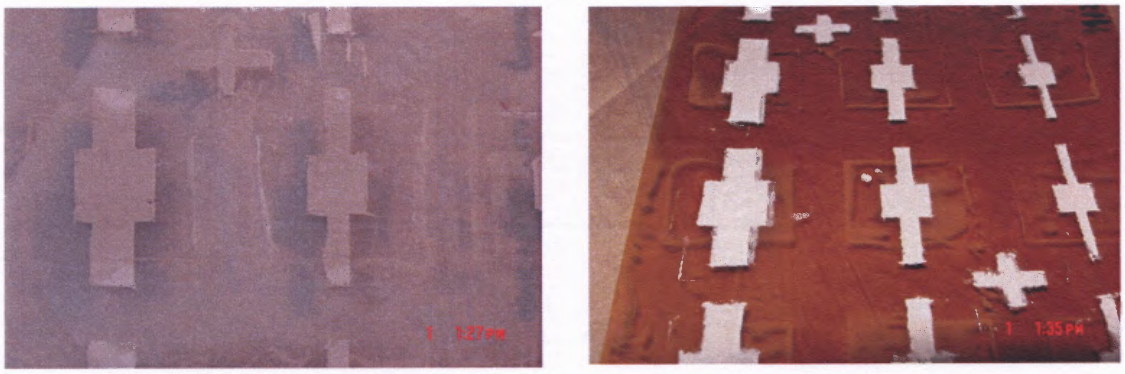

Figure 3.21 (a) Dried stencil printed Ag bottom contacts on transparency film with piezoelectric polymer stencil printed on top (b) Dried stencil printed Ag bottom contacts on Kapton film with piezoelectric polymer stencil printed on top.

Approximately 15 top silver films had been stencil printed on top of the polymer samples that were deposited on the Kapton and transparency film. They have been left to dry at room temperature. All the top contacts have been tested for resistance and all have exhibited resistances below 1 ohm as shown in Table 3.15.

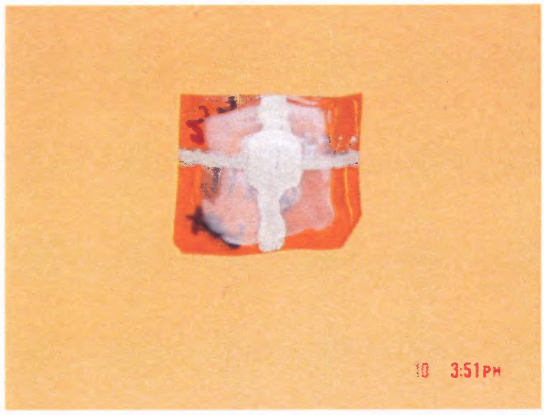

Figure 3.22 Pictures of the stencil printed silver top contact on Kapton.

Table 3.15 Range of Resistance Values of Top Silver Layer Deposited by Stencil Printing

Material	$R_t(\Omega)$	$R_{tb}(\Omega)$
Kapton	0.11 - 0.45	0.25 - ∞
Transparency	0.07 - 0.18	16 M - 120 M

The silver top contact on the Kapton film can be seen in Figure 3.22. As can be seen in the photo, the polymer had shrinkage but the top contact was still successfully printed and the top contacts were functional. Nine of the approximate fifteen top contacts were isolated from the bottom contacts; the potential cause is due to the layer thickness of the polymer being too thin. Further characterization of these films will be performed in Chapter 4 and Chapter 5.

3.4 Results and Discussions

As seen in Figure 3.6 through Figure 3.9 of the ink-jet printed films, both the silver and the polymer films had issues with definition of the printed pattern. Most of the silver films were not conductive and did not adhere. To resolve the issue of the conductivity of the silver layer and the adhesion issue, the printer platen temperature needs to be increased. Its current temperature limit is 60 C and needs to be adjusted to 85 – 100 C. This is possible through a modification to the platen in which a temperature controlled heated block is attached. Additional adjustments of fluid metering also appear to be necessary in order to reduce the number of time consuming printings needed in order to achieve sufficient homogeneous film build up. The largest nominal volume currently of a single drop is 10 pL, the drop spacing in x and y is 5μm. It appeared that the nozzles would clog leaving bare spots and missing rows on some depositions. Also the corners were not sharp on all of the depositions. It currently is not possible to adjust the volume of the drop, so multiple layers were deposited leading to lengthy depositions.

Better results were obtained with the H.C. Starck Baytron products. Repeatability was achieved, and well defined patterns were printed. Conductivity of the materials

available to this researcher was very low, but higher conductivity materials are available. All in all, issues with print speed and volume of ink deposited were still observed with this material.

The screen printed films have demonstrated the potential of rapid fabrication of thin metallic and polymer films and demonstrated excellent performance; all metallic films passed the scotch tape test and exhibited very low resistance. The silver films had issues with non-uniformity due to the screen lying in the wet ink during the deposition process and the polymer films had the same issue leading to forming bubbles in the polymer films. This issue can be resolved by using metal meshes and metal frames, and also by having better control of the frame height above the substrate. The metal mesh in a metal frame will control the tension in the screen such that it will not sag and lay in the wet ink. When the polymer was deposited and the mask was used for multiple depositions the mask was cleaned. The solvent used to clean the mask tended to soften the mask filler material. When the mask was used for the next deposition this mask filler material was transferred to the substrate. These issues with the screen printing process are easily resolved by either buying an inexpensive manual screen printer or building a simple frame to hold the screen and to control the height of the screen. The manual screen printing method was able to provide proof of the concept of isolated thin films. An automated system would be able to correct most if not all the issues, control over the pressure of the squeegee material through the screen, as well as metal screens fabricated with photolithography would also give better resolution of the circuits. There are many parameters involved which can be used to control the screen printed result. The thickness of the film depends on the viscosity of the ink, the mesh count, the screen emulsion, and

the squeegee. The resolution of the printed pattern depends on the screen mesh count and the resolution of the screen emulsion layer.

Stencil printing exhibited the best metallic films out of the three printing methods studied. The stencil for the stencil printing method was fabricated from a plastic transparency and there were occasions where the ink had gotten under the stencil deforming the desired pattern. The stencil in these cases was repairable by wiping with a solvent. Initial prototypes had the material squeegeed through the stencil which produced adequate films, but more uniform films were obtained by rolling the material through the stencil. If more consistent films were necessary a metal stencil and a frame similar to the screen printing frame could be fabricated.

3.5 Conclusions

In this study, screen printing and stencil printing have been successfully demonstrated as low temperature deposition methods for rapid fabrication of flexible thin films. Using these methods it has been possible to fabricate many low resistance contact layers on multiple substrates. Existing printing technology is capable of producing flexible thin films for flexible electronics with little modification to the commercially available systems and would require little capital investment. This study has shown the capability of the adhesion of the materials and the low resistance contacts. More work is necessary to achieve better resolution of the patterns. The simplicity of this process enables one to fabricate films rapidly. For more complex and better resolution circuit features commercially available systems could be used. Additionally, the proposed fabrication

techniques could be set up for roll to roll fabrication for high volume mass production of multi layer devices.

The issues with ink-jet printing appear to be related to the immaturity of the ink technology and the system used. Currently corporations like DuPont do not offer ink jettable conductive materials and materials available for ink jetting have adhesion issues with Kapton [122]. Also the inflexibility of the machine in terms of heating the substrate and the limitation of the volume of the ink dispensed with the current printer has impeded the success in fabricating good thin films.

CHAPTER 4

MATERIALS CHARACTERIZATION

4.1 Introduction

The ultimate goal of this study is to characterize the printed films described in Chapter 3. Three techniques are presented in this chapter. The first two, Raman spectroscopy and Fourier transform infrared spectroscopy, are both used to investigate the structure of the P(VDF-TrFE) films. The third characterization method is optical microscopy which is used to investigate the thickness and uniformity of the deposited films.

In this chapter, the infrared and Raman spectrum are evaluated and compared to theory. Raman and FT-IR spectrometry were chosen to characterize the P(VDF-TrFE) thin films due to the rapid, non-invasive, non-destructive nature of the techniques. The following section describes the use of an optical microscope to observe the films morphology. These techniques also require little sample preparation.

4.2 Raman Spectroscopy

Raman spectroscopy is a technique that identifies unknown materials by measuring how their vibrating molecular bonds scatter with an incident laser light into distinct frequencies. The advantage of Raman spectroscopy is its ability to penetrate a variety of glass and plastic materials. Raman spectroscopy was used to examine the structural and phase of P(VDF-TrFE) films. Raman spectroscopy in the wavenumber range of 4000 to 400 cm^{-1}, in transmission mode, was performed on the ink-jet, screen and stencil printed films.

The Raman spectra of the P(VDF-TrFE) films fabricated in Chapter 3 were taken with a Mesophotonics SE1000 Spectrometer. The Mesophotonics SE1000 Spectrometer is equipped with a 150 mW 785 nm ±1 nm laser. The films fabricated on the Kapton material saturated the detector due to luminescence of the Kapton at 785 nm. The films fabricated on the 3M transparency material exhibit a similar spectra as obtained by Constantino et al [123] shown in Figure 4.1. The screen and stencil printed films spectra are shown in Figure 4.2. The stencil printed film exhibited the strong peak at 841 cm^{-1} and a weaker peak at 813 cm^{-1}, which is similar to Constantino et al [7.1]. The screen printed film exhibited a strong peak at 855 cm^{-1} and a very weak peak at 846 cm^{-1}. The discrepancy in peaks and shifts is thought to be due to the mixture of the α and β phase in the screen printed films. Due to this inconsistency in the screen and stencil printed spectra further characterization was performed.

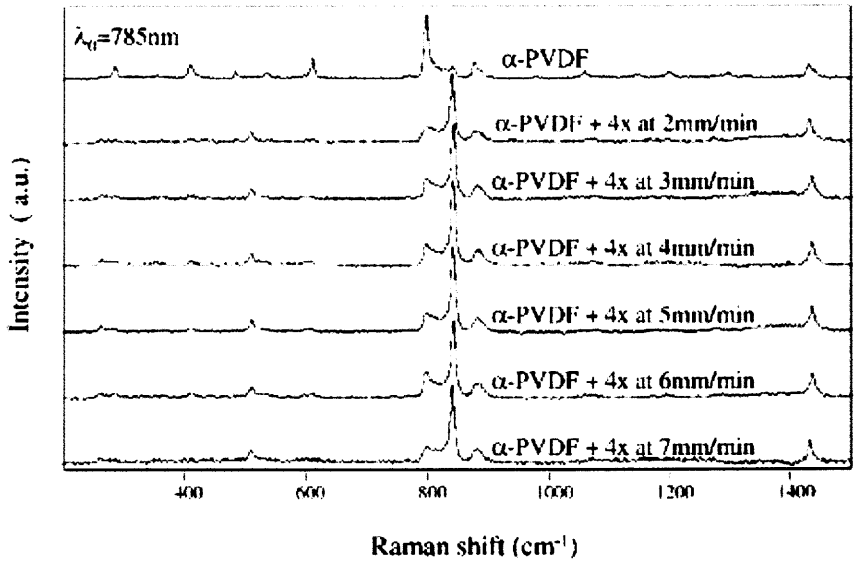

Figure 4.1 Raman Spectra of stretched PVDF [123].

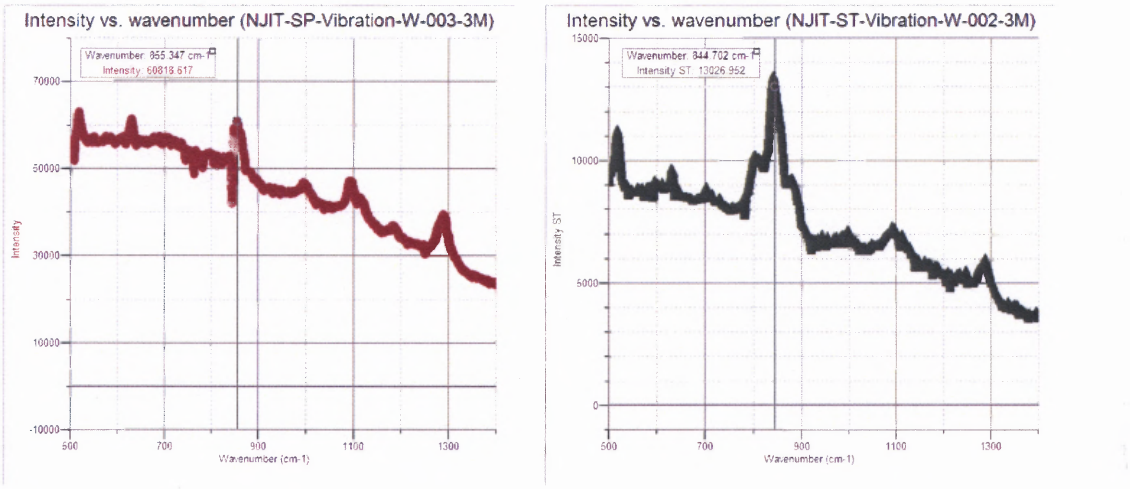

Figure 4.2 (a) Raman spectra of NJIT-SP-Vibration-W-003-3M (b) Raman spectra of NJIT-ST-Vibration-W-002-3M.

4.3 Fourier Transform Infrared Spectroscopy (FT-IR)

Due to the ambiguous results of the Raman spectroscopy, Fourier-Transform Infrared spectroscopy (FT-IR) was used to further investigate the phase of the P(VDF-TrFE) films. FT-IR, a complementary technology to Raman spectrometery, is a non-destructive analytical technique for the identification of unknown substances. This technique identifies unknown materials by the characteristic frequencies of these materials due to the molecular vibrations of the bonds and groups of bonds that hold the material together. This unique spectrum acts like a "molecular fingerprint" for distinct materials.

A Perkin Elmer Spectrum one FT-IR was used to examine the structural and phase of P(VDF-TrFE) films. FT-IR exposes a film to the full range of infrared frequencies. The infrared beam passes through the film and hit the detector, the resulting intensity of the beam is used to construct the spectra of the film. Screen and stencil printed thin films were removed from the flexible substrates. P(VDF-TrFE) pellets were dissolved in DMF and films were fabricated on glass slides and pealed off for the

measurement. Abdelsayed [124] and references there in state that the characteristic α-phase peaks are located at 614, 762, 795 and 975 cm^{-1} and the β-phase characteristic peaks are located at 440, 470, 510, 840 and 1280 cm^{-1}. FT-IR spectroscopy in the wavenumber range of 4000 to 400 cm^{-1}, in transmission modes was performed on the, screen printed, stencil printed and a DMF solution cast film.

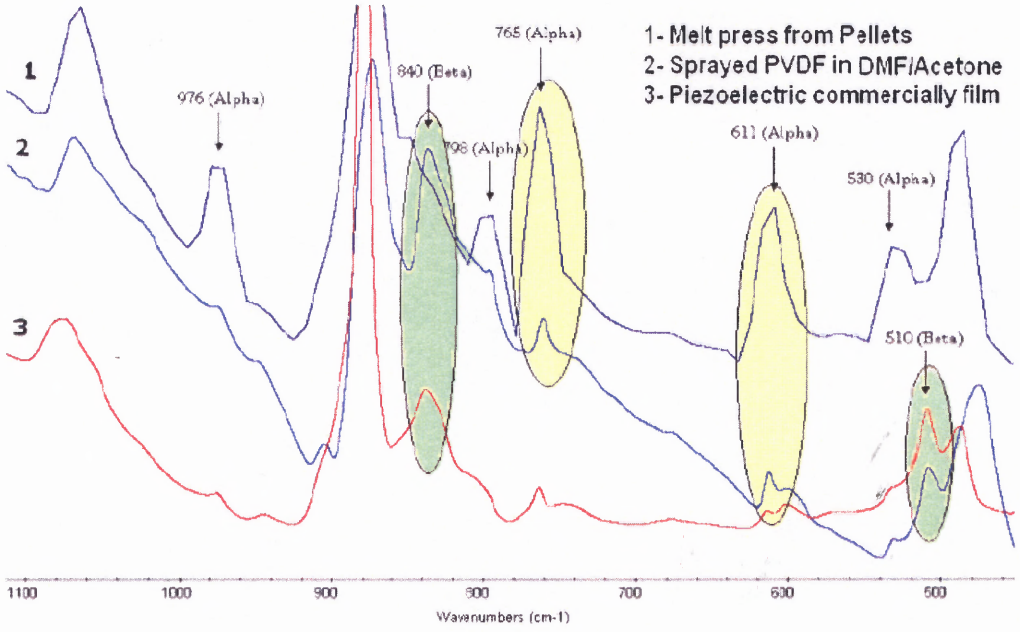

Figure 4.2 Absorption FT-IR spectrum of PVDF 1 – α-phase, 2 – sprayed PVDF in DMF/acetone, 3 – β-phase [124].

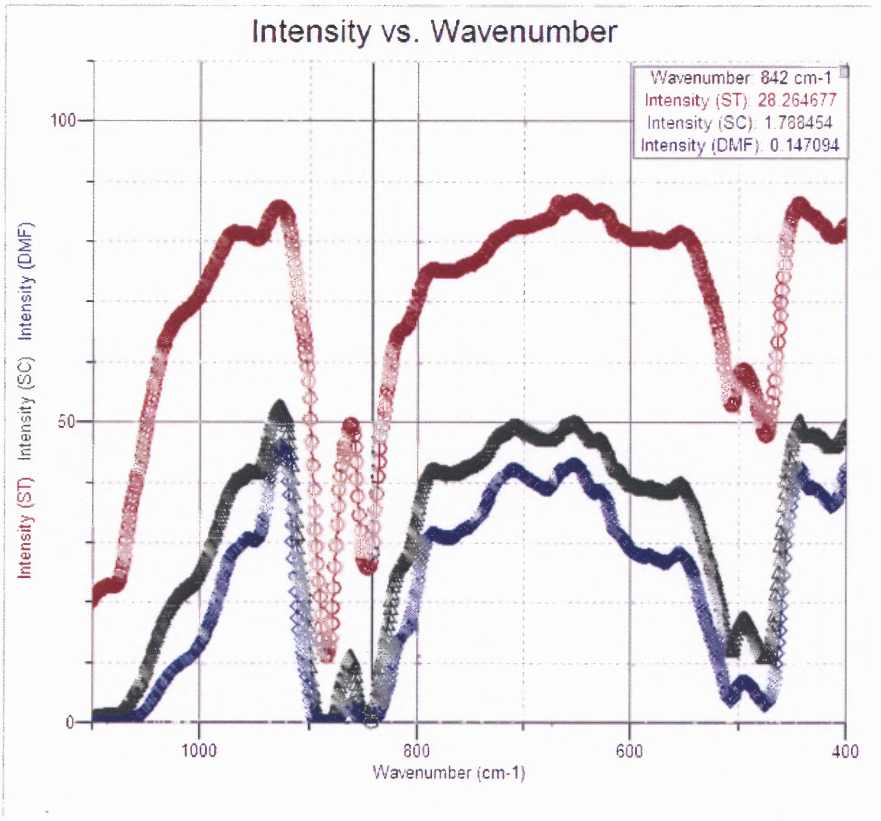

Figure 4.3 FT-IR spectrum of PVDF 1 – Stencil printed, 2 – Screen printed, 3 – P(VDF-TrFE) dissolved in DMF film.

The transmission FT-IR spectrum of the screen printed, stencil printed and a DMF solution cast films are shown if Figure 4.3. The three samples exhibit the same peaks while the intensities vary due to the thickness of the films. Comparing the peaks in Figure 4.3 to the characteristic peaks, these films contain the peaks related to the β-phase (474, 508 and 842 cm^{-1}), and none of the α-phase peaks. The FT-IR data shows that the films are in the piezoelectric β-phase.

4.4 Optical Microscopy

Optical microscopy is used to study the structure and morphology of thin films along with obtaining information about density, topography and various types of flaws. In this

study the optical microscope was used to examine the thickness and uniformity of the ink-jet, screen and stencil printed films P(VDF-TrFE) films.

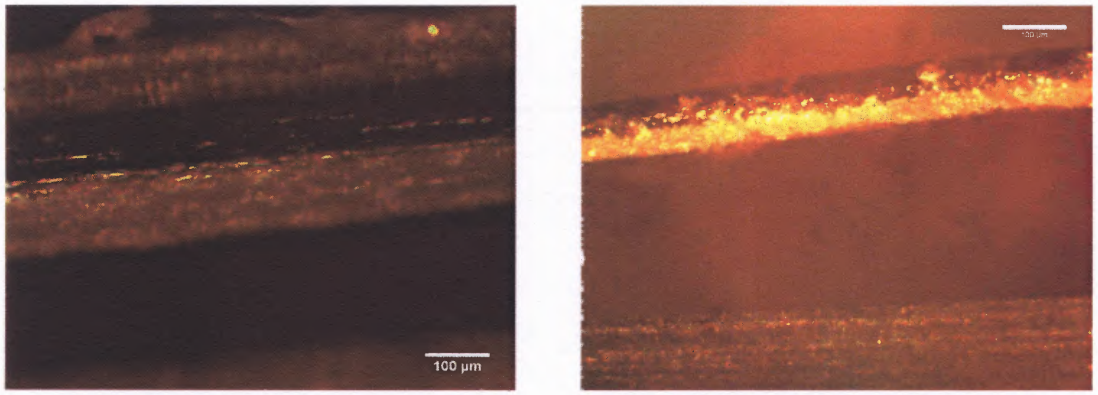

Figure 4.4 (a) Cross-section view of NJIT-ST-Vibration-W-002-3M (b) Cross-section view of NJIT-SP-Vibration-W-003-3M.

Figure 4.4 (a) shows a cross-section view of NJIT-ST-Vibration-W-002-3M. The thickness varied from 51 µm to 118 µm. The stencil printed films when measured with a micrometer demonstrated larger variation from sample to sample: 20 µm to 300 µm. Figure 4.4 (b) shows a cross-section view of NJIT-SP-Vibration-W-003-3M. The thickness varied from 204 µm to 559 µm. The screen printed films when measured with a micrometer demonstrated smaller variation (10 µm to 200 µm) from sample to sample.

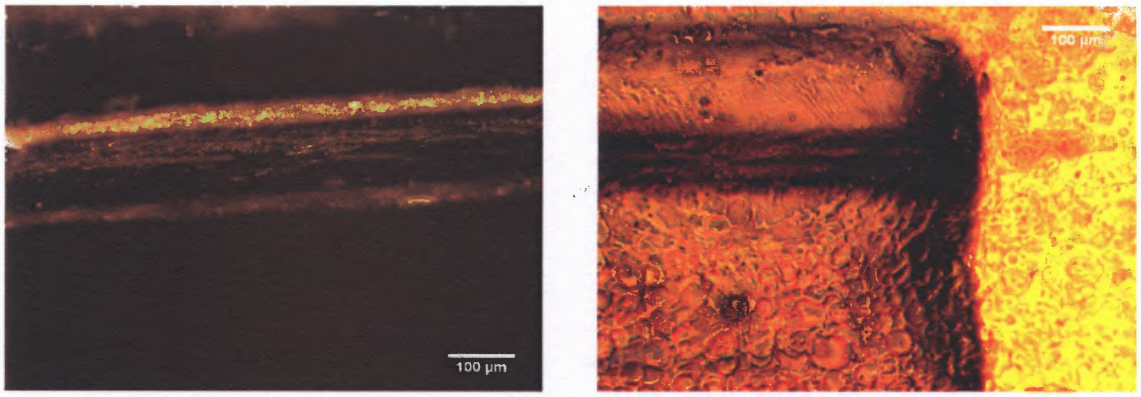

Figure 4.5 (a) Cross-section view of NJIT-IJ-W-002-HN (b) top view of NJIT-IJ-W-002-HN.

Figure 4.5 (a) shows a cross-section view of NJIT-IJ-W-002-HN. The thickness varied from 71 μm to 94 μm. The ink-jet printed films when measured with a micrometer demonstrated larger variation (5 μm to 10 μm) from sample to sample. Figure 4.5 (b) depicts the top view of NJIT-IJ-W-002-HN, in which the interface between the polymer and the bottom contact is visible along with a ridge due to printing. These ridges are seen with the naked eye on all the ink-jet printed sensors and are due to the drop spacing and drying temperature of the film. Similar ridges were observed by Tay al et. [40].

4.5 Conclusions

In this study, materials characterization of the printed P(VDF-TrFE) thin films were demonstrated to be in the piezoelectric β-phase. The Raman and FT-IR spectra were compared to the literature and were in good agreement. The Raman spectra were shifted slightly and the screen printed films did not clearly exhibit the 846 cm^{-1} peak. On the other hand, FT-IR exhibited sharp peaks (474, 508 and 842 cm^{-1}) as found in the literature. The optical microscope pictures demonstrated that the screen, stencil and ink-jet printed film thicknesses varied by 260 μm, 70 μm, and 20 μm respectively. The non-uniformity in film thickness leads to inaccuracies in calculating output voltages as will be seen in the next chapter.

CHAPTER 5

DEVICE FABRICATION AND CHARACTERIZATION

5.1 Introduction

The primary motivation of this study is to develop functional devices utilizing the printing methods described in Chapter 3. Two simple sensors are presented: the first a pyroelectric infrared sensor and the second an accelerometer. The aim of these two sensors is to observe the pyroelectric activity and piezoelectric activity in the Poly(vinylidene fluoride-trifluoroethylene) (P(VDF-TrFE)). Models for these sensors are based on the basic physics of piezoelectric and pyroelectric materials.

P(VDF-TrFE) had been chosen because it has been utilized as an infrared sensor and accelerometer on rigid substrates. The viscosity of the polymer was modified so both an ink-jettable and a screen printable formulation were developed.

Thin-film infrared and acceleration transducers on rigid substrates have been well received in the field of sensing technology. To date, fabrication by printing of these sensors on flexible substrates, such as polyimide, has not been reported.

Odon [125] demonstrated that commercial PVDF thin films could be realized as low cost pyroelectric sensors. In this case, the PVDF thin films are exposed to a short radiation pulse and the voltage response is studied. Satiadi et al. [126] have reported the design of an integrated pyroelectric P(VDF-TrFE) sensor on silicon with on chip step-wise poling at room temperature of the copolymer. They have tested the pyroelectric sensors voltage sensitivity and noise and found that the sensitivity depends on the thermal behavior of the sensor along with the transfer function of the readout electronics.

The methods of depositing thin films from the prior chapter have been utilized to fabricate functional devices on flexible substrates. In this chapter, the printed thin films have been utilized to form devices on transparency and on Kapton films. The resulting pyroelectric activity was evaluated by measuring the output potential when different light sources irradiated the device. The piezoelectric activity was evaluated from sensitivity measurements. In the next section infrared sensors will be investigated to observe the pyroelectric effect in the printed P(VDF-TrFE) thin film. The following section will investigate accelerometers to observe the piezoelectric effect.

5.2 Sensor Fabrication

The printing methods described in Chapter 3 were used to fabricate the sensors on flexible substrates.

5.2.1 Screen and Stencil Printed Sensor Fabrication

The flexible substrates used in fabricating the devices were a 51 μm thick Kapton E® polyimide film by DuPont, and a 100 μm thick transparent polyester film by 3M. The top-view of the sensor is shown in Figure 4.1 with the different geometries of the contacts fabricated in Figure 4.2. The P(VDF-TrFE) layer was one square inch in all devices. The side-view of the sensors is shown in Figure 5.3.

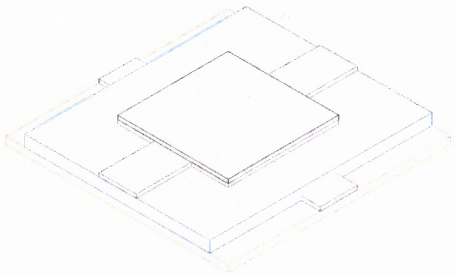

Figure 5.1 Top-view of the sensors.

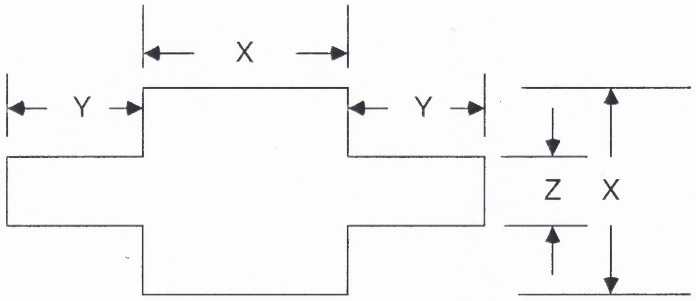

X	Y	Z
0.5	0.4	0.25
0.375	0.5	0.12
0.31	0.53	0.06

Figure 5.2 Geometries of the bottom and top contacts for the sensors.

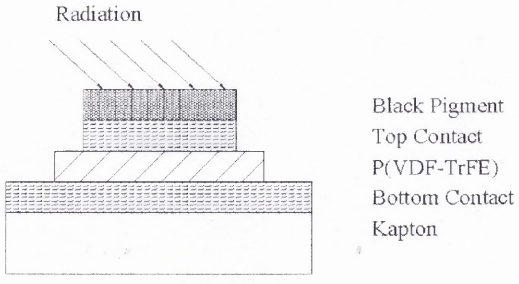

Figure 5.3 Side-view of the sensors.

All substrates were cleaned in acetone, isopropanol, and distilled water. The process flow of the sensors is depicted in Figure 5.4. The first layer deposited, the bottom contact, via screen and stencil printing was DuPont's microcircuit materials

CB028 silver conductor polymer thick film composition. The next layer printed via screen and stencil printing was P(VDF-TrFE) which was printed directly on top of the silver bottom contact layer. The next layer deposited, via screen and stencil printing, on top of the P(VDF-TrFE) was another layer of DuPont's silver for use as the top contact for the sensors. And the final layer, the black pigment, was spray coated. The final layer increased the absorption of incoming radiation for the IR sensors and had no effect in the operation of the accelerometers. The approximate thicknesses of the layers are stated in Table 5.1.

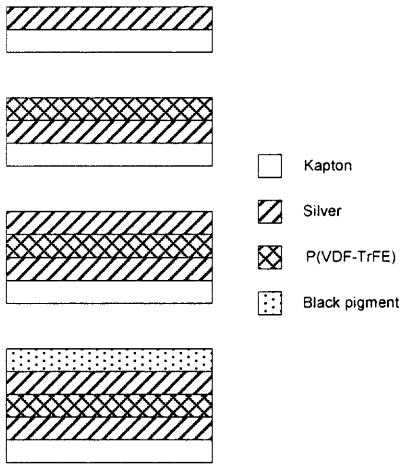

Figure 5.4 Process flow for the sensors. Top view is as depicted in Figure. 4.1. (a) Screen printing of Ag on Kapton substrate. (b) Screen printing of P(VDF-TrFE). (c) Screen printing of Ag on P(VDF-TrFE). (d) Spray coating of black pigment.

Table 5.1 Approximate Screen and Stencil Printed Sensor Layer Thicknesses Deposited

Layer	Approximate Screen Printed Thickness	Approximate Stencil Printed Thickness
Kapton E	51 μm	51 μm
3M Transparency	110 μm	110 μm
Bottom Electrode	20 - 130 μm	20 – 35 μm
P(VDF-TrFE)	10 - 200 μm	20 - 300 μm
Top Electrode	20 - 130 μm	20 - 35 μm
Black Pigment	0.1 -1 μm	0.1 -1 μm

5.2.2 Ink-jet Printed Sensor Fabrication

Due to the limitation of speed of the commercial print system utilized in this study the size of the sensors needed to be reduced in order to have reasonable print time, days compared to weeks. The flexible substrates used in fabricating the devices were a 51 μm thick Kapton HN® polyimide film by DuPont. The top-view of the sensor is shown in Figure 5.5 with the different geometries of the contacts fabricated in Figure 5.6. The side-view of the sensors is shown in Figure 5.7.

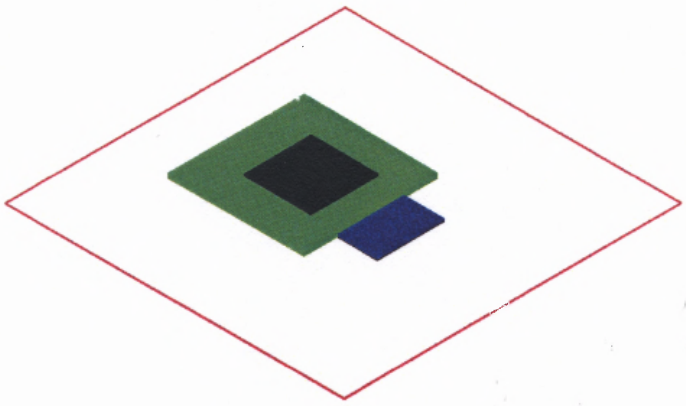

Figure 5.5 Top view of the sensors.

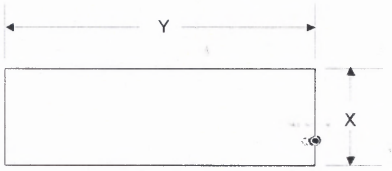

Bottom Contact		Middle Layer		Top Contact	
x (mm)	y (mm)	x (mm)	y (mm)	x (mm)	y (mm)
2.5	10	6.0	8.0	2.5	6
2.0	5.0	4.0	3.5	2.0	2
1.5	3.0	5.5	3.5	1.5	1

Figure 5.6 Geometries of the bottom, middle and top layers for the ink-jet printed sensors.

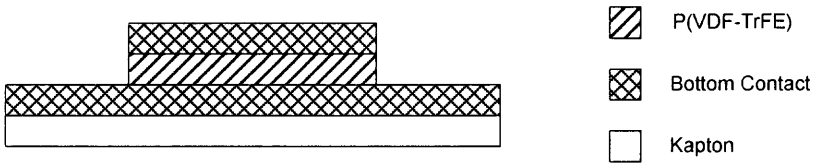

Figure 5.7 Side-view of the ink-jet printed sensors.

All substrates were cleaned in acetone, isopropanol, and distilled water. The process flow of the sensors is depicted in Figure 5.8. The first layer deposited, the bottom contact, was HC. Starck Baytron P JET conductive polymer. The next layer printed was P(VDF-TrFE) which was printed directly on top of the bottom contact layer. The next layer deposited, on top of the P(VDF-TrFE) was another layer of HC. Starck Baytron P JET for use as the top contact for the sensors.

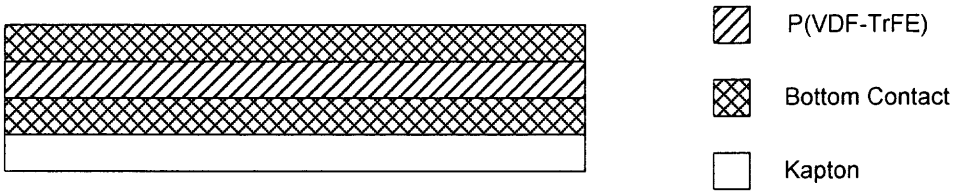

Figure 5.8 Process flow for the ink-jet printed sensors. Top view is as depicted in Figure. 5.5. (a) Printing of the Batron P Jet on Kapton substrate. (b) printing of P(VDF-TrFE). (c) printing of P Jet on P(VDF-TrFE).

Table 5.2 Approximate Ink-Jet Printed Sensor Layer Thicknesses

Layer	Approximate Thickness
Kapton E	51 μm
Bottom Electrode	7 - 30 μm
P(VDF-TrFE)	5 - 10 μm
Top Electrode	7 – 30 μm

5.3 Infrared Sensors

5.3.1 Infrared Sensor Design

The infrared sensors fabricated in this study are pyroelectric thermal-type. The pyroelectric element is sandwiched between two silver contacts. The sensitive area is defined by the overlap between these contacts. A black pigment is deposited on the top contact. When the pigment is irradiated with infrared radiation, the infrared radiation is converted into heat which is transferred to the pyroelectric element. The absorbed heat in the pyroelectric P(VDF-TrFE) leads to a change in temperature and consequently to a voltage change. A screen printed IR sensor is depicted in Figure 5.9.

The functionality of the presented IR sensor is based on the spontaneous polarization change of a pyroelectric film when the top contact is exposed to infrared radiation. The voltage produced in the film is given by,

$$V = \frac{pt\Delta T}{\varepsilon} \qquad (5.1)$$

where p is the pyroelectric coefficient, t is the film thickness, ΔT is the change in temperature, and ε is the permittivity of material.

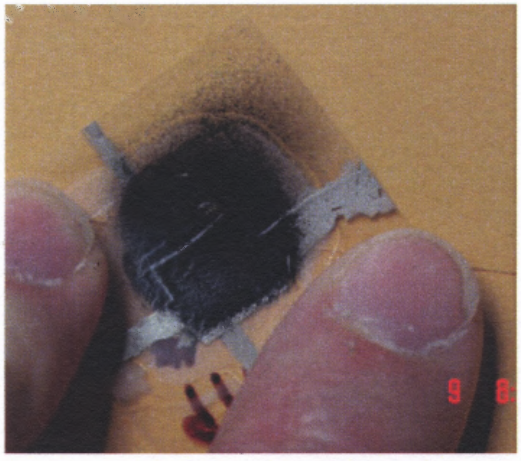

Figure 5.9 Screen printed IR sensor.

5.3.2 Infrared Sensor Testing

The measurement system that was used for detecting the voltage from the pyroelectric sensor is shown in Figure 5.6. The sensitivity of the sensors was measured using various light sources, such as a He-Ne laser (wavelength λ= 0.6328 μm), a Ti:Sa laser (wavelength λ= 0.78 μm), a CO2 laser (wavelength λ= 11.3 μm), and a heat lamp. For all experiments, the light beam was mechanically chopped at 100 Hz. The beam irradiated the top contact as shown in Figure 5.6. The pyroelectric voltage signal was measured using a lock-in amplifier (Model 7260, EG&G, Princeton, NJ) and a digitizing oscilloscope (Model HP- 54501A, Hewlett-Packard), while the detector was exposed to the incident chopped radiation. The power of the light source was measured by an optical power meter before the beam was chopped.

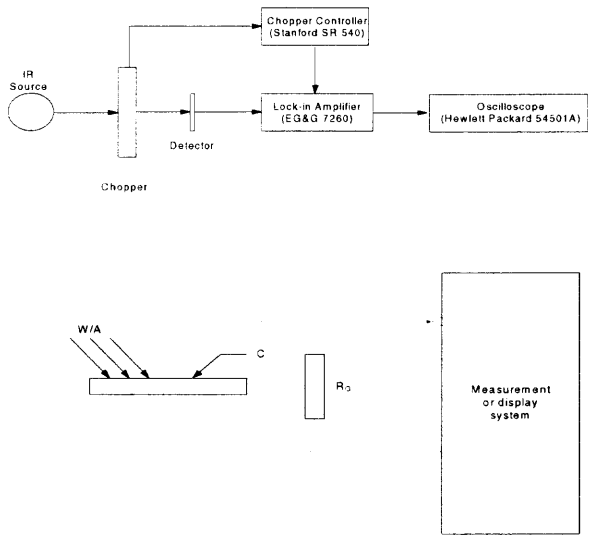

Figure 5.10 a) A common pyroelectric detecting system b) Schematic diagram for sensor response measurements.

5.4 Accelerometers

5.4.1 Accelerometer Design

The accelerometers fabricated in this study are compression-type, as opposed to the shear or bending type. The piezoelectric compression transducer incorporates a piezoelectric layer with contacts on the top and bottom of the piezoelectric layer. When the transducer is subjected to motion, a force is generated which acts on the piezoelectric layer to produce an electrical output proportional to the acceleration/deceleration. The accelerometer is depicted in Figure 5.11.

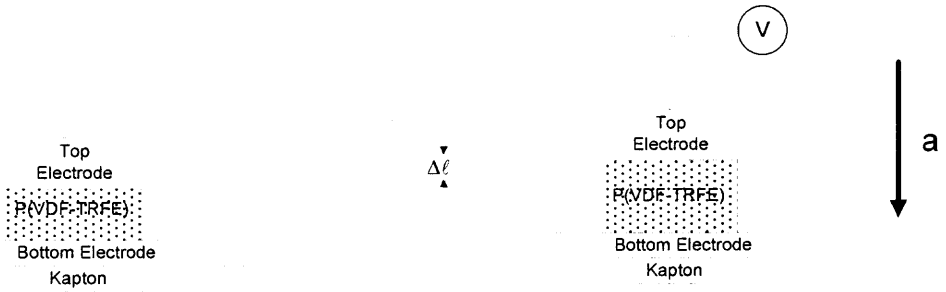

Figure 5.11 Compression accelerometer.

The fundamental linear relationships between the electrical and mechanical quantities of a piezoelectric material for determining the relationship between the voltage and force is described by the direct piezoelectric effect [127] and is given by,

$$E = -gT + \frac{D}{\varepsilon^T} \tag{5.2}$$

where E is the electric field, T is the stress, D is the electric displacement, ε^T is permittivity under the condition of constant stress and g is the piezoelectric voltage constant.

Setting D =0, due to the fact that the electrodes are not shorted and no current flows results in

$$E = -gT. \tag{5.3}$$

But voltage is related to the electric field times the thickness ℓ of the piezoelectric element, such that,

$$V = E\ell$$

where ℓ is the thickness of the piezoelectric layer and stress is force per area,

$$T = \frac{-F}{A}.$$

Inserting these relations in to Equation 5.3 for the electric field one readily obtains,

$$\frac{V}{\ell} = g\frac{F}{A}$$

a relationship between the voltage and force. Rearrangement results in,

$$V = g\frac{\ell}{A}F. \tag{5.4}$$

As can be seen in Equation 5.4 the voltage on the piezoelectric material due to an applied force is dependent on the geometry and g the piezoelectric voltage constant which happens to be temperature dependent.

The natural resonant frequency is given by,

$$f_r = \frac{1}{2\pi}\sqrt{\frac{k}{M + \frac{1}{3}m}} \tag{5.5}$$

where k is the stiffness of the piezoelectric element, M is the mass of the seismic mass, and $m = \rho V$ is the mass of the piezoelectric element.

The stiffness of the piezoelectric element is given by,

$$k = \frac{Ac_{33}^{E}}{\ell} \tag{5.7}$$

where c_{33}^{E} is the stiffness coefficient of the piezoelectric element. The sensitivity can be determined starting with Equation 5.3 that relates voltage to stress,

$$V = -g\ell T \tag{5.8}$$

Using the relation where stress is force per area and force is mass times acceleration (a),

$$T = \frac{Ma}{A}$$

and substituting back into Equation 5.8 one readily obtains,

$$V = ga\ell\frac{M}{A}$$

The sensitivity when the mass of the piezoelectric element is negligible is

$$S_V = \frac{V}{a} = g\frac{\ell}{A}M \tag{5.9}$$

The sensitivity when the mass of the piezoelectric element is not negligible is

$$S_V = \frac{V}{a} = g\frac{\ell}{A}\left(M + \frac{m}{2}\right) \tag{5.10}$$

And the sensitivity when there is no seismic mass is

$$S_V = \frac{V}{a} = g\frac{\ell}{A}\frac{m}{2} = \frac{1}{2}\rho g\ell^2 \tag{5.11}$$

5.4.2 Accelerometer Testing

The back-to-back method has been used to measure the sensitivity of the printed sensors. The back-to-back method is an industry standard method used by accelerometer manufacturers to calibrate devices [128, 129].

The vibration test system in Figure 5.12 was constructed to test the fabricated sensors. The Bruel & Kjaer 4809 vibration exciter is capable of 44.5 N sine peak rated force and 60 N rated force with air cooling, at frequencies from 10 Hz to 20 kHz, with maximum acceleration of 75 g and 100 g with air cooling. The fabricated sensors have been tested using a comparison calibration method. This method entails mounting both a known accelerometer (Endevco 2221D) and the printed accelerometer to a fixture. This fixture was then mounted on the Bruel & Kjaer 4809 vibration exciter as shown in Figure 5.8. The 2221D has a transverse sensitivity of 0.9%, capacitance of 870 pF and a charge sensitivity of 16.5 pC/g over the range 1 Hz to 6 kHz [130, 131]. The input acceleration is the same for both devices and the ratio of their outputs is also the ratio of their sensitivities. The sensitivity of the printed sensors has been calculated using Equation 5.12.

$$S_u = S_r \frac{V_u}{V_r} \tag{5.12}$$

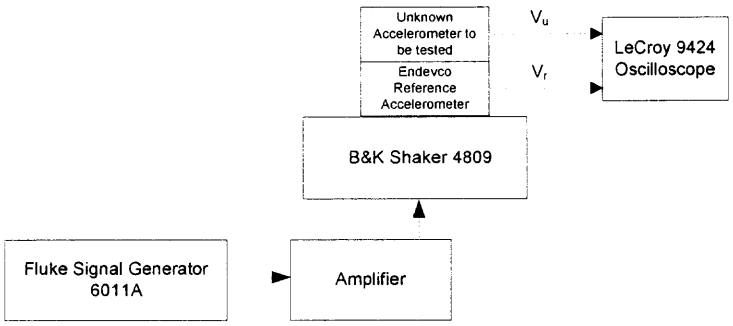

Figure 5.12 Back to back calibration of accelerometer.

5.5 Results and Discussions

5.5.1 Results and Discussions on the Pyroelectric Sensor

For each of the light sources employed, there was no detectable pyroelectric response. Even in the case of physical damage (burning) of the sample using a powerful CO_2 laser beam, no pyroelectric response was detected. In each test, if some pyroelectric response were present, its value was below the noise limits of the detection system.

In order to determine if the sensors should have produced an observable signal, an estimate of the expected signal based on the known thermal and pyroelectric properties of the materials used in the sensor was performed. Using Equation 5.1 and values from the literature, the pyroelectric conversion has been calculated as seen in Table 5.2. The calculated pyroelectric conversion factor ($\Delta V / \Delta T = pt / \varepsilon$ from Equation 5.1) for a commercial PVDF film (Measurement Specialties, Hampton Va.) as seen in Table 5.2 is half the value of the deposited P(VDF-TrFE) film.

The temperature difference ΔT is estimated based on a thermal diffusion equation,

$$\rho s \frac{\partial \Delta T}{\partial t} = \sigma \nabla^2 \Delta T + Q_L \tag{5.13}$$

where Q_L is the rate of laser energy deposited per unit volume per unit time. The spot size of the illumination was approximated to be 2 mm. The layer thicknesses and thermal properties of the two layers are tabulated in Table 5.3. Since the layers are so thin, heat will equilibrate much more rapidly perpendicular to the plane of the film compared to parallel to the film. Consequently, it is assumed that the films under the area being illuminated by the light are all at the same temperature and all of these films are in equilibrium. In the lateral direction, however, the heat is dissipated predominately by thermal conduction in the silver conductor due to the high thermal conductivity compared to the pigment/ P(VDF-TrFE) layers.

The rate of the lateral heat dissipation can be estimated from Equation 5.13 by balancing the equation with no laser heating term (eg. The chopper blocks the illuminating radiation). In that case, Equation 5.13 reduces to

$$\frac{\partial \Delta T}{\partial t} = \frac{\sigma}{\rho s} \nabla^2 \Delta T \tag{5.14}$$

In the lateral direction, the spatial scale over which there is a gradient in the temperature is the spot size of the laser. Therefore, one can estimate that

$$\nabla^2 \Delta T \sim \frac{\Delta T}{d^2} \tag{5.15}$$

where d is the spot size of the laser. Using Equations 5.14 and 5.15, the time scale for lateral dissipation of heat is estimated as

$$\tau_{Lat} \sim \frac{\rho s}{\sigma} d^2 \sim \frac{d^2}{\alpha} \tag{5.16}$$

where α is the thermal diffusivity. Using d = 0.2 cm and α from Table 5.3 gives a lateral diffusion time of 23 ms corresponding to ~43Hz. Therefore, for a chopper modulation

rate of ~100Hz the heat should be laterally diffusing. When the sample is illuminated, the estimated temperature rise is given by the right-hand side of Equation 5.13. For short time periods, there is not sufficient time for lateral diffusion of heat. The light induced temperature change can then be approximated from

$$0 = \sigma \nabla^2 \Delta T + Q_L \tag{5.17}$$

to be

$$\Delta T \sim \frac{d^2}{\sigma} Q_L \tag{5.18}$$

In estimating Q_L, we account for the emissivity of the $\varepsilon_n = 0.876$ of the black pigment [132]. About 10% power is approximated to be absorbed by the material as the black pigment is intended as a layer to reduce the reflection of the incoming heat. Assuming that the optical energy is distributed evenly in the volume defined by the combined thickness of the three layers and the spot size of the optical beam, we estimate the corresponding temperature rise and expected pryoelectric voltage for each light source in Table 5.5.

Table 5.3 Parameters used for Calculating IR Sensor Performance

	Thickness t (μm)	Specific heat s (J/mg K)	Density ρ (mg/cm^3)	Pyroelectric coefficient p (Cm^{-2}K^{-1})	Permittivity ε (Fm^{-1})	Pyro-electric conversion (V/K)
PVDF	2.80E-05	1.28	1.8	3.00E-05	1.09E-10	8
P(VDF-TrFE)	2.80E-05	1.28	1.8	4.00E-05	7.00E-11	16

Table 5.4 Parameters Used for Calculation of Expected Output Voltage

	Thickness t (cm)	Area A (cm^2)	Thermal Conductivity σ (W/cm K)	Specific heat* Density s*ρ (J/ cm K)	Thermal diffusivity α (cm^2/s)
Black pigment	0.00001	0.03142	0.0030	0.14	0.0214
Silver contact	0.00008	0.03142	4.1700	2.4	1.7375
P(VDF-TrFE)	0.00028	0.03142	0.0013	2.3	0.0006

Table 5.5 Expected Output Voltages for the Various Light Sources

Laser Source	Absorbed Power q_k (W)	Temperature Difference (ΔT) (K)	Expected Voltage V_e (V)
HeNe	0.0005	7.181E-05	0.0011
Ti:Sa	0.0300	4.376E-03	0.0700
CO_2	0.1000	1.436E-02	0.2298

A potential of the order of 1 mV is calculated in Table 5.5 for the HeNe laser. This potential of 1 mV would not have been detectable with a measured noise level of 55 mV on the oscilloscope. When the EG&G 7260 lock-in amplifier is used, the average measured noise level was 0.65 μV. This noise level is lower than the expected voltage level for all three different light sources. In conclusion, we should have had enough experimental sensitivity to detect the pryoelectric response of the film provided that the response was comparable to previously published values.

The negligible pyroelectric response of these samples is attributed to the lack of poling of the sample. While there have been no reports on the value of the pyroelectric coefficient of PVDF or any copolymers prior to poling, the expected enhancement can be estimated based on other materials. Butler et al. [133] has reported that a YBaCuO thin film deposited by RF magnetron sputtering at room temperature with gold contacts have exhibited pyroelectric coefficients in the range of 65 nC/ cm^2-K prior to poling. When poled, the pyroelectric coefficient was found to increase to 18 μC/cm^2-K. The pyroelectric behavior in Butler's device prior to poling has been explained as a strain-poled case when the films are fabricated a mechanical strain is induced in which the domains line up in one direction.

For comparison, we calculate the expected output of our device based on the pyroelectric value of poled PVDF reported by Capineri et al. [134]. The expected output voltage of their sensor is in good agreement with our fabricated sensor, as seen in Table 5.6. They fabricated their sensor on a glass-epoxy substrate that had a copper electrode. A PVDF film was epoxied to the contact and a black pigment was spray coated to enhance absorption. The PVDF film that was epoxied to the substrate was pre-poled from the manufacturer.

The deposited P(VDF-TrFE) films exhibited piezoelectric activity. As Lee et al. [135] state, the copolymer directly crystallizes in the piezoelectric β phase, which is the polar form of PVDF and its copolymers. It is possible to increase the piezoelectric and pyroelectric activity by poling the material, capacitive poling can be performed at room temperature on the samples that had a lack of response as described by Kohler et al. [136].

Table 5.6 Expected Output Voltages for Capineri Sensor [134]

	Thickness t (cm)	Specific heat s ($Jcm^{-3}K^{-1}$)	Thermal Conductivity σ ($Wcm^{-1}K^{-1}$)	Power (q_k) W	T_1-T_4 (K)	Expected Voltage V (V)
Black Pigment	0.0004	0.14	0.0030	0.000165	1.577E-04	0.0013
Silver Contact	0.00004	2.4	4.1700			
P(VDF-TrFE)	0.00028	2.3	0.0013			

5.5.2 Results and Discussions on the Accelerometer

The anticipated performance of the screen and stencil printed devices was calculated for the three geometries shown in Figure 5.2. The expected performance of the ink-jet printed devices was calculated for the three geometries shown in Figure 5.6. The piezoelectric voltage constant was calculated using the values of the piezoelectric charge constant and the average values of the permittivity with the typical values of the material properties for P(VDF-TrFE) given in Table 2.2. The sensitivity was calculated for the fabricated sensors using Equation 5.11 ($S_V = \frac{1}{2}\rho g \ell^2$). The calculated sensitivity for the ink-jet, screen and stencil printed sensors is shown in Table 5.7 and Table 5.8. A Mitutoyo digital micrometer with a resolution of 0.001 mm and an accuracy of ±.00005 in. (0.00127 mm) was used to measure film thickness for the devices in Table 5.7. The film thickness measures for Table 5.8 were made by cross sectioning the device and making the measurements under an Olympus Vanox microscope with a Mitutoyo 164-162 digital micrometer with a resolution of 0.001 mm and an accuracy of ±.00015 in. (0.00381 mm). From this data it can be seen that the film thickness variations and sensitivities of the devices varies significantly in all cases.

Table 5.7 Thickness of Piezoelectric Pads and Anticipated Sensitivity for the Ink-Jet, Screen and Stencil Printed Sensors Measured With a Mututoyo 293-335 Digital Micrometer

	Screen	Stencil	Ink-jet
Thickness of PE mt (μm)	10 - 200	20 - 300	5 - 10
Minimum Sensitivity (mV/g)	0.049	0.197	0.012
Maximum Sensitivity (mV/g)	19.729	44.39	0.049

These devices have NJIT part numbers NJIT-SC/ST/IJ-Vibration-W-XXX-52HN/52E/3M

Table 5.8 Thickness of Piezoelectric Pads and Anticipated Sensitivity for the Ink-Jet, Screen and Stencil Printed Sensors Measured Under an Olympus Vanox Microscope with a Mututoyo 164-162 Digital Micrometer

	Screen	Stencil	Ink-jet
Thickness of PE mt (μm)	200 - 560	50 - 120	70 - 90
Minimum Sensitivity (mV/g)	19.729	1.233	2.417
Maximum Sensitivity (mV/g)	154.674	7.102	3.995

Film thicknesses variations in the case of the screen printed devices are due to the manual screen printing set-up and the use of fabric screens. These discrepancies are due to the fabric screens lying in the ink as the ink is being deposited and the when the screen is removed the ink creates non-uniformities as it is pulled out of the wet ink. Further improvement in fabrication consistency can be achieved by controlling the process. Building a print box to control the screen position and using metal screens that have their patterns generated by photolithography will remedy these issues.

Film thicknesses variations of the stencil printed devices were due to the use of the roller in applying the ink through the stencil. The roller was used to apply the ink due to the squeegee having issues with pushing the ink under the stencil. Improvements in fabrication can be achieved by building a print box to control the stencil position and using metal stencils.

Film thickness variations were minimal for the ink-jet printed films and were generally caused by defective ink-jet cartridges and nozzles. While printing the nozzles would clog and in worst case the cartridge would only out put a fraction of the ink specified leading to non-uniformities in film thicknesses. In other cases there were complete failures of the cartridge in which the ink was no longer being jetted from the nozzle but was sprayed out parallel to the substrate surface resulting in undefined films as seen in Figure 3.11. Further improvement in fabrication consistency can be achieved by

being very aware of the ink-jet cartridge and at any sign of malfunction replacing it with a new cartridge.

Vibration measurement accuracy depends on device mounting, measurement location is repeatable and ensuring device mass is much less than the fixture (to ensure there is no mass load effects). The initial fixture constructed for the testing is shown in Figure 5.13. The fixture was designed to verify that the devices had an output voltage. This fixture has a top plate fabricated out of thin plastic that cover the printed sensor. The under side of this top plate has a spongy foam material covered by conductive tape at the contact region and is bare in the active region. This material was intended so that the top plate would not be in contact with the active region (i.e. the top plate would not add mass to the sensor). Also the underside of this top plate had guide marks so that the sensor could be placed in the same location for repeatability of measurements. Between the bottom surface of the sensor and the bottom fixture plate was a thin sheet of rubber to ensure that there was good electrical contact.

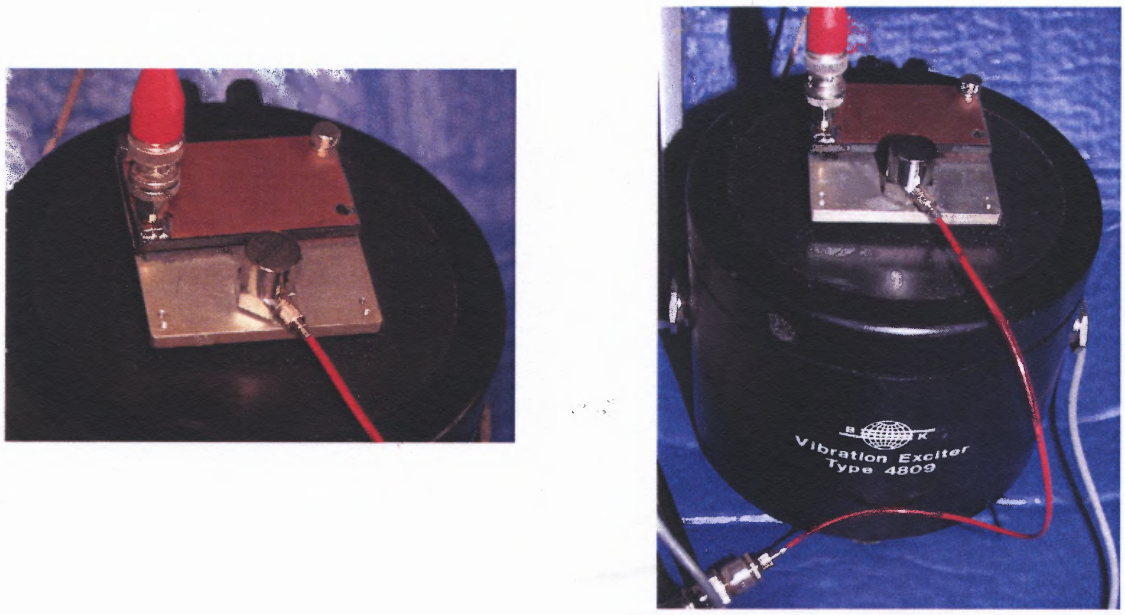

Figure 5.13 Initial test fixture for the back-to-back measurement of the printed accelerometer.

The vibration test system in Figure 5.8 was used to test the fabricated sensors. Initial testing was performed from 10 Hz to 100 Hz in steps of 5 Hz from 10 to 30 Hz, then in steps of 25 Hz from 50 to 100 Hz. Between the 50 and 75 Hz measurements there was a dramatic jump in output voltage for both the commercial and printed sensors. This increase was thought to be a resonance of that fixture and all measurements were made from 10 to 30 Hz in 5 Hz steps. Table 5.9 compares the measured sensitivity to the calculated. In all cases, with the exception of NJIT-ST-Vibration-W-003-52E, the measured value is an order of magnitude greater then the calculated. To verify that the top plate was in fact not adding mass to the sensor the top plate of the fixture was modified

Table 5.9 Average Measured Results Compared to the Calculated Sensors Performance

Sensor	Sensitivity Measured (mV/g)	Sensitivity Calculated (mV/g)	Variation in film thickness
NJIT-ST-Vibration-W-003-52E	39.5	0.2 to 22	0.020 to 0.200 μm
NJIT-ST-Vibration-W-004-52E	39.7	2.4 to 4	0.07 to 0.09 μm
NJIT-SP-Vibration-W-002-3M	38.5	1.8 to 9.0	0.06 to 0.135 μm
NJIT-SP-Vibration-W-002-52E	31.1	0.4 to 6.0	0.03 to 0.110 μm
NJIT-IJ-Vibration-W-006-52HN	5.67	0.012 to 0.049	0.005 to 0.010 μm
NJIT-IJ-Vibration-W-002-52HN	9.68	0.012 to 0.049	0.005 to 0.010 μm

Figure 5.14 shows the modified fixture. The devices were placed on the fixture such that the active region of the sensor was aligned with the hole in the top plate of the modified fixture and additional measurements were made such that the active region was under the top plate. In the case of the ink-jet printed sensors, the sensors were placed under the smaller hole on the left side of the top plate. Measurements of the ink-jet printed sensors were made with the sensor the right and left of the hole such that the devices were covered by the top plate plus measurements were obtained where the sensors active region was between the hole in the fixture. Table 5.10 compares the

measured sensitivity to the calculated. The measured output voltage of the sensor with the active region not exposed to the top plate increase by four times that of the unmodified fixture and the measurement on either side of the hole varied as initially expected. To determine that this was no due to increased distance that the active region could move the rubber insert was removed and the measurements repeated.

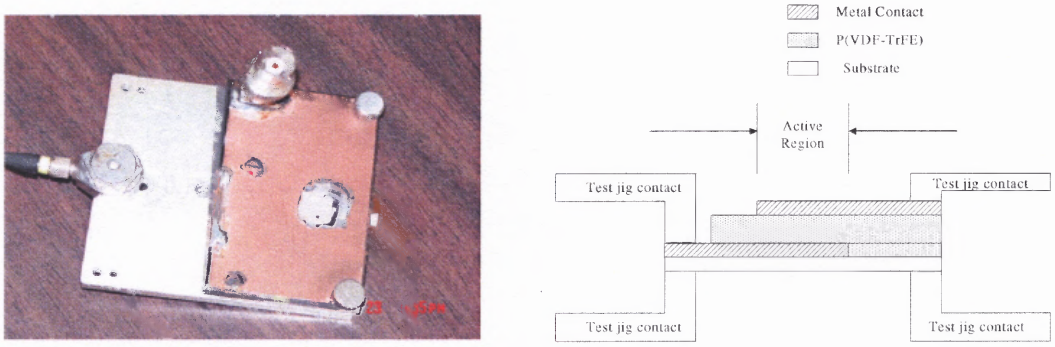

Figure 5.14 Modified test fixture for the back-to-back measurement of the printed accelerometer.

Table 5.10 Average Measured Results Compared to the Calculated Sensors Performance for the Modified Fixture

Sensor NJIT-IJ-Vibration-W-002-52HN	Sensitivity Measured (mV/g)	Sensitivity Calculated (mV/g)	Variation in film thickness
Active region exposed	39.9	9.68	0.012 to 0.049
Active region to the right of the hole	24	9.68	0.012 to 0.049
Active region to the left of the hole	16.7	9.68	0.012 to 0.049

The rubber insert was removed fro8m the modified fixture. The devices were placed on the fixture again such that the active region of the sensor was aligned with the hole in the top plate of the modified fixture and to the left and right side of the hole in the top plate. Table 5.11 compares the measured sensitivity to the calculated. The measured output voltage of the sensor with the active region not exposed to the top plate was measured to be 10.1 mV/g which within 2.1% of the calculated value. The

measurements on either side of the hole were as much as 22% lower then the calculated value. To further see the effects of the top plate the fixture was further modified and the measurements repeated.

Table 5.11 Average Measured Results Compared to the Calculated Sensors Performance for the Modified Fixture Without the Rubber Insert

Sensor NJIT-IJ-Vibration-W-002-52HN	Sensitivity Measured (mV/g)	Sensitivity Calculated (mV/g)	Variation in film thickness
Active region exposed	10.1	9.68	0.012 to 0.049
Active region to the right of the hole	7.61	9.68	0.012 to 0.049
Active region to the left of the hole	6.2	9.68	0.012 to 0.049

Figure 5.15 shows the typical response curves for the Endevco and the ink-jet printed sensor. From Equation 5.4 ($V = g\frac{\ell}{A}F$) and Newton's second law ($F = ma$) we see that the curve of the output voltage verses gravitational force is linear. The curve of output voltage verses frequency goes as the square of the frequency as acceleration is the second derivative of the displacement ($a = x_0\omega^2 \sin(\omega t)$).

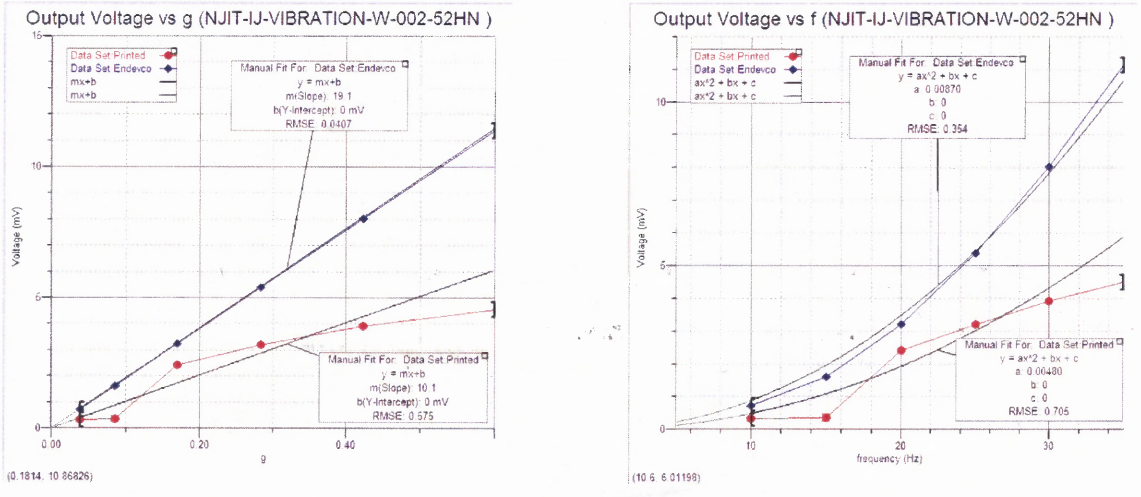

Figure 5.15 Active region of the sensor exposed .

Figure 5.16 and Figure 5.17 shows the typical response curves for the Endevco and the ink-jet printed sensor shifted slightly to the right and slightly to the left of the hole in the fixture. Again in both cases we see that the data falls within the linear and quadratic fits as they should. When the sensor is moved to different positions the vibration measurement accuracy is not repeatable.

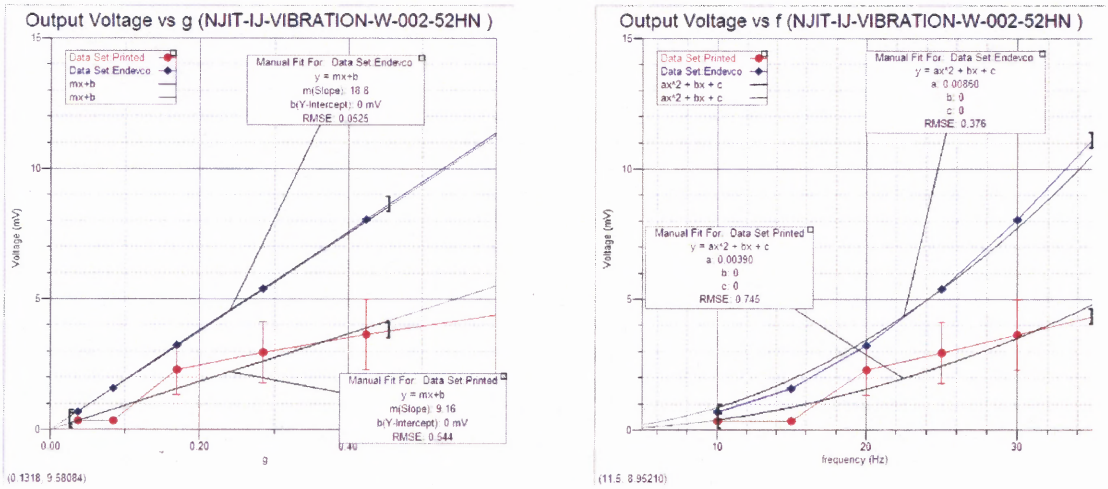

Figure 5.16 Sensor measured toward the edge of the top plate

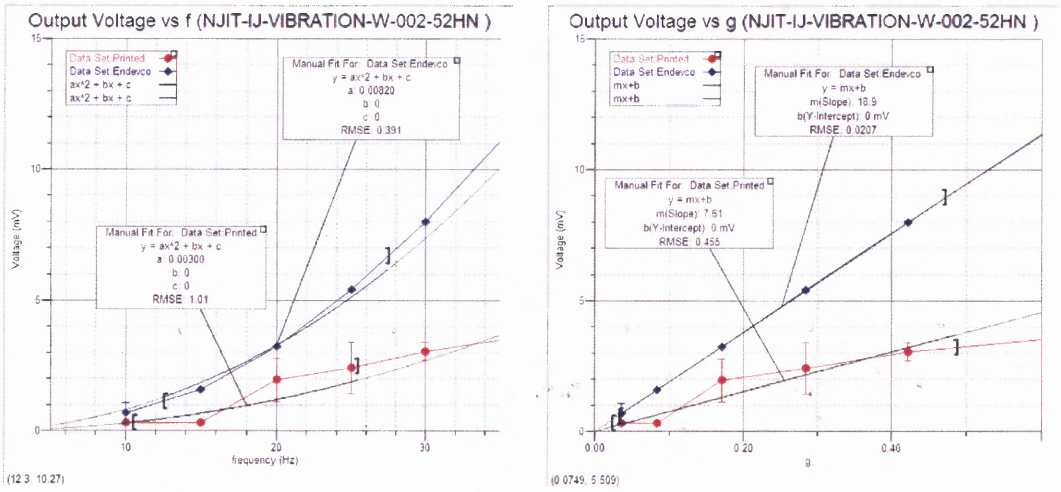

Figure 5.17 Sensor measured toward the center of the top plate.

Figure 5.14 shows the modified fixture. The devices were stuck on double sided tape to the base of the fixture. 0.007 inch diameter gold wire was solder with indium from the sensor to a printed circuit board which had leads soldered to them. Initial testing was performed from 10 Hz to 500 Hz in steps of 5 Hz from 10 to 30 Hz, then in steps of 25 Hz from 50 to 100 Hz and then in steps of 100 Hz from 100 Hz to 500 Hz. No response was measured in the printed sensor below 50 Hz. Between the 300 and 400 Hz measurement there was a dramatic drop in output voltage for the commercial sensor. This decrease was thought to be a resonance of that fixture and all measurements were made from 50 to 300 Hz in 25 Hz steps from 50 to 100 Hz and then in 100 Hz steps from 100 to 300 Hz. The measured sensitivity of NJIT-IJ-Vibration-W-002-52HN was 0.039 mV/g. A potential cause to this low value is that when the thin gold wires where repeatedly vibrated they would break. Also the Indium solder joint would break and the connection was intermittent.

Figure 5.14 Redesigned test fixture.

The deposited P(VDF-TrFE) films exhibited piezoelectric activity. The fixture was found to be critical in measuring these devices. As seen with the data the fixture with the hole and the rubber insert removed gave the best results. Further engineering of the fixture is required to get optimum results.

5.6 Conclusions

This study demonstrates the potential of a flexible polyimide infrared sensor, with a unique inexpensive fabrication technique. There has been no output voltage from the printed IR sensors to date; the potential reason may be due to non-crystalline polymer films or the incorrect phase of the polymer. The films need to be poled to see if the pyroelectric coefficients can be increased.

Initial poling of the current IR sensors can potentially be done utilizing capacitive poling where by the fabricated sensors are inserted between two plates and a potential applied. Kohler et al. [136] has successfully poled P(VDF-TrFE) sensors at room temperature with a poling strength of 120 v/μm, the time that the potential is applied will need to be studied. Also, when more samples are fabricated prior to the deposition of the top contact, the samples can be corona poled. The samples would be placed on a heated grounded metal plate, a probe would be located approximately 2 cm above the sample to supply a charge to the surface creating a potential difference between the top and bottom surfaces.

This study was able to demonstrate the piezoelectric activity in the P(VDF-TrFE) films by fabrication of accelerometers. The output voltage from the printed accelerometers was compared to the output of an Endevco accelerometer and the sensitivity of the printed device was calculated and measured. The crystallinity of the polymer films was sufficient in the case of the accelerometers; the tested device exhibits average voltage sensitivity within 2.1% of the calculated value. The films did not need to be poled to observe their piezoelectric activity.

The data obtained utilizing the finial fixture shown in Figure 5.14, was plotted and did not exhibit the quadratic trend as expected from Equation 5.11. This is due to the changing amplitude of the exciter, as the frequency is increased the impedance of the

exciter changes leading to the changing amplitude. Therefore the sensitivity of the printed sensors was calculated with the ratio given in Equation 5.12. The original fixture with the modifications did not exhibit this effect, but the sensors were tested at much lower frequencies from 10 to 30 Hz.

CHAPTER 6

CONCLUSION AND FUTURE WORK

6.1 Conclusion

From the early concepts of flexible electronics at the turn of the 20th century, this technology has come a long way. The initial concepts of flexible interconnects have evolved into versatile devices with applications from areas such as flexible display technology and wearable electronics to sensing. Flexible electronics is just beginning to develop. This rapidly changing area of study is on the cusp of great advances as new materials are engineered and new fabrication techniques are developed.

The present work has documented some of the preliminary issues with the ink-jet printing of a metal organic silver ink. Due to the immaturity of the commercial ink-jet print system used in this study, issues with adhesion and conductivity were observed. These issues were overcome by the use of commercial inks. The H.C. Starck Baytron P Jet material was printed on Kapton and on P(VDF-TrFE). Adhesion was adequate while conductivity was low but working accelerometers were fabricated.

Table 6.1 Comparison of Printing Techniques

	Ink-Jet	Screen	Stencil
Mask generation	Easy	Moderate	Moderate
Cost of Masks	No Cost	Inexpensive	Inexpensive
Cost of Consumables	Moderate	Inexpensive	Inexpensive
Speed of depositing films	Slow	Fast	Fast
Available inks	Few	Many	Many
Synopsis	High resolution devices	Refined proto-types	Quick proto-types

The attributes of the three printing techniques used in this study are compared in Table 6.1. Generation of masks for ink-jet printing entailed specifying the dimensions in the software provided with the printer. On the other hand the masks for screen and stencil printing required transferring the pattern to specific media, screen or stencil. The cost of all the screens and stencils generated for this study were under $100 for the screens and under $35 for the stencils. The cost of the consumables for ink-jet printing were relatively high, each layer requires a cartridge at a cost of $59 plus the syringe to fill the cartridge. From the printer company these cartridges are one time use items. The screens and stencils on the other hand can be reused and were reused without any major problems. Other consumables have equivalent costs for the three methods of printing. The main hindrance to ink-jet printing was found to be the speed of printing. Multiple sheets of sensor devices could be printed with the other two methods in the same time required to print the bottom contact layers using ink-jet printing. Over all the ink-jet method produced uniform, high quality devices where as the screen and stencil methods generated rapid devices.

The present work has also documented the success with the deposition of thin films by screen and stencil printing. DuPont screen printable inks were deposited via screen and stencil printing on Kapton, transparency films and copy paper. All the conductive films exhibited excellent adhesion and very high conduction. Multi-layer films were successfully fabricated. These low temperature, rapid, simple printing methods could be adapted for mass production.

6.2 Future Work

The ultimate goal of this project was to develop simpler cost effective methods for fabricating flexible electronics. Screen and stencil printing have provided quick methods

for depositing many different thin films on flexible substrates. While ink jet printing was slower over all it allows for rapid art work modifications and high print resolution. These three methods open the area up to the researcher without access to fabrication facilities. First and foremost, cost effective and simpler methods were demonstrated and successful working devices were fabricated.

Finally in this concluding section, with particular reference to this present dissertation, some further research is posed below. The aim is to incite future researchers to continue the present quest to further development of low temperature active flexible thin films with not only the application of sensors but also for display technology and energy scavenging.

- Preliminary electrical measurements were made on the devices. Further characterization of frequency response, and impact spectrum could be ascertained.
- Initial studies of aqueous solution techniques for the synthesis of flexible ceramic thin films have been carried out but not reported in this research. Aqueous solution techniques are well published in journals and very inexpensive to realize. Further work in structural characterization and then transferring the process to ink-jet printing could lead to vast possibilities.
- Investment in a semi-automated screen printing set-up could lead to better results in terms of better agreement in electrical performance from device to device.
- Development of composite inks, such as PZT powder with polymer, could be formulated to improve the sensor performance.
- Modifications to the commercial ink-jet materials printer system should be implemented to increase the system's effectiveness. Increases in speed, platen temperature and drop volume could improve the overall performance of this system.

APPENDIX A

INK FORMULATION RECIPE FOR INK-JET, SCREEN AND STENCIL PRINTING

The HC Starck materials and solvents should be at room temperature when mixing the inks.

Ink-jet metal contacts:

1. Place a 30 ml beaker on a digital scale and then zero the scale.
2. Shake the Baytron P Jet (P Jet) bottle vigorously for approximately 10 seconds.
3. Dispense approximately 5 mL of the P Jet material into a 30 ml beaker.
4. With a syringe remove approximately 3 mL from the dispensed P Jet material and dispense the syringed material into the 30 ml beaker on the scale (this material should weight approximately 3 grams).
5. Calculate 4% of the measured value (in the case of 3 grams the calculated value is 0.12g ±0.03 (c) this is the amount of solvent to be added to the P Jet material.
6. Dispense approximately 2 ml of ethylene glycol into a 30 ml beaker.
7. With a syringe remove approximately 1 mL from the dispensed ethylene glycol material and dispense the calculated value from the syringe into the 30 ml beaker on the scale (this material should be approximately 8 drops).
8. Remove the beaker with the P Jet material and ethylene glycol (ink) from the scale and place it on a hotplate that is capable of stirring.
9. Place a small magnetic stirrer in the beaker with the ink that is on the hotplate.
10. Set the hotplate to room temperature and the stirrer to 3 or approximately 100 rpm. The ink should be stirring with the magnetic stirrer lying in the ink. The stirrer should not be violently rotating if the stirrer is lower the sped or move the beaker to a different spot on the hotplate.
11. After 30 minutes remove the beaker of ink from the hotplate.
12. Use a syringe to remove the ink from the beaker and it is ready to dispense into the ink-jet cartridge.

Notes:

a. All beaker sizes are recommended sizes bigger beakers can be used if the size stated is unavailable.

b. If HC Starch Baytron P Jet N is available skip steps 4 -11.

c. This tolerance is ±1% of the calculated 4%.

Ink-jet polymer:

1. Place a 30 ml beaker on a digital scale and then zero the scale.

2. Place 0.2 g (approximately 20 pellets) of the polymer into the beaker on the scale.

3. Dispense approximately 12 mL of the DMF into a 30 ml beaker.

4. With a syringe remove approximately 10 mL from the dispensed DMF material and dispense the syringed material into the 30 ml beaker on the scale (this material should weight approximately 9 grams).

5. Remove the beaker with the polymer and DMF (ink) from the scale and place it on a hotplate that is capable of stirring.

6. Place a small magnetic stirrer in the beaker with the ink that is on the hotplate.

7. Set the hotplate to 50 C and the stirrer to 3 or approximately 100 rpm. The ink should be stirring with the magnetic stirrer lying in the ink. The stirrer should not be violently rotating if the stirrer is lower the sped or move the beaker to a different spot on the hotplate.

8. After 30 minutes check to see that the polymer pellets have dissolved. If they have then remove the beaker of ink from the hotplate.

9. Use a syringe to remove the ink from the beaker and it is ready to dispense into the ink-jet cartridge.

Screen and stencil printed polymer:

1. Place a 30 ml beaker on a digital scale and then zero the scale.
2. Place 2 g (approximately 100 pellets) of the polymer into the beaker on the scale.
3. Dispense approximately 12 mL of the Acetone into a 30 ml beaker.
4. With a syringe remove approximately 10 mL from the dispensed Acetone material and dispense the syringed material into the 30 ml beaker on the scale (this material should weight approximately 9 grams).
5. Remove the beaker with the polymer and Acetone (ink) from the scale and place it on a hotplate that is capable of stirring.
6. Place a small magnetic stirrer in the beaker with the ink that is on the hotplate.
7. leave the hotplate at room temperature 22 C and set the stirrer to 3 or approximately 100 rpm. The ink should be stirring with the magnetic stirrer lying in the ink. The stirrer should not be violently rotating if the stirrer is lower the sped or move the beaker to a different spot on the hotplate.
8. After 30 minutes check to see that the polymer pellets have dissolved. If they have then remove the beaker of ink from the hotplate.

H.C. Starck contact:
Paul Poirier
Customer Service Representative
Electronics & Optics Group
H.C. Starck Inc.
Newton, MA 02461/USA
T 617-630-5831
F 617-559-3906
paul.poirier@hcstarck.com

Baytron P Jet - http://www.clevios.com/index.php?page_id=995&prod_service_id=310
Baytron P Jet N -
http://www.clevios.com/index.php?page_id=995&prod_service_id=1051

Solvent contact:
Frank Grodio
KEM Chemical Corporation
P.O. Box 3019
Mount Vernon, NY 10553
(914) 699-3110

Ethylene glycol - http://www.jtbaker.com/msds/englishhtml/E5125.htm

Dimethylformamide (DMF) - http://www.jtbaker.com/msds/englishhtml/D6408.htm

VF2-TRFE Contact:
Solvay Solexis
Michael Krauss
Hylar Segment Manager
NAFTA Sales Manager - Melts Fluoropolymers
Office: 856-251-3439
Mobile: 856-693-5638

Solef VF2TrFe 75/25 (P(VDF-TrFE) 75:25)

APPENDIX B

FABRICATION RECIPE

The power to the Dimatix system should be switched on and the lid to the system should be closed. Next, open the Dimatix Drop Manager (DDM) software, either by the clicking on the shortcut on the desktop or under the start button.

The first tab of the DDM software prompts you to install the cartridge. Prepare the ink and cartridge as per Appendix A. Open the lid of the printer. Insert the cartridge firmly into the holder on the printer with the electrical connection side toward the back of the printer. Pull the latch forward and down until it clicks and firmly puts the cartridge into place, the cartridge should sit flat in the holder. Close the lid to the print system. The Select Cartridge Settings window will pop up and prompt for the cartridge settings file. Click yes to load the last file used.

Click on the second tab, select pattern, choice the appropriate file to be printed. Table B.1 lists the files and the geometries for the fabricated sensors.

The third tab prompts you to load the substrate. Under "Substrate Settings:" thickness [in microns] and temperature [degrees C] select the appropriate setting from Table B.2. If an individual sensor is to be printed use the higher temperature value to drive off the solvent more rapidly.

To load the substrate, open the lid of the print system. Align the clean substrate to the register mark in the back left corner on the platen. Use Scotch tape on the four corners to assure that the substrate does not move during printing. Close the lid on the print system. Back in the DDM software under the Substrate Settings section click on the on button to turn on the vacuum.

Click on the forth tab, Printer Set-up. Under cartridge settings select the file kate.jst. In the bottom right corner of the DDM window click on the Drop Watcher button. Both the Cartridge Settings window and the Drop Watcher window will pop up.

In the Drop Watcher window under cleaning select the file kate.clc. Click on the Waveform tab in the Cartridge Settings window. In the Firing voltage section of this tab, click on the button Reset, to reset all the nozzle firing voltages to sixteen volts. Back in the Drop Watcher window on the right side is an image of the nozzles. With the mouse click in this area, and hold the left mouse button as you drag the mouse to the left. You want to get nozzle one on the screen. Once you have nozzle one on the screen click on the box below the number 1. If ink jets from the nozzle unselect the box other wise leave it selected and move to the next nozzle until you have checked each nozzle. If all the nozzles do not jet increase the jetting potentials of those that do not jet to twenty volts. Starting at nozzle 16 click the box below the number 16 if it jets unselect the box otherwise leave it selected. Continue until all the nozzles have been checked. Increase the jetting potential of those nozzles that did not jet by five volts and repeat the above procedure until all jets are firing. All nozzles may not have the same jetting potential and may differ from one printing to the next.

In the Cartridge Settings window select the Cartridge tab. Set the Cartridge Temperature to ambient by clicking on the down arrow until a dashed line appears in the Temperature Setpoint box. Leave the Meniscus Setpoint and the Cartridge Print Height at the default of 2.5 and 1.000 respectively. If the first or last nozzles do not jet change the number of Jets to reflect this and the Starting jet if applicable.

In the Cartridge Settings window select the Cleaning Cycle tab. Change the Start of Printing and During Printing files to NONE. Set the End of printing and While Idle

files to kate.clc. leave the Run every value set to the default of 300 seconds. In order for the changes to take effect, go to file and save the changes.

In the Drop Watcher window go to file and exit to return to the DDM window and to return the cartridge carriage to it original position.

In the DDM window under the Print Pattern section select edit and verify that the drop spacing, number of layers and the other dimensions are the same as in Table B.1 and B.2. Once these data are verified save the changes, if there are any, and close the window.

In the bottom right of the DDM window click on the print button, the print preview window will appear. This window shows the pattern to be printed and then gives the number of jets to be used if these appear to be correct click on the print button, if the information is not correct click on the cancel button and fix the error.

Table B.1 Sensor File Pattern Block Drop Position Details

Pattern Block Drop Position				Pattern Block Array					
Shock_B.ptn									
x start	x width	y start	y height	x start	x width	x pitch	y start	y width	y pitch
6.75	1.5	6	3	5	15	30	5	15	30
Shock_M.ptn									
x start	x width	y start	y height	x start	x width	x pitch	y start	y width	y pitch
4.75	5.5	4.5	3.5	5	15	30	5	15	30
Shock_T.ptn									
x start	x width	y start	y height	x start	x width	x pitch	y start	y width	y pitch
6.75	1.5	6	1	5	15	30	5	15	30
IR_B.ptn									
x start	x width	y start	y height	x start	x width	x pitch	y start	y width	y pitch
6.5	2	5	5	5	15	30	5	15	30
IR_M.ptn									
x start	x width	y start	y height	x start	x width	x pitch	y start	y width	y pitch
5.5	4	7	3.5	5	15	30	5	15	30
IR_T.ptn									
x start	x width	y start	y height	x start	x width	x pitch	y start	y width	y pitch
6.5	2	7.75	2.25	5	15	30	5	15	30

Table B.2 Sensor Jetting Parameters

	Sensor		Substrate Settings		Pattern Editor	
Layer	Shock	IR	Thickness [microns]	Temperature [degrees C]	Drop Spacing	Layers
Bottom Contact	Shock_B	IR_B	100	ambient - 28	50/25	10/90
P(VDF-TrFE)	Shock_M	IR_M	500	ambient - 35	75/50	100/100
Top Contact	Shock_T	IR_T	700	ambient - 28	50/25	10/90

APPENDIX C

DEVICE FABRICATION MATRIX

The following tables describe the differences in the fabricated devices.

Mesh material in Table C.1 is Screen Fabric-Multifilament Polyester purchased at Jerrys artist outlet, West Orange, New Jersey

8XX = 86 holes per linear inch
12XX = 124 holes per linear inch
14XX = 138 holes per linear inch

Fabric with an undefined hole spacing was purchased at Jo-Ann Fabric, Middletown, NY and is called Shear in the Mesh of Table C.1

Table C.1 Screen Printed Device Matrix

	Bottom Contacts					Polymer Layer		
	Start Date	Mesh	Method of Drying	Temp (C)	Time (min)	Start Date	Mesh	Layers
NJIT-SP-Vibration-W-001-52E	9/7/2007	12XX	Box oven	165	60	9/24/2007	Shear	2
NJIT-SP-Vibration-W-002-52E	9/10/2007	12XX	Box oven	165	90	9/13/2007	M8/Painted	2
NJIT-SP-Vibration-W-003-52E	9/10/2007	12XX	Box oven	165	70	9/13/2007	M12/M8/Shear	4
NJIT-SP-Vibration-W-004-52E	9/17/2007	8XX	Hot plate	55	45	9/18/2007	M12/M8/Shear	6
NJIT-SP-Vibration-W-001-3M	9/17/2007	12XX	Air Dry		24 Hr	9/22/2007	M8	1
NJIT-SP-Vibration-W-002-3M	9/17/2007	8XX	Hot plate	40	120	9/18/2007	M8/Shear	3
NJIT-SP-Vibration-W-003-3M	9/17/2007	8XX	Hot plate	45	90	9/20/2007	M12/M8/Shear	4

	Top Contacts			
	Start Date	Mesh	Method of Drying	Time (Hr)
NJIT-SP-Vibration-W-001-52E	9/25/2007	12XX	Air Dry	24
NJIT-SP-Vibration-W-002-52E	9/25/2007	12XX	Air Dry	24
NJIT-SP-Vibration-W-003-52E	9/25/2007	12XX	Air Dry	24
NJIT-SP-Vibration-W-004-52E	9/25/2007	12XX	Air Dry	24
NJIT-SP-Vibration-W-001-3M	9/25/2007	12XX	Air Dry	24
NJIT-SP-Vibration-W-002-3M	9/25/2007	12XX	Air Dry	24
NJIT-SP-Vibration-W-003-3M	9/25/2007	12XX	Air Dry	24

Table C.2 Stencil Printed Device Matrix

	Bottom Contacts			Polymer Layer		Top Contact		
	Start Date	Method of Drying	Time (Hr)	Start Date	Number of layers	Start Date	Method of Drying	Time (Hr)
NJIT-ST-Vibration-W-001-52E	9/28/2007	Air Dry	24	10/1/2007	3	10/2/2007	Air Dry	24
NJIT-ST-Vibration-W-002-52E	9/28/2007	Air Dry	24	10/1/2007	3	10/2/2007	Air Dry	24
NJIT-ST-Vibration-W-003-52E	9/28/2007	Air Dry	24	10/1/2007	3	10/2/2007	Air Dry	24
NJIT-ST-Vibration-W-004-52E	10/1/2007	Air Dry	24	10/2/2007	4	10/2/2007	Air Dry	24
NJIT-ST-Vibration-W-001-3M	9/28/2007	Air Dry	24	10/1/2007	4	10/2/2007	Air Dry	24
NJIT-ST-Vibration-W-002-3M	9/28/2007	Air Dry	24	10/1/2007	4	10/2/2007	Air Dry	24
NJIT-ST-Vibration-W-003-3M	9/28/2007	Air Dry	24	10/1/2007	4	10/2/2007	Air Dry	24
NJIT-ST-Vibration-W-004-3M	9/28/2007	Air Dry	24	10/2/2007	1	10/2/2007	Air Dry	24
NJIT-ST-Vibration-W-005-3M	9/28/2007	Air Dry	24	10/2/2007	1	10/2/2007	Air Dry	24
NJIT-ST-Vibration-W-006-3M	9/28/2007	Air Dry	24	10/2/2007	1	10/2/2007	Air Dry	24

Table C.3 Ink-jet Printed Device Matrix

	Bottom Contacts				
	Start Date	Layers	Voltage	Spacing	# Jets
NJIT-IJ-Vibration-W-001-52HN	3/14/2008	25/44/51/30	27	75/25/30/35	16
NJIT-IJ-Vibration-W-002-52HN	3/17/2008	25/125	23	75/25	16
NJIT-IJ-Vibration-W-003-52HN	3/20/2008	99	16	30	16
NJIT-IJ-Vibration-W-004-52HN	3/19/2008	50/50	20	35/25	15
NJIT-IJ-Vibration-W-005-52HN	3/20/2008	99	16	30	16
NJIT-IJ-Vibration-W-006-52HN	3/17/2008	25/100	24	50/25	16
NJIT-IJ-IR-W-002-52HN	3/17/2008	25/125	23	75/25	16
NJIT-IJ-IR-W-003-52HN	3/20/2008	99	16	30	16

	Polymer Layer				
	Start Date	Layers	Voltage	Spacing	# Jets
NJIT-IJ-Vibration-W-001-52HN	3/15/2008	100/110/75	31	50/75/50	15
NJIT-IJ-Vibration-W-002-52HN	3/18/2008	25/100/50/203/99	25	75/50/45/55/75	15
NJIT-IJ-Vibration-W-003-52HN	3/21/2008	495	25	50	15
NJIT-IJ-Vibration-W-004-52HN	3/19/2008	352	25	75	15
NJIT-IJ-Vibration-W-005-52HN	3/21/2008	495	25	50	15
NJIT-IJ-Vibration-W-006-52HN	3/17/2008	55/100/100	25	50/25/75	15
NJIT-IJ-IR-W-002-52HN	3/18/2008	25/100/50/203/99	25	75/50/45/55/75	15
NJIT-IJ-IR-W-003-52HN	3/21/2008	495	25	50	15

Table C.3 (Cont.) Ink-jet Printed Device Matrix

	Start Date	Layers	Top Contact Voltage	Spacing	# Jets
NJIT-IJ-Vibration-W-001-52HN	3/16/08	25/75	-	75/30	13/12
NJIT-IJ-Vibration-W-002-52HN	3/18/08	5/93	27	50/25	15
NJIT-IJ-Vibration-W-003-52HN	3/21/08	99	-	35	16
NJIT-IJ-Vibration-W-004-52HN	3/20/2008	99	-	35	15
NJIT-IJ-Vibration-W-005-52HN	3/21/08	99	-	35	16
NJIT-IJ-Vibration-W-006-52HN	3/17/08	99	-	30	15
NJIT-IJ-IR-W-002-52HN	3/18/08	5/93	27	50/25	15
NJIT-IJ-IR-W-003-52HN	3/21/08	99	-	35	16

REFERENCES

[1] M. A. Dubois and P. Muralt, "Properties of aluminum nitride thin films for piezoelectric transducers and microwave filter applications," *Applied Physics Letters,* vol. 74, pp. 3032-3034, 1999.

[2] C. K. Chiang, C. R. Fincher, Y. W. Park, A. J. Heeger, H. Shirakawa, E. J. Louis, S. C. Gau, and A. G. MacDiarmid, "Electrical conductivity in doped polyacetylene," *Physical Review Letters,* vol. 39, pp. 1098-1101, 1977.

[3] H. Shirakawa, E. J. Louis, A. G. MacDiarmid, C. K. Chiang, and A. J. Heeger, "Synthesis of electrically conducting organic polymers: Halogen derivatives of polyacetylene, (CH)x," *Journal of the Chemical Society, Chemical Communications,* pp. 578-580, 1977.

[4] M. Jayakannan, S. R. Amrutha, and K. V. Sindhu, "Effect of composition on the conductivity and morphology of ligno sulfonic acid sodium salt doped polyaniline," *Journal of Applied Polymer Science,* vol. 101, pp. 2650-2655, 2006.

[5] L. R. Bao, B. Wei, and A. Y. Xiao, "Conductive coating formulations with low silver content," in *Proceedings - Electronic Components and Technology Conference*, 2007, pp. 494-500.

[6] R. N. Das, H. Lin, K. I. Papathomas, J. M. Lauffer, N. Card, and V. R. Markovich, "Printable nanocomposites for advanced organic packaging," in *Proceedings - Electronic Components and Technology Conference*, 2007, pp. 316-322.

[7] G. Dennler and N. S. Sariciftci, "Flexible conjugated polymer-based plastic solar cells: From basics to applications," *Proceedings of the IEEE,* vol. 93, pp. 1429-1439, 2005.

[8] S. E. Shaheen, Radspinner, R., Peyghambarian, N., Jabbour, G.E.,, "Fabrication of bulk heterojunction plastic solar cells by screen printing," *Applied Physics Letters,* vol. 79, pp. 2996 - 2998, 2001.

[9] S. Choi and Z. Jiang, "A novel wearable sensor device with conductive fabric and PVDF film for monitoring cardiorespiratory signals," *Sensors and Actuators, A: Physical,* vol. 128, pp. 317-326, 2006.

[10] H.-h. Chang, C.-c. Wu, C.-c. Yang, C.-w. Chen, and C.-c. Lee, "Multicolor organic LEDs processed by integration of screen printing and thermal transfer printing," in *Proceedings of SPIE - The International Society for Optical Engineering*, 2000, pp. 127-134.

[11] R. Mannerbro, M. Ranlof, N. Robinson, and R. Forchheimer, "Inkjet printed electrochemical organic electronics," *Synthetic Metals.*

[12] Independent research and analysis on Printed Electronics IDTechEx Inc Retrieved April 24, 2008 from the World Wide Web: http://printedelectronics.idtechex.com/printedelectronics/en/

[13] ORGANIC ELECTRONICS: Materials, Physics, Chemistry and Applications http://www.elsevier.com/wps/find/journaldescription.cws_home/620806/description#description

[14] H. C. Lim, B. Schulkin, M. J. Pulickal, S. Liu, R. Petrova, G. Thomas, S. Wagner, K. Sidhu, and J. F. Federici, "Flexible membrane pressure sensor," *Sensors and Actuators, A: Physical,* vol. 119, pp. 332-335, 2005.

[15] A. Mahmood, D. P. Butler, and Z. Celik-Butler, "Micromachined bolometers on polyimide," *Sensors and Actuators, A: Physical,* vol. 132, pp. 452-459, 2006.

[16] S. Y. Xiao, L. F. Che, X. X. Li, and Y. L. Wang, "A novel fabrication process of MEMS devices on polyimide flexible substrates," *Microelectronic Engineering,* vol. 85, pp. 452-457, 2008.

[17] Mylar® Polyester Film, Professional Plastics Retrieved from the World Wide Web: http://www.professionalplastics.com/cgi-bin/pp.pl?pgm=co_disp&func=displ&strfnbr=3&prrfnbr=85435&sesent=0,0&srch_pid=94463&search_id=118080

[18] DuPont Kapton® HN Polyimide Film Data Sheet, DuPont Retrieved March 7, 2008 from the World Wide Web: http://www2.dupont.com/Kapton/en_US/assets/downloads/pdf/HN_datasheet.pdf

[19] Polyimide, Wikipedia Retrieved March 7, 2008 from the World Wide Web: http://en.wikipedia.org/wiki/Polyimides

[20] Si - Silicon Thermal Properties, Ioffe Physico-Technical Institute Retrieved from the World Wide Web: http://www.ioffe.ru/SVA/NSM/Semicond/Si/thermal.html

[21] Laminates and Flexible Circuit Materials, Rogers Corporation Retrieved February 13, 2007 from the World Wide Web: http://www.rogerscorporation.com/acm/about_our_products.htm#1000

[22] DuPont Pyralux AX Copper-Clad Laminate All-Polyimide Flexible Laminate, DuPont Electronic Materials Retrieved Febrauary 13, 2007 from the World Wide Web: http://www2.dupont.com/Pyralux/en_US/assets/downloads/pdf/AX_datasheet.pdf

[23] T. Afentakis, M. Hatalis, A. T. Voutsas, and J. Hartzell, "Design and fabrication of high-performance polycrystalline silicon thin-film transistor circuits on flexible steel foils," *IEEE Transactions on Electron Devices,* vol. 53, pp. 815-822, 2006.

[24] Semiconductor film transfer process Concept of "flexible devices" Kanagawa Academy of Science and Technology Retrieved March 3, 2008 from the World Wide Web: http://www.newkast.or.jp/english/projects/pro_fujioka.html

[25] Lehigh University Center for Optical Technologies Flexible Electronics Brochure, Lehigh University Center for Optical Technologies Retrieved January 12, 2008 from the World Wide Web: http://www.lehigh.edu/optics/Documents/2003OpenHouse/PDF%20Posters/Flexible_Electronics_poster.pdf

[26] J. Stringer, X. Bojun, and B. Derby, "Characterization of photo-reduced silver organometallic salt deposited by inkjet printing," in *International Conference on Digital Printing Technologies*, 2007, p. 960.

[27] N. Zhao, M. Chiesa, H. Sirringhaus, Y. Li, Y. Wu, and B. Ong, "Self-aligned inkjet printing of highly conducting gold electrodes with submicron resolution," *Journal of Applied Physics,* vol. 101, 2007.

[28] M. Green, "Organometallic based strategies for metal nanocrystal synthesis," *Chemical Communications,* pp. 3002-3011, 2005.

[29] Z. Liu, Y. Su, and K. Varahramyan, "Inkjet-printed silver conductors using silver nitrate ink and their electrical contacts with conducting polymers," *Thin Solid Films,* vol. 478, pp. 275-279, 2005.

[30] Use of Inherently Conductive Polymers in Coatings & Inks, SpecialChem Coating & Inks Retrieved May 8, 2008 from the World Wide Web: http://www.specialchem4coatings.com/resources/articles/article.aspx?id=6858

[31] A. Morrin, O. Ngamna, E. O'Malley, N. Kent, S. E. Moulton, G. G. Wallace, M. R. Smyth, and A. J. Killard, "The fabrication and characterization of inkjet-printed polyaniline nanoparticle films," *Electrochimica Acta,* vol. 53, pp. 5092-5099, 2008.

[32] U. Lang, P. Rust, and J. Dual, "Towards fully polymeric MEMS: Fabrication and testing of PEDOT/PSS strain gauges," *Microelectronic Engineering.*

[33] A. Michalska, M. Skompska, J. Mieczkowski, M. Zago?rska, and K. Maksymiuk, "Tailoring solution cast poly(3,4-dioctyloxythiophene) transducers for potentiometric all-solid-state ion-selective electrodes," *Electroanalysis,* vol. 18, pp. 763-771, 2006.

[34] M. Al-Ibrahim, A. Konkin, H. K. Roth, D. A. M. Egbe, E. Klemm, U. Zhokhavets, G. Gobsch, and S. Sensfuss, "Phenylene-ethynylene/phenylene-vinylene hybrid polymers: Optical and electrochemical characterization, comparison with poly[2-methoxy-5-(3 ,7 -dimethyloctyloxy)-1,4-phenylene vinylene] and application in flexible polymer solar cells," *Thin Solid Films,* vol. 474, pp. 201-210, 2005.

[35] J. W. Andreasen, S. A. Gevorgyan, C. M. Schleputz, and F. C. Krebs, "Applicability of X-ray reflectometry to studies of polymer solar cell degradation," *Solar Energy Materials and Solar Cells,* vol. 92, pp. 793-798, 2008.

[36] J. P. Lock, J. L. Lutkenhaus, N. S. Zacharia, S. G. Im, P. T. Hammond, and K. K. Gleason, "Electrochemical investigation of PEDOT films deposited via CVD for electrochromic applications," *Synthetic Metals,* vol. 157, pp. 894-898, 2007.

[37] B. D. Chin, N. S. Kang, J. W. Yu, S. Mu Jo, and J. Y. Lee, "Role of the interfacial layer in the efficiency and lifetime of polymeric light emitting devices," *Journal of Applied Physics,* vol. 102, 2007.

[38] J. Jang, J. Ha, and K. Kim, "Organic light-emitting diode with polyaniline-poly(styrene sulfonate) as a hole injection layer," *Thin Solid Films,* vol. 516, pp. 3152-3156, 2008.

[39] J. Windle and B. Derby, "Ink jet printing of PZT aqueous ceramic suspensions," *Journal of Materials Science Letters,* vol. 18, pp. 87-90, 1999.

[40] B. Y. Tay and M. J. Edirisinghe, "Investigation of some phenomena occurring during continuous ink-jet printing of ceramics," *Journal of Materials Research,* vol. 16, pp. 373-384, 2001.

[41] New buffer sublayers with crystal structure of cubic syngony for growing the heteroepitaxial films of nitride compounds of type AIIIBV on sapphire substrates, MRS Internet Journal Nitride Semiconductor Research Retrieved December 22, 2006 from the World Wide Web: http://nsr.mij.mrs.org/4/13/text.html

[42] J. Molarius, J. Kaitila, T. Pensala, and M. Ylilammi, "Piezoelectric ZnO films by r.f. sputtering," *Journal of Materials Science: Materials in Electronics,* vol. 14, pp. 431-435, 2003.

[43] M. Ortega-Lopez, A. Avila-Garcia, M. L. Albor-Aguilera, and V. M. Sanchez Resendiz, "Improved efficiency of the chemical bath deposition method during growth of ZnO thin films," *Materials Research Bulletin,* vol. 38, pp. 1241-1248, 2003.

[44] T. Trindade, P. O'Brien, and N. L. Pickett, "Nanocrystalline semiconductors: Synthesis, properties, and perspectives," *Chemistry of Materials,* vol. 13, pp. 3843-3858, 2001.

[45] C. B. Murray, D. J. Norris, and M. G. Bawendi, "Synthesis and characterization of nearly monodisperse CdE (E = S, Se, Te) semiconductor nanocrystallites," *Journal of the American Chemical Society,* vol. 115, pp. 8706-8715, 1993.

[46] W. R. Small, F. Masdarolomoor, G. G. Wallace, and M. In Het Panhuis, "Inkjet deposition and characterization of transparent conducting electroactive

polyaniline composite films with a high carbon nanotube loading fraction," *Journal of Materials Chemistry,* vol. 17, pp. 4359-4361, 2007.

[47] A. J. Sandee, C. K. Williams, N. R. Evans, J. E. Davies, C. E. Boothby, A. Kohler, R. H. Friend, and A. B. Holmes, "Solution-processible conjugated electrophosphorescent polymers," *Journal of the American Chemical Society,* vol. 126, pp. 7041-7048, 2004.

[48] S. Supothina, M. R. De Guire, and A. H. Heuer, "Nanocrystalline tin oxide thin films via liquid flow deposition," *Journal of the American Ceramic Society,* vol. 86, pp. 2074-2081, 2003.

[49] R. Kumaresan, M. Ichimura, N. Sato, and P. Ramasamy, "Application of novel photochemical deposition technique for the deposition of indium sulfide," *Materials Science and Engineering B: Solid-State Materials for Advanced Technology,* vol. 96, pp. 37-42, 2002.

[50] P. O'Brien, T. Saeed, and J. Knowles, "Speciation and the nature of ZnO thin films from chemical bath deposition," *Journal of Materials Chemistry,* vol. 6, pp. 1135-1139, 1996.

[51] B. E. McCandless and W. N. Shafarman, "Chemical surface deposition of ultra-thin cadmium sulfide films for high performance and high cadmium utilization," in *Proceddings of the 3rd World Conference on Photovoltaic Energy Conversion,* 2003, pp. 562-565.

[52] B. E. McCandless and W. N. Shafarman, Chemical surface deposition of ultra-thin semiconductors US Patent and Trademark office granted patent #6,537,845,(2003)

[53] MicroFab Technote 99-01 Background on Ink-Jet Technology, MicroFab Technologies, Inc. Retrieved February 3, 2007 from the World Wide Web: http://www.microfab.com/equipment/technotes/technote99-01.pdf

[54] M. Dietze and M. Es-Souni, "Structural and functional properties of screen-printed PZT-PVDF-TrFE composites," *Sensors and Actuators, A: Physical,* vol. 143, pp. 329-334, 2008.

[55] I. Hafaiedh, S. Helali, K. Cherif, A. Abdelghani, and G. Tournier, "Characterization of tin dioxide film for chemical vapors sensor," *Materials Science and Engineering C,* vol. 28, pp. 584-587, 2008.

[56] S. Ito, T. N. Murakami, P. Comte, P. Liska, C. Gratzel, M. K. Nazeeruddin, and M. Gratzel, "Fabrication of thin film dye sensitized solar cells with solar to electric power conversion efficiency over 10%," *Thin Solid Films,* vol. 516, pp. 4613-4619, 2008.

[57] R. W. Kay, S. Stoyanov, G. P. Glinski, C. Bailey, and M. P. Y. Desmulliez, "Ultra-fine pitch stencil printing for a low cost and low temperature flip-chip assembly process," *IEEE Transactions on Components and Packaging Technologies,* vol. 30, pp. 129-136, 2007.

[58] R. Kisiel, J. Borecki, J. Felba, and A. Moscicki, "Technological aspects of applying conductive adhesives for inner connections in PCB," in *2004 4th IEEE International Conference on Polymers and Adhesives in Microelectronics and Photonics*, 2004, pp. 121-125.

[59] S. Aravamudhan, D. Santos, G. Pham-Van-Diep, and F. Andres, "A study of solder paste release from small stencil apertures of different geometries with constant volumes," in *Proceedings of the IEEE/CPMT International Electronics Manufacturing Technology (IEMT) Symposium*, 2002, pp. 159-165.

[60] J. Belmonte, "Trends in the stencil printing process," *SMT Surface Mount Technology Magazine,* vol. 19, pp. 18-20, 2005.

[61] S. Ufer, C. Mundt, B. Ash, and R. P. Buck, "Stencil printing of ion-selective membranes on flexible planar sensor arrays for cardiovascular applications," in *Annual International Conference of the IEEE Engineering in Medicine and Biology - Proceedings*, 1994, pp. 840-841.

[62] H. H. C. de Moor, J. Hoornstra, A. W. Weeber, A. R. Burgers, and W. C. Sinke, "Printing high and fine metal lines using stencils," in *Proceedings of the 14th European Photovoltaic Solar Energy Conference, Barcelona, Spain* 1994, pp. 404-407.

[63] B. Jaffe, "Piezoelectric Ceramics," Academic Press, 1971.

[64] W. G. Cady, *Piezoelectricity; an introduction to the theory and applications of electromechanical phenomena in crystals* vol. 1: New York, Dover Publications 1964.

[65] Y. Tajitsu, H. Ogura, A. Chiba, and T. Furukawa, "Investigation of switching characteristics of vinylidene fluoride/trifluoroethylene copolymers in relation to their structures," *Japanese Journal of Applied Physics, Part 1: Regular Papers & Short Notes,* vol. 26, pp. 554-560, 1987.

[66] R. G. Kepler and R. A. Anderson, "Ferroelectric polymers," *Advances in Physics,* vol. 41, pp. 1-57, 1992.

[67] P. Ueberschlag, "PVDF piezoelectric polymer," *Sensor Review,* vol. 21, pp. 118-125, 2001.

[68] H. P. Loebl, M. Klee, C. Metzmacher, W. Brand, R. Milsom, and P. Lok, "Piezoelectric thin AlN films for bulk acoustic wave (BAW) resonators," *Materials Chemistry and Physics,* vol. 79, pp. 143-146, 2003.

[69] R. S. Muller, "From IC's to microstructures: materials and technologies," *Acta Polytechnica Scandinavica, Electrical Engineering,* pp. 143-146, 1988.

[70] R. S. Naik, J. J. Lutsky, R. Reif, C. G. Sodini, A. Becker, Fetter, H. Huggins, R. Miller, J. Pastalan, G. Rittenhouse, and Y. H. Wong, "Measurements of the bulk, c-axis electromechanical coupling constant as a function of aln film quality," *IEEE Transactions on Ultrasonics, Ferroelectrics, and Frequency Control,* vol. 47, pp. 292-296, 2000.

[71] U. Ozgur, Y. I. Alivov, C. Liu, A. Teke, M. A. Reshchikov, S. Dog?an, V. Avrutin, S. J. Cho, and H. Morko, "A comprehensive review of ZnO materials and devices," *Journal of Applied Physics,* vol. 98, pp. 1-103, 2005.

[72] G. W. Bohannan, V. H. Schmidt, R. J. Conant, J. Hallenberg, C. Nelson, A. Childs, C. Lukes, J. Ballensky, J. Wehri, B. Tikalsky, and E. McKenzie, "Piezoelectric polymer actuators in a vibration isolation application," *Proceedings of SPIE - The International Society for Optical Engineering,* vol. 3987, pp. 331-342, 2000.

[73] G. Carlotti, F. S. Hickernell, H. M. Liaw, L. Palmieri, G. Socino, and E. Verona, "Elastic constants of sputtered aluminum nitride films," in *Proceedings of the IEEE Ultrasonics Symposium*, 1995, pp. 353-356.

[74] I. S. Didenko, "The experimental and theoretical characterization of the saw propagation properties for zinc oxide films on silicon carbide," *IEEE Transactions on Ultrasonics, Ferroelectrics, and Frequency Control,* vol. 47, pp. 179-187, 2000.

[75] T. Furukawa, "Piezoelectricity and pyroelectricity in polymers," *IEEE transactions on electrical insulation,* vol. 24, pp. 375-394, 1989.

[76] J. G. Gualtieri, J. A. Kosinski, and A. Ballato, "Piezoelectric materials for acoustic wave applications," *IEEE Transactions on Ultrasonics, Ferroelectrics, and Frequency Control,* vol. 41, pp. 53-59, 1994.

[77] F. S. Hickernell, "ZnO PROCESSNG FOR BULK- AND SURFACE-WAVE DEVICES," *Ultrasonics Symposium Proceedings,* vol. 2, pp. 785-794, 1980.

[78] F. S. Hickernell, "Measurement techniques for evaluating piezoelectric thin films," in *Proceedings of the IEEE Ultrasonics Symposium*, 1996, pp. 235-242.

[79] P. Muralt, "PZT thin films for microsensors and actuators: Where do we stand?," *IEEE Transactions on Ultrasonics, Ferroelectrics, and Frequency Control,* vol. 47, pp. 903-915, 2000.

[80] W. Tjhen, T. Tamagawa, C. P. Ye, C. C. Hsueh, P. Schiller, and D. L. Polla, "Properties of piezoelectric thin films for micromechanical devices and systems," in *Micro Electro Mechanical Systems, 1991, MEMS '91, Proceedings. An*

Investigation of Micro Structures, Sensors, Actuators, Machines and Robots. IEEE, 1991, pp. 114-119.

[81] F. Xu, S. Trolier-McKinstry, W. Ren, B. Xu, Z. L. Xie, and K. J. Hemker, "Domain wall motion and its contribution to the dielectric and piezoelectric properties of lead zirconate titanate films," *Journal of Applied Physics,* vol. 89, pp. 1336-1348, 2001.

[82] Q. M. Zhang, Z. Y. Cheng, V. Bharti, T. B. Xu, H. Xu, T. Mai, and S. J. Gross, "Piezoelectric and electrostrictive polymeric actuator materials," *Proceedings of SPIE - The International Society for Optical Engineering,* vol. 3987, pp. 34-50, 2000.

[83] A. Arora, V. K. Dwivedi, P. J. George, K. Sreenivas, and V. Gupta, "Zinc oxide thin film-based MEMS acoustic sensor with tunnel for pressure compensation," *Sensors and Actuators, A: Physical,* vol. 141, pp. 256-261, 2008.

[84] C. C. Chang and S. K. Fang, "A study of the design of ZnO thin film pressure sensors," *International Journal of Electronics,* vol. 87, pp. 1013-1023, 2000.

[85] D. L. DeVoe, "Piezoelectric thin film micromechanical beam resonators," *Sensors and Actuators, A: Physical,* vol. 88, pp. 263-272, 2001.

[86] D. L. DeVoe and A. P. Pisano, "Fully surface-micromachined piezoelectric accelerometer," in *International Conference on Solid-State Sensors and Actuators, Proceedings*, 1997, pp. 1205-1208.

[87] D. L. DeVoe and A. P. Pisano, "Surface micromachined piezoelectric accelerometers (PiXLs)," *Journal of Microelectromechanical Systems,* vol. 10, pp. 180-186, 2001.

[88] A. Kuoni, R. Holzherr, M. Boillat, and N. F. De Rooij, "Polyimide membrane with ZnO piezoelectric thin film pressure transducers as a differential pressure liquid flow sensor," *Journal of Micromechanics and Microengineering,* vol. 13, pp. S103-S107, 2003.

[89] X. Ma, P. Chen, D. Li, Y. Zhang, and D. Yang, "Electrically pumped ZnO film ultraviolet random lasers on silicon substrate," *Applied Physics Letters,* vol. 91, 2007.

[90] M. Wang and X. Wang, "P3HT/ZnO bulk-heterojunction solar cell sensitized by a perylene derivative," *Solar Energy Materials and Solar Cells,* vol. 92, pp. 766-771, 2008.

[91] M. Allahverdi, A. Hall, R. Brennan, M. E. Ebrahimi, N. Marandian Hagh, and A. Safari, "An overview of rapidly prototyped piezoelectric actuators and grain-oriented ceramics," *Journal of Electroceramics,* vol. 8, pp. 129-137, 2002.

[92] P. Muralt and J. Baborowski, "Micromachined ultrasonic transducers and acoustic sensors based on piezoelectric thin films," *Journal of Electroceramics,* vol. 12, pp. 101-108, 2004.

[93] B. Sun and V. Qiu, "Rectangular shape distributed piezoelectric actuator: Analytical analysis," *Smart Materials and Structures,* vol. 13, pp. 337-349, 2004.

[94] Q. M. Wang, Z. Yang, F. Li, and P. Smolinski, "Analysis of thin film piezoelectric microaccelerometer using analytical and finite element modeling," *Sensors and Actuators, A: Physical,* vol. 113, pp. 1-11, 2004.

[95] G. T. Davis, M. G. Broadhurst, A. J. Lovinger, and T. Furukawa, "Hysteresis in copolymers of vinylidene fluoride and trifluoroethylene," *Ferroelectrics,* vol. 57, pp. 73-84, 1983.

[96] Y. Higashihata, J. Sako, and T. Yagi, "Piezoelectricity of vinylidene fluoride-trifluoroethylene copolymers," *Ferroelectrics,* vol. 32, pp. 85-92, 1981.

[97] J. C. Hicks, T. E. Jones, and J. C. Logan, "Ferroelectric properties of poly(vinylidene fluoride-tetrafluoroethylene)," *Journal of Applied Physics,* vol. 49, pp. 6092-6096, 1978.

[98] K. J. Humphrey, G. M. Garner, N. M. Shorrocks, and R. W. Whatmore, "The Dielectric Piezoelectric and Pyroelectric Properties of VDF-TrFE Copolymers," in *Applications of Ferroelectrics. 1986 Sixth IEEE International Symposium on*, 1986, pp. 543-546.

[99] N. C. Banik, F. P. Boyle, T. J. Sluckin, P. L. Taylor, S. K. Tripathy, and A. J. Hopfinger, "Theory of structural phase transitions in crystalline poly(vinylidene fluoride)," *The Journal of Chemical Physics,* vol. 72, pp. 3191-3196, 1979.

[100] T. Danno, H. Matsumoto, M. Nasir, S. Shimizu, M. Minagawa, J. Kawaguchi, H. Horibe, and A. Tanioka, "Fine structure of PVDF nanofiber fabricated by electrospray deposition," *Journal of Polymer Science, Part B: Polymer Physics,* vol. 46, pp. 558-563, 2008.

[101] Y. Hui, W. Liu, W. Luo, C. Yang, and X. Niu, "Effect of electric field on oriented poly(vinylidene fluoride) (PVDF) thin films prepared by vacuum evaporation," in *Proceedings of SPIE - The International Society for Optical Engineering*, 2007.

[102] Z. Dong, D. G. Huang, and D. Y. Zhang, "Preparation and design of PVDF pyroelectric thin film infrared and ultraviolet fire sensor," in *Proceedings of SPIE - The International Society for Optical Engineering*, 2005.

[103] T. M. Lee, A. P. Anderson, and F. A. Benson, "Microwave field-detecting element based on pyroelectric effect in PVDF," *Electronics Letters,* vol. 22, pp. 200-202, 1986.

[104] C. Christofides and A. Mandelis, "Photopyroelectric Pd-PVDF hydrogen sensor," in *Ultrasonics Symposium Proceedings*, 1989, pp. 613-616.

[105] J. J. Simonne, V. V. Pham, D. Esteve, J. Clot, A. Mahrane, and J. P. Beconne, "Visible/infrared integrated double detector: application to obstacle detection in automotive (Phase 2)," in *Proceedings of SPIE - The International Society for Optical Engineering*, 1991, pp. 139-147.

[106] Piezoelectric Ceramic Sensors (PIEZOTITE), Murata Manufacturing Co., Ltd. Retrieved March 11, 2008 from the World Wide Web: http://www.murata.com/catalog/p19e.pdf

[107] A. J. Lovinger, "Ferroelectric polymers," *Science,* vol. 220, pp. 1115-1121, 1983.

[108] A. J. Lovinger, *Developments in Crystalline Polymers; Bassett, D. C., Ed.; Applied Science Publishers: Oxford,* p. 5, 1982.

[109] H. S. Chavan, PhD Thesis, "Investigation of beta-phase poly(vinylidene fluoride) films using small-angle X-ray scattering", University of Cincinnati Cincinnati Ohio, (2006).

[110] R. W. Tyler, J. H. Webb, and W. C. York, "Measurements of electrical polarization in thin dielectric materials," *Journal of Applied Physics,* vol. 26, pp. 61-68, 1955.

[111] S. N. Fedosov, A. E. Sergeeva, and J. N. Marat-Mendes, "Anomalous apparent conductivity of PVDF and PT:P(VDF-TrFE) composites," in *Ferroelectrics*, 2003, pp. 93-103.

[112] B. Gross, R. Gerhard-Multhaupt, A. Berraissoul, and G. M. Sessler, "Electron-beam poling of piezoelectric polymer electrets," *Journal of Applied Physics,* vol. 62, pp. 1429-1432, 1987.

[113] D. Setiadi, T. D. Binnie, P. Regtien, and M. Wubbenhorst, "Poling of VDF/TrFE copolymers using a step-wise method," in *Proceedings - International Symposium on Electrets*, 1996, pp. 831-835.

[114] J. Krumpton, Personal Communication dated September 6, 2007.

[115] Dimatix Materials Printer DMP - 2800 Series Data sheet, Fujifilm Dimatic, Inc. Retrieved June 17, 2007 from the World Wide Web: http://www.dimatix.com/files/DMP-2831-Datasheet.pdf

[116] D. B. Bogy and F. E. Talke, "Experimental and theoretical study of wave propagation phenomena in drop-on-demand ink jet devices," *IBM Journal of Research and Development,* vol. 28, pp. 314-321, 1984.

[117] Sankir, PhD Thesis, "Flexible Elextronics: Materials and Device Fabrication", Virginia Polytechnic Institute and State University, Blacksburg, Virginia, (2005).

[118] F. Keohan, Personal Communication dated March 5, 2008 and March 6, 2008.

[119] Y. Chen, I. Smith, A. L. Geiler, C. Vittoria, V. Zagorodnii, Z. Celinski, and V. G. Harris, "Realization of hexagonal barium ferrite thick films on Si substrates using a screen printing technique," *Journal of Physics D: Applied Physics,* vol. 41, 2008.

[120] IDEAS Microwave Laboratory, Purdue University, West Lafayette, Indiana https://engineering.purdue.edu/IDEAS

[121] The Center for Microwave Magnetic Materials and Integrated Circuits, Northeastern University, Boston, MA. http://www.cm3ic.neu.edu/index.htm

[122] DuPont's microcircuit materials CB028 silver conductor polymer thick film composition data sheet, DuPont Microcircuit Materials Retrieved September 3, 2007 from the World Wide Web: http://www2.dupont.com/MCM/en_US/PDF/datasheets/CB028.pdf

[123] C. J. L. Constantino, A. E. Job, R. D. Simoes, J. A. Giacometti, V. Zucolotto, O. N. Oliveira Jr, G. Gozzi, and D. L. Chinaglia, "Phase transition in poly(vinylidene fluoride) investigated with micro-Raman spectroscopy," *Applied Spectroscopy,* vol. 59, pp. 275-279, 2005.

[124] I. Abdelsayed, "Characterization of electrosprayed Poly(vinylidene fluoride) and Poly(vinylidene fluoride)/CNT Nanocomposite," May 2006.

[125] A. Odon, "A Study for a PVDF sensor for detecting optical pulse radiation," in *Proceedings of SPIE - The International Society for Optical Engineering*, 2005, pp. 1-8.

[126] D. Setiadi, P. P. L. Regtien, and P. M. Sarro, "Realization of an integrated VDF/TrFE copolymer-on-silicon pyroelectric sensor," *Microelectronic Engineering,* vol. 29, pp. 85-88, 1995.

[127] B. Jaffe, Cook, W., Jaffe, H., *Piezoelectric Ceramics*. London: Academic Press, 1971.

[128] M. Serridge, Licht, T.R., *Piezoelectric accelerometer and vibration preamplifier handbook*: Bruel & Kjaer, 1987.

[129] B. F. Payne, "Application of back-to-back accelerometers to precision vibration measurements," *Journal of Research of the National Bureau of Standards (United States),* vol. 88, pp. 171-174, 1983.

[130] Piezoelectric Accelerometer -- Model 2221D SPECIFICATIONS, GlobalSpec the Engineering Search Engine Retrieved January 9, 2008 from the World Wide Web: http://sensors-transducers.globalspec.com/SpecSearch/PartSpecs?VID=605&Comp=5&PartId={bfdb5156-c8d4-4187-9713-e1530a05088b}

[131] Model 2221D Piezoelectric Accelerometer Data Sheet, Endevco Corporation Retrieved January 9, 2008 from the World Wide Web: http://www.endevco.com/product/prodpdf/2221D.pdf

[132] F. Kreith, Bohn, M.S., *Principles of heat transfer*: Brooks/Cole, 2001.

[133] D. P. Butler, Z. Celik-Butler, A. Jahanzeb, J. E. Gray, and C. M. Travers, "Micromachined YBaCuO capacitor structures as uncooled pyroelectric infrared detectors," *Journal of Applied Physics,* vol. 84, pp. 1680-1687, 1998.

[134] L. Capineri, "Pyroelectric PVDF sensor modeling of the temporal voltage response to arbitrarily modulated radiation," *IEEE Transactions on Ultrasonics, Ferroelectrics, and Frequency Control,* vol. 47, pp. 1406-1412, 2000.

[135] C. S. Lee, J. Y. Kim, D. E. Lee, J. Joo, S. Han, Y. W. Beag, and S. K. Koh, "An approach to durable poly(vinylidene fluoride) thin film loudspeaker," *Journal of Materials Research,* vol. 18, pp. 2904-2911, 2003.

[136] J. M. Kohler, R. Pechmann, A. Schaper, A. Schober, T. M. Jovin, M. Thurk, and A. Schwienhorst, "Micromechanical elements for detection of molecules and molecular design," *Microsystem Technologies,* vol. 1, pp. 202-208, 1995.